Dynamic Ferrite Transformation in Fe-6Ni-0.1C Alloy

2013

Nokeun Park

Dynamic Ferrite Transformation in

Fe-6Ni-0.1C Alloy

by

Nokeun Park

A Dissertation submitted to Kyoto University for

Doctor of Engineering

Department of Materials Science and Engineering

Graduate School of Engineering

Kyoto University

2013

Table of Contents

Chapter 3

Kinetics of dynamic transformation

Chapter 4

Characteristics of dynamically transformed ferrite

Chapter 5
Summary and Conclusions

Acknowledgements

List of Publications

CHAPTER 1

BACKGROUND AND PURPOSES

1.1 Grain refinement of ferrite

Steels are the fundamental resource as important structural materials in human civilization. Demand about development of mechanical properties in steels has been severely increased. For metallic materials, there are several strengthening mechanisms, and these are shown in **Fig. 1.1a** that displays the correlation between the strength and the strengthening mechanisms in steels. The yield strength levels caused by strengthening mechanisms of precipitation, dislocation, solid solution and matrix are almost constant, but only the portion of grain refinement strengthening is proportionally increased. **Figure 1.1b** shows the correlation between the yield stress of ferrite and the inverse square root of ferrite grain size, so-called 'Hall-Petch relationship' which can be expressed as [1–4],

$$\sigma_y = \sigma_i + k \cdot D^{-1/2} \tag{1.1}$$

where σ_y is the yield stress, σ_i is the friction stress, k is a constant and D is the mean grain size of ferrite. It is well known that most strengthening mechanisms mentioned above have trade-off relationship with the enhancement in toughness and ductility of materials, so that the improvement of strength makes toughness and ductility decrease. It has been reported, however, that the grain refinement of ferrite improves the toughness in ferrite, and the ductile-brittle transition temperature (DBTT) decreases as ferrite grain size decreases, which is described in the following relationship [5],

$$DBTT = A - k' \cdot D^{-1/2} \tag{1.2}$$

1
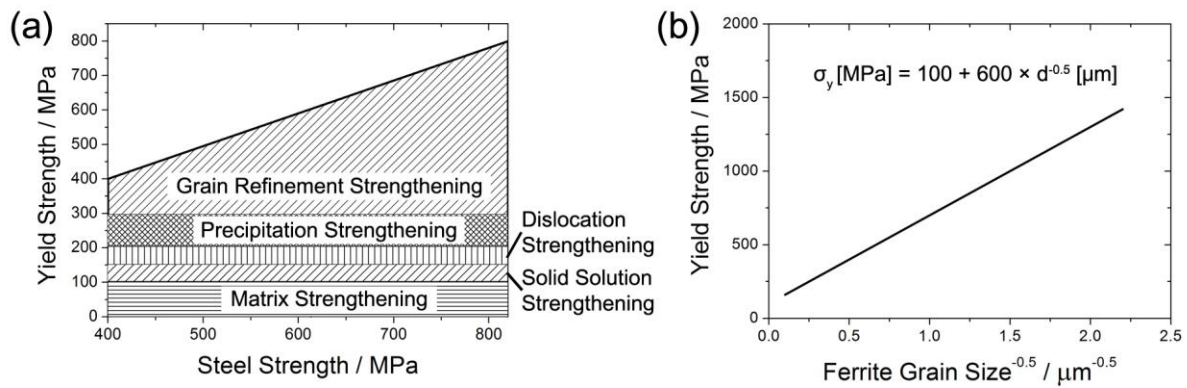
Fig. 1.1 (a) Scheme of various strengthening effects and (b) Hall-Petch relationship of ferrite in steels. Reproduction of Ref. [1].

where A and k' are constants, and D is the mean grain size of ferrite. Thus it has been believed that grain refinement of ferrite is the most effective way to improve both strength and toughness in steels.

1.2 Methods to make grain size of ferrite fine

Various processes have been tried to achieve grain refinement of ferrite in low-carbon steels in order to improve their mechanical properties. The concepts for grain refinement of ferrite are basically classified into two categories: one is the grain refinement using plastic deformation of austenite before ferrite transformation, and the other is to apply plastic deformation to ferrite after phase transformation.

1.2.1 Plastic deformation of austenite before ferrite transformation

Various ways have been proposed to maximize the number of nucleation sites for ferrite in austenite and/or to inhibit the growth of ferrite. One of the representative ways is to

increase the fraction of austenite grain boundary through plastic deformation of austenite prior to ferrite transformation. Because austenite grain boundary acts as a preferential nucleation site for ferrite transformation, the higher fraction of austenite grain boundary gives the higher density of nucleation site for ferrite transformation. **Figure 1.2** illustrates different stages in the controlled rolling process, which is a representative thermomechanical process used for ferrite grain refinement of steel plates, and the change in microstructures during the process. After reheating slabs, austenite (**Fig. 1.2a**) is hot-deformed in recrystallization region, resulting in recrystallized fine austenite grains, leading to the increase of austenite grain boundaries (**Fig. 1.2.b**). When deformation of austenite is carried out at lower temperatures where recrystallization of austenite does not occur, austenite grains are plastically deformed and elongated (**Fig. 1.2c**). As a result, austenite grain boundary per unit volume is significantly increased [6]. Additionally, plastic deformation of austenite generates high density of lattice defects, such as deformation bands and microbands that can be additional nucleation sites for ferrite transformation [7]. In the commercial controlled rolling, some carbide-forming alloying elements, such as Nb and Ti, are added to the steels for inhibiting recovery and recrystallization of austenite. Furthermore, accelerated cooling of the hot-rolled plates are sometimes applied to increase the nucleation frequency of ferrite through enhancing undercooling (i.e., driving force for ferrite transformation), and suppresses the growth of ferrite by lowering temperatures. Consequently, ferrite grain size around 5 µm is achieved in manufacturing process through plastic deformation of austenite before ferrite transformation [8].

1.2.2 Plastic deformation of ferrite

Plastic deformation of ferrite can also decrease its grain size. One example is the

3

dynamic recrystallization of ferrite that takes place when plastic deformation is applied to ferrite or tempered martensite under appropriate conditions at elevated temperatures [9–11]. Much finer ferrite grain (less than 3 μm) can be achieved through severe plastic deformation processes, where very large amount of plastic deformation is applied to the materials by special processes, such as equal channel angular pressing [12], accumulative roll bonding [13], high pressure torsion [14], large plain strain [15] and so on. It is thought that the original grains are subdivided to form ultrafine grained structures during severe plastic deformation [8,16]. The common features of these processes to decrease grain size of ferrite are that plastic deformation is applied to ferrite after completion of ferrite transformation and that the mechanisms of plastic deformation and subsequent recovery and recrystallization are used for microstructure refinement.
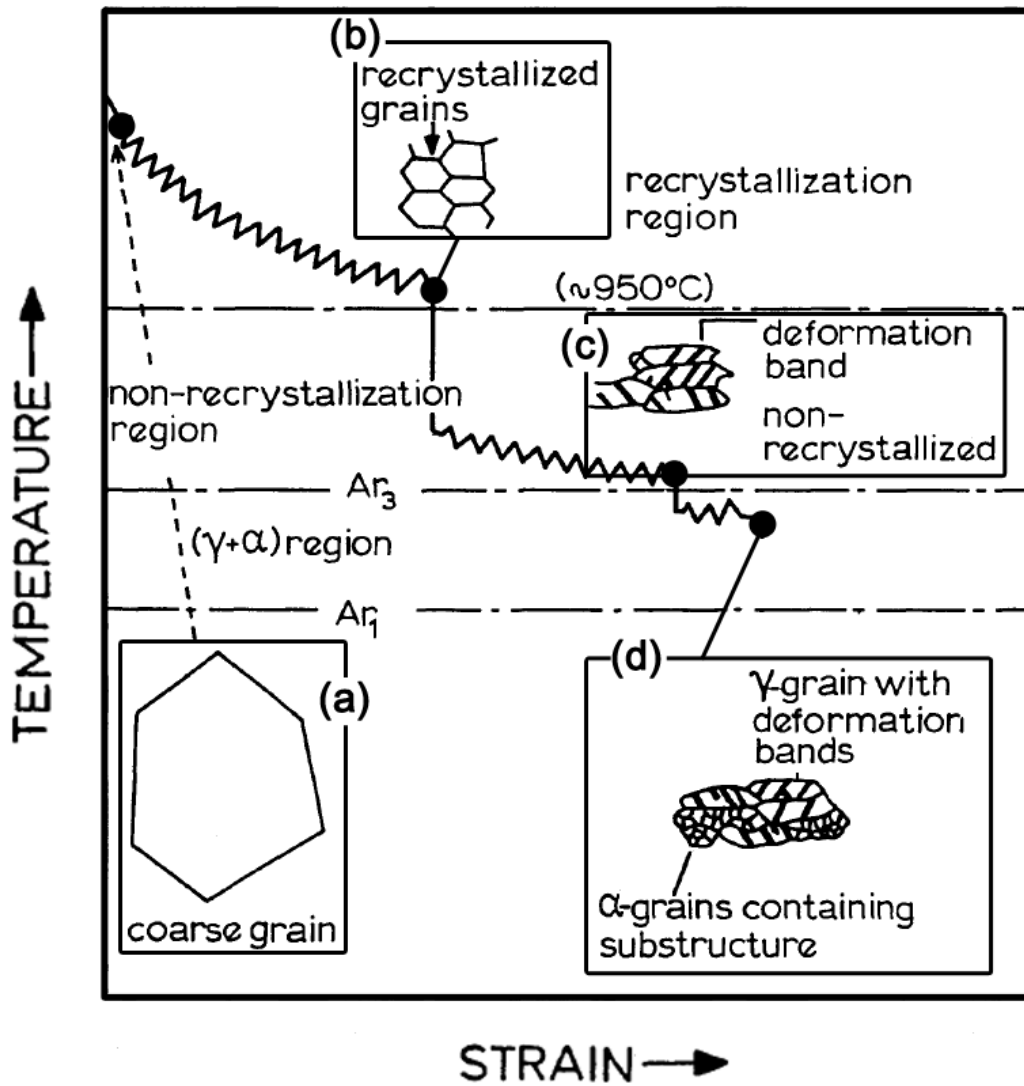
Fig. 1.2 Schematic illustration of the controlled rolling process and the change in microstructure with deformation.   Reproduction of Ref. [7].

1.3 Dynamic ferrite transformation

As mentioned in section 1.2, the fundamental methods to achieve fine ferrite grains are categorized into two types depending on whether the plastic deformation is applied to either austenite or ferrite. In the former route, i.e., plastic deformation of austenite before ferrite transformation, in development of thermomechanical process, as shown in **Fig. 1.2**, temperature for the final rolling pass has been decreased to apply larger plastic deformation of austenite. Finally it reached to intercritical temperature regime where both austenite and ferrite are stable, as shown in **Fig. 1.2d**. As a result, ferrite could be formed during deformation of austenite at low temperatures, which is defined as 'dynamic transformation' to ferrite.

Yada and his colleague [17–19], who were pioneers of studies about dynamic ferrite transformation, reported the occurrence of dynamic transformation to ferrite in low-carbon steels, and the ferrite grain size was much finer than that obtained from a conventional TMCP. **Figure 1.3** shows (a) Strain-Temperature-Phase map of a Fe-0.15C-1Mn steel (wt.%) and (b) average ferrite grain size as a function of accumulated strain at rolling temperatures ranging from 750 to 800 ℃ [17]. When accumulated strain in austenite by rolling was larger than 0.7 at around 750 ℃, dynamic ferrite transformation occurred according to **Fig. 1.3a**. With increasing accumulated strain, grain size of ferrite decreased, as shown in **Fig. 1.3b**, and it finally reached to 1 μm at large accumulated strain. Many studies about dynamic transformation in commercial alloys have been reported in last 30 years [20–42]. Although mechanisms of dynamic ferrite transformation have not been fully understood yet due to the lack of systematic approaches, many interesting topics have been reported, especially about thermodynamics and kinetics of ferrite transformation during deformation of austenite. One of controversial topics is the occurrence of dynamic transformation at temperatures above the
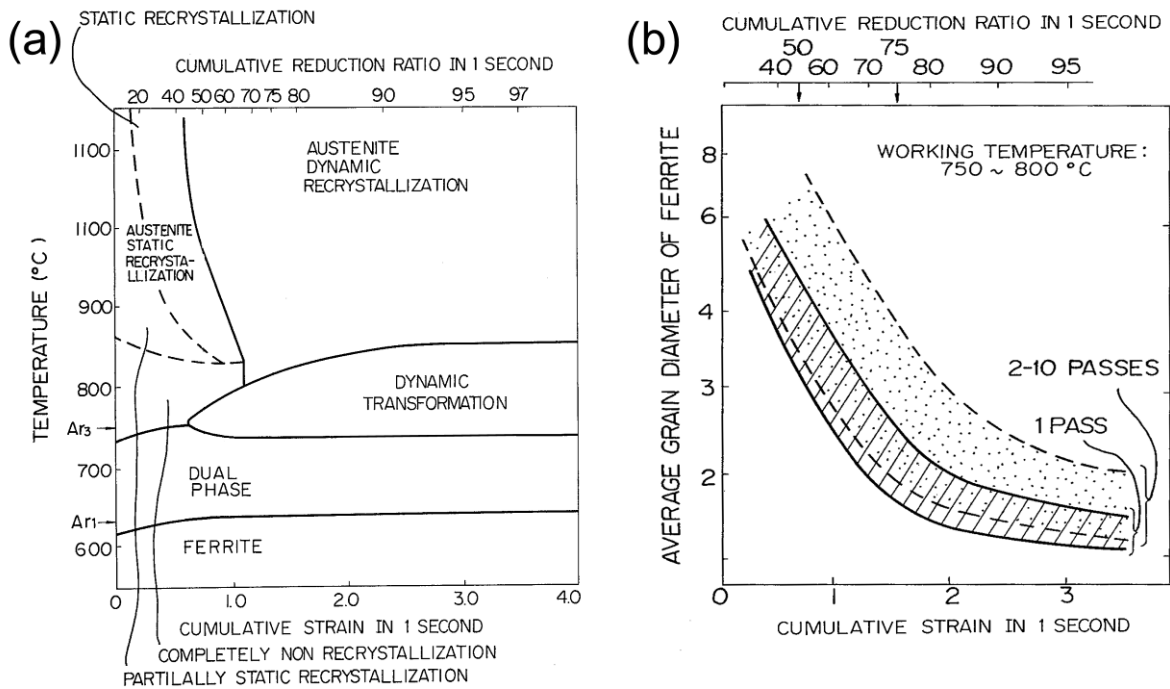
Fig. 1.3 (a) Strain-Temperature-Phase map of a Fe-0.15C-1Mn steel (wt.%). Multi-pass rolling was applied within one second, and then specimens were air-cooled at a rate of 20 ℃ s^{-1}. (b) The relationship between the accumulative strain in less than one second and the ferrite grain diameter of specimens deformed at temperature ranging from 750 to 800 ℃. Reproduction of Ref. [17].

ortho-equilibrium transformation temperature (Ae$_3$), which was proposed firstly by Yada *et al.* as seen in **Fig. 1.3a** [17]. The mechanism of dynamic transformation above Ae$_3$ was qualitatively explained in **Fig. 1.4**. When plastic deformation is applied to austenite, free energy of austenite is raised by stored energy due to the generation of dislocations in austenite (**Fig. 1.4a**), resulting in the increase in Ae$_3$ temperature (**Fig. 1.4b**) so that ferrite could be formed even above Ae$_3$ [20,24,43]. Computer-aided studies about the occurrence of dynamic transformation above Ae$_3$ have been performed, and experimentally obtained deformation microstructures of ferrite were reported as the evidence of dynamic transformation above Ae$_3$ [29,30,33–37]. However, it is still possible that the observed

7
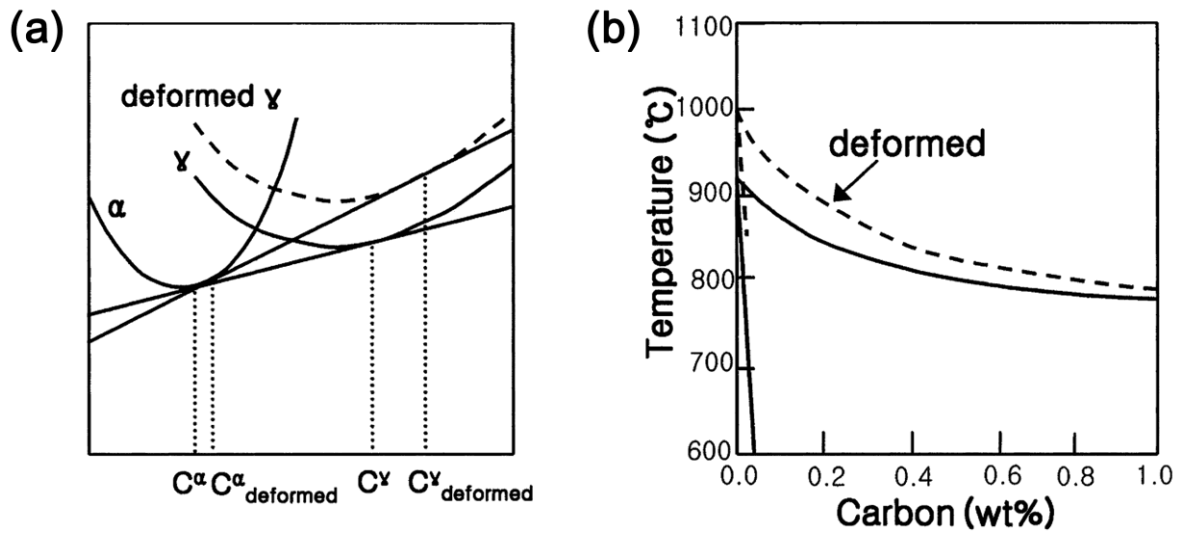
Fig. 1.4 Schematic diagram showing change in free energy curve of deformed austenite, (b) Fe–C phase diagram showing change in transformation temperature by deformation.   Reproduction of Ref. [43].

ferrite, which was suggested as the evidence of dynamic transformation above Ae_3, might form during cooling from deformation temperature to room temperature because driving force for ferrite transformation is increased and kinetics of ferrite transformation is accelerated due to plastic deformation of austenite.   The direct evidence for the occurrence of dynamic transformation was experimentally demonstrated through *in-situ* X-ray diffraction during torsion test [23].   Nevertheless, the mechanism of the occurrence of dynamic transformation, the role of deformation of austenite and the kinetics of dynamic transformation above Ae_3, have not been clarified yet.

The other interesting viewpoint about dynamic transformation is the acceleration of transformation kinetics.   It is well known that static ferrite transformation is accelerated when austenite is plastically deformed [6,7].   This is because plastic deformation of austenite introduces high density of lattice defects in austenite which could be potential nucleation sites for ferrite.   In the case of dynamic transformation, it has been reported that

8

kinetics of dynamic transformation was accelerated as well [41,42]. The previous concept of static transformation from deformed austenite could be adopted to explain why dynamic transformation was accelerated. Additionally, the continuous deformation during dynamic transformation could play a role to influence on kinetics of dynamic transformation. Zheng *et al.* [34,35] studied the role of deformation on kinetics of dynamic transformation using cellular automaton calculation, and proposed that 'unsaturated nucleation of ferrite' at interphase boundary between austenite and ferrite was a key mechanism for the acceleration of dynamic transformation. However, no *in-situ* experimental study has been reported about kinetics of dynamic transformation yet. As mentioned above, microstructure at room temperature may contain not only dynamically transformed ferrite but also statically transformed ferrite grains which formed during cooling procedure from deformed austenite. Therefore, it is necessary to study about the kinetics of dynamic transformation in detail, which may give us deeper understanding on mechanisms of dynamic transformation.

Not only two topics shown above, but many interesting topics on dynamic transformation still exist, such as morphologies, crystallographic orientations, mechanical properties of dynamically transformed ferrite and formation of precipitates, and so on. They are also studied in the present dissertation.

1.4 Variables affecting dynamic ferrite transformation

There are several variables that control *static* ferrite transformation from austenite, such as chemical composition of alloy, prior austenite grain size, transformation temperature, cooling rate, and so on. Most of those variables are consequently controlled to modulate thermodynamics and kinetics of ferrite transformation. It should be noted that other two

variables are additionally involved in dynamic transformation, i.e., strain (amount of deformation) and strain rate.   When two variables are set, *deformation period*, which equals to *strain divided by strain rate* (under a constant strain rate), is determined.   Under a constant strain rate, the density of lattice defects in the deformed austenite would increase with increasing strain.   Under the same amounts of applied strain, on the other hand, the density of lattice defects in the deformed austenite would be higher when the strain rate is faster.   Combination of strain rate and strain determines deformation period, i.e., time period at the temperature, which is also important variable for studying dynamic ferrite transformation.   Therefore, additional variables, i.e., strain and strain rate, should be involved in dynamic transformation together with the variables which are usually considered in static transformation because the effects of strain and strain rate significantly affect thermodynamics and kinetics of dynamic ferrite transformation.

1.5 Design of experiments

1.5.1 Chemical composition of alloy

Most previous studies about dynamic transformation have used commercial low-carbon steels with few percent of Mn and small amounts of additional elements, such as P, Si, Ni, Ti, N, and so on.   For example, Basabe and Jonas [37] studied dynamic transformation using a low carbon steel (C: 0.09, Si: 0.02, Mn: 1.3, Al: 0.07, Nb: 0.036, P< 0.004, S: 0.0028, Fe: bal. (wt. %)), and they reported dynamic recrystallization (DRX) of austenite occurred together with dynamic transformation to ferrite, and dynamic softening of flow stress in stress-strain curves was observed.   Since dynamic softening in flow stress resulted from a mixture of the effects of both DRX of austenite and dynamic transformation, it was difficult to separate the

effect of each phenomenon for dynamic softening in flow stress. In order to understand the sole effect of dynamic transformation to ferrite on both dynamic softening and the microstructure of deformed specimens, it is better to minimize or to suppress the influence of DRX of austenite.

It is well known that some elements, such as Ni and Mn, representatively, are effective to lower Ae_3 of a given steel and to delay the kinetics of ferrite transformation. By adding such elements, the effects between DRX of austenite and dynamic transformation on dynamic softening of flow stress can be separated when experiment is conducted at relatively low temperatures where DRX of austenite does not take place but still ferrite transformation is possible to occur. Especially, Ni does not change stacking-fault energy of austenite significantly and does not make precipitates (like MnS), compared with Mn.

The alloy used in the present dissertation was therefore designed to be Fe-6Ni-0.1C (C: 0.11, Si: 0.01, Mn: 0.003, P: 0.002, S: 0.0015, Ni: 5.97, Fe: bal. (wt.%)), which was a model alloy to widen austenite range for lowering processing temperatures. Ae_3 of this alloy is 728 ℃ calculated by Thermo-Calc software, and that is quite low enough not to occur DRX of austenite.

1.5.2 Thermomechanical process simulation

Dynamic transformation from austenite can be investigated through several kinds of deformation modes, such as plain strain compression (rolling), tension, uniaxial compression and torsion, using thermomechanical processing simulators or other equipments in a laboratory scale. In the present dissertation, uniaxial compression mode is chosen to simulate dynamic transformation using Thermecmastor-Z, a thermomechanical processing simulator made by Fuji Electronic Industrial Co., Ltd, which can perform compressive

deformation at wide range of temperatures at various strain rates.   Information of the applied

load and stroke during hot-compression can be converted into flow stress and true strain so

that true stress-true strain curve of each specimen is obtained.

The temperature of the specimen is recorded during the process by using a thermocouple

welded on the side surface of the specimen.   The high-frequency induction heating system

in Thermecmastor-Z controls temperature of the specimen precisely.   One example about the

change in temperature of a specimen during a thermomechanical process is shown in **Fig. 1.5**.

Figure 1.5a shows the temperature change during the process from austenitization at 800 ℃

to the completion of compression by 60% reduction in height at 750 ℃ at a strain rate of 10^{-1}

s^{-1}.   **Figures 1.5b** and **c** are enlarged parts of **Fig. 1.5a** marked as **A** and **B**, respectively.

After the onset of isothermal holding process in **Fig. 1.5b**, it takes 4.5 s for the temperature to

be stabilized.   The maximum decrease of the temperature during 4.5 s is -6 ℃ (at 744 ℃).

In order to stabilize temperature distribution in the specimen, the specimen is kept for 60 s at

deformation temperature.   When the deformation starts, the temperature drops but the

maximum decrease is only -3 ℃ (down to 747 ℃) in **Fig. 1.5c**.   Temperature fluctuation of

the specimen during deformation is recorded as ± 2 ℃.   Thus, it could be concluded that
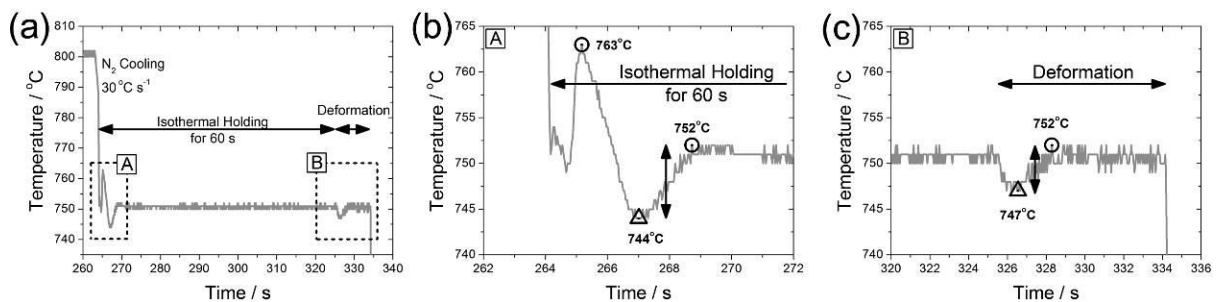
Fig. 1.5 Temperature of the compression specimen during a thermomechanical process, recorded by a thermocouple welded on the side surface of the specimen.   (a) Temperature change during a period from austenitization at 800 ℃ to completion of compression at 750 ℃ at a strain rate of 10^{-1} s^{-1} to a strain of 0.96, (b)-(c) enlarged parts (A and B) of (a).

temperature during thermomechanical process is controlled well by induction heating system.

Microstructural observations of the as-deformed specimens are necessary to understand characteristics of dynamically transformed ferrite. Thus, precisely controlled cooling condition with an appropriate coolant having large heat capacity is required to freeze microstructures of the as-deformed specimens within short period. In the present
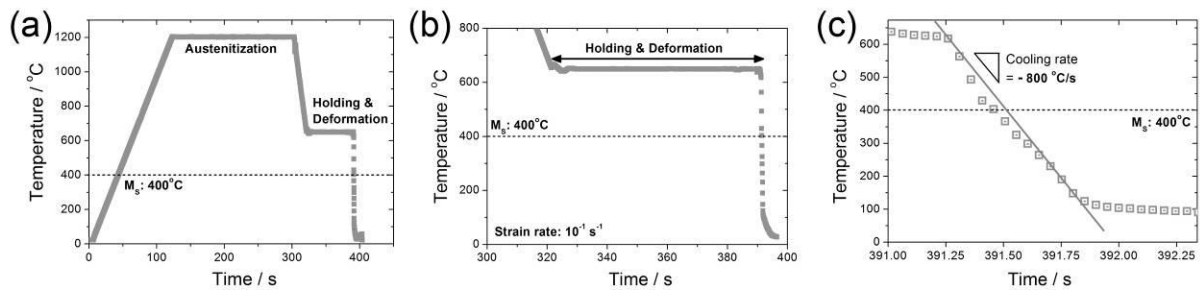
Fig. 1.6 Temperature of the compression specimen during thermomechanical process, recorded by a thermocouple welded on the surface of the specimen. (a) Whole period of the compression test at 650°C and 10^{-1} s^{-1} to a strain of 0.96, (b) enlarged area of (a), and (c) enlarged area of (b) especially around cooling procedure. M_S indicates martensite-start-temperature.

experiments, water is chosen as a coolant. Cooling condition is optimized to minimize the time interval between the finish of deformation and the initiation of water cooling. The cooling rate measured at the surface of the specimen is about 800 °C s^{-1} as shown in **Fig. 1.6**.

1.6 Outline of the dissertation

The present dissertation consists of five chapters. First of all, in **Chapter 1** (this chapter), background, purpose and experimental details of this dissertation are explained.

It is well known that flow stress during deformation of austenite reflects the existence of dislocations [44,45]. Because ferrite is softer than strain-hardened austenite at elevated temperatures [46–48], flow stress might decrease when dynamic transformation occur. In

Chapter 2, critical deformation condition for the occurrence of dynamic transformation is studied through analyzing stress-strain curves, and the microstructures of dynamically transformed ferrite are compared with those of statically formed ones. Chemical and mechanical driving force for dynamic transformation is also discussed from a viewpoint of thermodynamics.

In the case of DRX of austenite, its kinetics has been interpreted through stress-strain curve analysis [49–52]. The onset of softening in the flow stress indicates the annihilation of dislocations owing to DRX of austenite, and subsequent softening is related to the increase in the fraction of dynamically recrystallized austenite. In the case of dynamic transformation, it is obvious that, when dynamic transformation to ferrite occurs, the softening of flow stress should be observed because ferrite is softer than strain-hardened austenite at elevated temperatures. However, there is no report about the kinetics of dynamic transformation which corresponds to the softening of the flow stress. In **Chapter 3**, the correlation between the change in flow stress and the fraction of ferrite is revealed first, and then, the kinetics of dynamic transformation is interpreted by analyzing stress-strain curves.

In **Chapter** 4, the effects of deformation variables, such as strain, strain rate and deformation temperature, on microstructural characteristics, such as morphology and crystallography, of dynamically transformed ferrite are discussed. Additionally, mechanical properties of the dynamically transformed ferrite are compared with those of the statically transformed ferrite in order to clarify the differences between them.

In **Chapter 5**, conclusions with achievements in the present dissertation are summarized.

1.7 References

[1]   Y. Weng, *Ultra-fine grained steels*. Springer, 2009.

[2]   E. O. Hall, "The deformation and ageing of mild steel: III Discussion of results," *Proceedings of the Physical Society. Section B*, vol. 64, pp. 747–753, 1951.

[3]   N. J. Petch, *Journal of the Iron and Steel Institute*, vol. 174, p. 25, 1953.

[4]   N. Hansen, "Hall-Petch relation and boundary strengthening," *Scripta Materialia*, vol. 51, pp. 801–806, 2004.

[5]   T. Hanamura, F. Yin, and K. Nagai, "Ductile–brittle transition temperature of ultrafine ferrite/cementite microstructure in a low carbon steel," *ISIJ International*, vol. 44, pp. 610–617, 2004.

[6]   A. Hiramatsu and M. Umemoto, "Computer modelling of phase transformation from work-hardened austenite," *ISIJ International*, vol. 32, pp. 306–315, 1992.

[7]   G. Anan, S. Nakajima, M. Miyahara, S. Nanba, M. Umemoto, A. Hiramatsu, A. Moriya, and T. Watanabe, "A model for recovery and recrystallization of hot deformed austenite considering structural heterogeneity," *ISIJ international*, vol. 32, pp. 261–266, 1992.

[8]   N. Tsuji and T. Maki, "Enhanced structural refinement by combining phase transformation and plastic deformation in steels," *Scripta Materialia*, vol. 60, pp. 1044–1049, 2009.

[9]   N. Tsuji, Y. Matsubara, and Y. Saito, "Dynamic recrystallization of ferrite in interstitial free steel," *Scripta Materialia*, vol. 37, pp. 477–484, 1997.

[10]   L. Longfei, Y. Wangyue, and S. Zuqing, "Dynamic recrystallization of ferrite in a low-carbon steel," *Metallurgical and Materials Transactions A*, vol. 37, pp. 609–619, 2006.

[11]   B. Poorganji, G. Miyamoto, T. Maki, and T. Furuhara, "Formation of ultrafine grained ferrite by warm deformation of lath martensite in low-alloy steels with different carbon content," *Scripta Materialia*, vol. 59, pp. 279–281, 2008.

[12]   D. H. Shin, B. C. Kim, K.-T. Park, and W. Y. Choo, "Microstructural changes in equal channel angular pressed low carbon steel by static annealing," *Acta Materialia*, vol. 48, pp. 3245–3252, 2000.

[13]   R. Yoda, K. Shibata, T. Morimitsu, D. Terada, and N. Tsuji, "Formability of ultrafine-grained interstitial-free steel fabricated by accumulative roll-bonding and subsequent annealing," *Scripta Materialia*, vol. 65, pp. 175–178, 2011.

[14] Y. Ivanisenko, W. Lojkowski, R. Z. Valiev, and H.-J. Fecht, "The mechanism of formation of nanostructure and dissolution of cementite in a pearlitic steel during high pressure torsion," *Acta Materialia*, vol. 51, pp. 5555–5570, 2003.

[15] A. Ohmori, S. Torizuka, K. Nagai, N. Koseki, and Y. Kogo, "Effect of deformation temperature and strain rate on evolution of ultrafine grained structure through single-pass large-strain warm deformation in a low carbon," *Materials transactions*, vol. 45, pp. 2224–2231, 2004.

[16] N. Hansen, R. F. Mehl, and A. Medalist, "New discoveries in deformed metals," *Metallurgical and Materials Transactions A*, vol. 32, pp. 2917–2935, 2001.

[17] H. Yada, Y. Matsumura, and K. Nakajima, "Ferritic steel having ultra-fine grains and a method for producing the same," U.S. Patent US 446684221-Aug-1984.

[18] Y. Matsumura and H. Yada, "Evolution deformation of ultrafine-grained ferrite in hot successive deformation," *Transactions ISIJ*, vol. 27, pp. 492–498, 1987.

[19] H. Yada, T. Matsumura, and T. Senuma, *Proc. Int. Conf. Physical Metallurgy of Themomechanical Processing of Steels and Other Metals, ISIJ*, vol. Thermec 88, pp. 200–207, 1988.

[20] S. W. Lee, D. H. Seo, and W. Y. Choo, "Study of ferrite refinement using heavy deformation in plain low carbon steels," *Korean Journal of Metals and Materials*, vol. 36, pp. 1966–1973, 1998.

[21] P. Hodgson, M. R. Hickson, and R. K. Gibbs, "Ultrafine ferrite in low carbon steel," *Scripta Materialia*, vol. 40, pp. 1179–1184, 1999.

[22] P. J. Hurley, P. D. Hodgson, and B. C. Muddle, "Analysis and characterisation of ultra-fine ferrite produced during a new steel strip rolling process," *Scripta Materialia*, vol. 40, pp. 433–438, 1999.

[23] H. Yada, C.-M. Li, and H. Yamagata, "Dynamic $\gamma \to \alpha$ transformation during hot deformation in iron-nickel-carbon alloys," *ISIJ international*, vol. 40, pp. 200–206, 2000.

[24] R. Priestner and A. K. Ibraheem, "Processing of steel for ultrafine ferrite grain structures," *Materials Science and Technology*, vol. 16, pp. 1267–1272, 2000.

[25] Y. Choi, W. Y. Choo, and D. Kwon, "Analysis of mechanical property distribution in multiphase ultra-fine-grained steels by nanoindentation," *Scripta Materialia*, vol. 45, pp. 1401–1406, 2001.

[26] J.-K. Choi, D.-H. Seo, J.-S. Lee, K.-K. Um, and W.-Y. Choo, "Formation of ultrafine ferrite by strain-induced dynamic transformation in plain low carbon steel," *ISIJ International*, vol. 43, pp. 746–754, 2003.

[27] S. C. Hong, S. H. Lim, H. S. Hong, K. J. Lee, D. H. Shin, and K. S. Lee, "Effects of Nb on strain induced ferrite transformation in C-Mn steel," *Materials Science and Engineering A*, vol. 355, pp. 241–248, 2003.

[28] S. C. Hong, S. H. Lim, K. J. Lee, D. H. Shin, and K. S. Lee, "Effect of undercooling of austenite on strain induced ferrite transformation behavior.," *ISIJ International*, vol. 43, pp. 394–399, 2003.

[29] M. Tong, J. Ni, Y. Zhang, D. Li, and Y. Li, "Temporal oscillatory behavior in deformation induced ferrite transformation in an Fe–C binary system," *Scripta Materialia*, vol. 50, pp. 909–913, 2004.

[30] M. Tong, D. Li, Y. Li, J. Ni, and Y. Zhang, "Monte carlo-method simulation of the deformation-induced ferrite transformation in the Fe-C system," *Metallurgical and Materials Transactions A*, vol. 35, pp. 1565–1577, 2004.

[31] H. Beladi, G. Kelly, A. Shokouhi, and P. Hodgson, "Effect of thermomechanical parameters on the critical strain for ultrafine ferrite formation through hot torsion testing," *Materials Science and Engineering A*, vol. 367, pp. 152–161, 2004.

[32] H. Beladi, G. L. Kelly, and P. D. Hodgson, "Ultrafine grained structure formation in steels using dynamic strain induced transformation processing," *International Materials Reviews*, vol. 52, pp. 14–28, 2007.

[33] X. Sun, H. Luo, H. Dong, Q. Liu, and Y. Weng, "Microstructural evolution and kinetics for post-dynamic transformation in a plain low carbon steel," *ISIJ International*, vol. 48, pp. 994–1000, 2008.

[34] C. Zheng, D. Li, S. Lu, and Y. Li, "On the ferrite refinement during the dynamic strain-induced transformation: A cellular automaton modeling," *Scripta Materialia*, vol. 58, pp. 838–841, 2008.

[35] C. Zheng, N. Xiao, L. Hao, D. Li, and Y. Li, "Numerical simulation of dynamic strain-induced austenite–ferrite transformation in a low carbon steel," *Acta Materialia*, vol. 57, pp. 2956–2968, 2009.

[36] V. V Basabe and J. J. Jonas, "The ferrite transformation in hot deformed 0.036 % Nb austenite at temperatures above the Ae 3," *ISIJ international*, vol. 50, pp. 1185–1192, 2010.

[37] V. V Basabe, J. J. Jonas, and H. Mahjoubi, "Dynamic transformation of a low carbon steel at temperatures above the Ae3," *ISIJ international*, vol. 51, pp. 612–618, 2011.

[38] J. J. Jonas and V. V. Basabe, "Ferrite formation above the Ae3 in a medium-carbon steel," *Solid State Phenomena*, vol. 172–174, pp. 372–377, 2011.

[39] J. J. Jonas and V. V Basabe, "The transformation of hot deformed austenite above the Ae3," in *THERMEC'2011*, 2011, p. 596.

[40] Y. M. Kim, T.-H. Ahn, K. K. Park, K. H. Oh, and H. N. Han, "Identification of dynamic ferrite formed during the deformation of super-cooled austenite by image-based analysis of an EBSD map," *Metals and Materials International*, vol. 17, pp. 181–186, 2011.

[41] Y. Adachi, P. G. Xu, and Y. Tomota, "Crystallography and kinetics of dynamic transformation in steels," *ISIJ International*, vol. 48, pp. 1056–1062, 2008.

[42] H. Dong and X. Sun, "Deformation induced ferrite transformation in low carbon steels," *Current Opinion in Solid State and Materials Science*, vol. 9, pp. 269–276, 2005.

[43] S. C. Hong and K. S. Lee, "Influence of deformation induced ferrite transformation on grain refinement of dual phase steel," *Materials Science and Engineering A*, vol. 323, pp. 148–159, 2002.

[44] Y. Estrin and H. Mecking, "A unified phenomenological description of work hardening and creep based on one-parameter models," *Acta Metallurgica*, vol. 32, pp. 57–70, 1984.

[45] C. M. Sellars, "The kinetics of softening processes during hot working of austenite," *Czechoslovak Journal of Physics*, vol. 35, pp. 239–248, 1985.

[46] A. Z. Hanzaki, R. Pandi, P. D. Hodgson, and S. Yue, "Continuous cooling deformation testing of steels," *Metallurgical Transactions A*, vol. 24, pp. 2657–2665, 1993.

[47] R. Pandi and S. Yue, "Dynamic transformation of austenite to ferrite in low carbon steel," *ISIJ international*, vol. 34, pp. 270–279, 1994.

[48] R. Wang and T. Lei, "Deformation and restoration behaviour of ferrite-austenite two-phase structures," *Materials Science and Engineering A*, vol. 165, pp. 19–27, 1993.

[49] T. Sakai and J. Jonas, "Overview no. 35 Dynamic recrystallization: mechanical and microstructural considerations," *Acta Metallurgica*, vol. 32, pp. 189–209, 1984.

[50] E. Poliak and J. Jonas, "A one-parmenter approach to determining the critical conditions for the initiation of dynamic recrystallization," *Acta Materialia*, vol. 44, pp. 127–136, 1996.

[51] H. Mecking and U. F. Kocks, "Kinetics of flow and strain-hardening," *Acta Metallurgica*, vol. 29, pp. 1865–1875, 1981.

[52] U. F. Kocks and H. Mecking, "Physics and phenomenology of strain hardening: the FCC case," *Progress in Materials Science*, vol. 48, pp. 171–273, 2003.

CHAPTER 2

OCCURRENCE OF DYNAMIC TRANSFORMATION IN 6NI-0.1C

STEEL

2.1 Introduction

As mentioned in Chapter 1, dynamic ferrite transformation is defined as a ferrite transformation occurring during deformation of austenite. Many studies discussed the occurrence of dynamic transformation in commercial low-C steels [1–23]. Yada and Matsumura [1,2] firstly reported that ferrite could be formed under deformation, and they also proposed a possibility that dynamic transformation would occur even above the ortho-equilibrium transformation temperature (Ae_3) in low-C steels composed of 0.07-0.13C, 0.02-0.47Si, and 0.97-1.07Mn (wt.%). Yada *et al.* [6] actually demonstrated the occurrence of dynamic transformation through in-situ X-ray diffraction experiment during torsion test. Lee *et al.* [3] and Priestner *et al.* [7] explained qualitatively how Ae_3 was increased by plastic deformation. On the other hand, Choi *et al.* [9] reported dynamic transformation occurred at intercritical temperature regime, i.e. below Ae_3, but only dynamic recrystallization of austenite took place at higher temperature above Ae_3 in a plain carbon steel (C 0.15, Si 0.40, Mn 1.51 (wt.%)). As decreasing deformation temperature, i.e. increasing undercooling, the required strain for the occurrence of dynamic transformation was decreased [11], and the fraction of ferrite after completing deformation was increased [9]. It was concluded that kinetics of ferrite transformation under deformation was greatly accelerated. Computer-aided study about dynamic transformation has been performed as well. Monte Carlo simulations by Tong *et al.* [12,13] showed that ferrite transformation in a 0.13C steel (wt.%)

could occur at Ae₃, and a reverse transformation to austenite from the dynamically transformed ferrite could also happen during subsequent isothermal holding at Ae₃. Zheng *et al.* [17,18] proposed, using cellular automaton calculation for a steel with a chemical composition of 0.13C-0.19Si-0.49Mn (wt.%), that transformation during deformation was accelerated by continuous nucleation of ferrite around austenite/ferrite phase boundaries as well as at austenite grain interiors. Although a variety of studies about the dynamic transformation to ferrite have been reported, current literatures lack a coherent explanation of the fundamental transformation mechanism.

Supposing dynamic transformation happens in steels at elevated temperatures, it would affect the stress-strain behaviors during hot-deformation sensitively, like the case of dynamic recrystallization of austenite [24–26]. However, by using commercial alloys, it is difficult to understand the stress-strain behavior of dynamic transformation because the occurrence of dynamic recrystallization of austenite competes with that of dynamic transformation at high temperature regime [9,27]. Therefore, a Fe-6Ni-0.1C model alloy is designed in the present study to enlarge austenite range to lower temperature regime, so that the occurrence of dynamic recrystallization of austenite could be prohibited at that temperature regime.

Chapter 2 consists of following two sections. The occurrence of dynamic transformation in the Fe-6Ni-0.1C model alloy should be firstly confirmed by systematic analyses of stress-strain curves with microstructure observations. Then, the occurrence of dynamic transformation at wide temperature ranges including temperatures above Ae₃ will be demonstrated based on the results of the first section.

2.2 Flow stress analysis for determining critical condition of dynamic ferrite transformation in 6Ni-0.1C Steel

2.2.1 Introduction

Choi et al. [9] reported that the occurrence of dynamic transformation in a plain carbon steel competed with that of dynamic recrystallization of austenite. It is because temperature range for the occurrence of dynamic transformation for commercial steels is overlapped with that of dynamic recrystallization of austenite. Once temperature ranges for two different phenomena in an identical alloy are separated, it is possible to interpret the occurrence of dynamic transformation only, irrespective of dynamic recrystallization of austenite. It is well known that addition of Ni in steels decreases Ae_3 effectively so that it is possible to obtain the temperature range where austenite is solely stable but no dynamic (and static) recrystallization of austenite occurs.

In this section, the occurrence of dynamic transformation in the Fe-6Ni-0.1C model alloy is confirmed both by systematical analyses of stress-strain curves obtained under various deformation conditions, including regions of dynamic recrystallization of austenite, and by microstructure observation of the specimens deformed under different conditions.

2.2.2 Experimental procedure

2.2.2.1 Material

The material used in the present study is a 6Ni-0.1C steel (wt.%), which was designed as a model alloy to enlarge austenite temperature range and to have enough incubation time for the onset of ferrite transformation during isothermal holding of austenite. The detailed chemical composition of the alloy investigated is shown in **Table 2.2.1**. The Ae_3 and the para-equilibrium temperature (Ap_3) of the 6Ni-0.1C steel were calculated to be 728 and 684 ℃, respectively, by Thermo-Calc software. As-received hot rolled plate of the 6Ni-0.1C steel 15 mm in thickness was homogenized at 1100 ℃ for 24 hours.

Table 2.2.1 Chemical composition of the investigated alloy (wt.%).

C	Ni	Mn	Si	Al	P	S	Fe
0.112	5.97	0.003	0.008	0.037	0.002	0.0015	bal.

2.2.2.2 Time-Temperature-Transformation (TTT) diagram

In order to determine the onset of static transformation from austenite to ferrite during isothermal holding below Ae_3, volume change accompanying transformation was measured by dilatometer (Fuji Electronic Industrial Co., Ltd, Formastor-F). Cylindrical specimens 3 mm in diameter and 10 mm in height was installed, and was austenitized at 1200 ℃ for 180 s. The mean austenite grain size after austenitization was approximately 400 μm. After austenitization, the specimen was cooled using He gas at a rate of 30 ℃ s^{-1} to the intercritical temperature region ranging from 550 to 625 ℃, and isothermally held until volume change of

the specimen was observed.   To eliminate undercooling below desired temperatures, the flow of cooling gas was precisely controlled.

2.2.2.3 Thermomechanical process

To obtain stress-strain behaviors of both austenite and ferrite phases, two different cooling procedures were designed after the homogenization treatment.   In the first case, the austenitized plate was quenched into water to obtain martensite.   In the other case, the austenitized plate was furnace-cooled to obtain ferrite.   The former was provided for deformation experiments of austenite, while the latter for deformation experiments of ferrite. Cylindrical specimens 12 mm in height and 8 mm in diameter were machined from the homogenized plate, and were hot-compressed at various temperatures and strain rates in a thermomechanical processing simulator (Fuji Electronic Industrial Co., Ltd, Thermecmastor-Z).   Mica with glass powder was used in the hot-compression test as insulator and lubricant, and temperature of the specimens was precisely controlled by the induction-heating system.

Figure 2.2.1a and **b** show the procedures for the hot-compression of austenite and ferrite, respectively.   In the case of the hot-compression of austenite (**Fig. 2.2.1a**), the specimens consisting of martensite were firstly austenitized at 1200 ℃ for 180 s to obtain coarse austenite.   The average grain size of austenite was approximately 400 μm.   The austenitized specimens were cooled by N_2 gas at a cooling rate of 30 ℃ s^{-1} to the deformation temperature ranging from 600 to 1000 ℃.   After holding for 60 s at the deformation temperature to homogenize the temperature distribution within the specimen, uniaxial compressive deformation of 60% reduction in height (equivalent strain ε ~ 0.96) was applied at various strain rates ranging from 10^{-3} s^{-1} to 10^{0} s^{-1}.   Immediately after completing the deformation,

the specimens were cooled with water injection precisely controlled to minimize the time interval till cooling initiation. The cooling rate measured at the surface of the specimen was about 800 °C s^{-1}. In the case of the hot-compression of ferrite (**Fig. 2.2.1b**), the specimens composed of ferrite was heated from room temperature to the deformation temperature ranging from 400 to 700 °C, followed by isothermal holding for 60 s. Uniaxial compression of 60% reduction in height was applied at a strain rate of 10^{-2} s^{-1}, and the specimen was cooled with water injection. True stress-true strain data were obtained from the load-displacement data taken during the hot deformation.
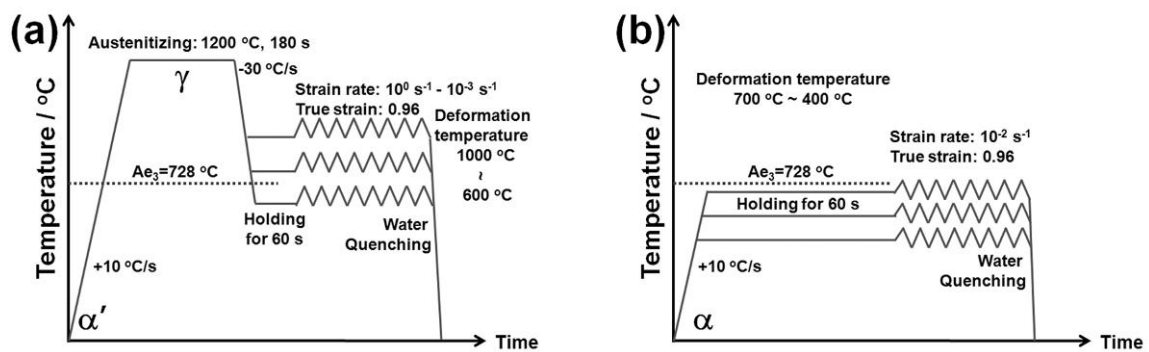
Fig. 2.2.1 Schematic illustrations of the thermomechanical processes in compression deformation of (a) austenite and (b) ferrite.

2.2.2.4 Microstructural observation

Microstructural observation was carried out by using optical microscopy (OM), electron back-scattering diffraction (EBSD) analyzer attached to a field-emission scanning electron microscope (FE-SEM, FEI XL30S FEG), and a transmission electron microscope (TEM, Philips CM200 FEG). For the OM and EBSD observation, the cross-section parallel to the compressive axis of the specimens was mechanically polished, and then electrically polished

in an aqueous solution of 10% of perchloric acid ($HClO_4$) and 90% of acetic acid (CH_3COOH) at 25 ℃. 3% nital solution was used to reveal microstructures. The EBSD measurement by OIM (Orientation Imaging Microscopy™) system was performed with a step size of 0.15 μm on a hexagonal grid. The inverse pole figure (IPF) map and the grain average misorientation (GAM) map were used to analyze the microstructures obtained by EBSD. IPF map shows the crystal orientations of each measured point parallel to a particular direction of the specimen [28]. GAM, which is the average misorientation angle among all pairs of adjacent points in a grain, is used to evaluate the degree of misorientation inside the grains [29]. For the TEM observation, thin-foil specimens were prepared by twin-jet electro-polishing using the same solution as that used for the EBSD observation. To measure misorientation between neighboring ferrite grains, Kikuchi diffraction patterns obtained in TEM were used.

2.2.3 Results

2.2.3.1 Kinetics of static transformation to ferrite

Figure 2.2.2 is the time-temperature-transformation (TTT) diagram of the Fe-6Ni-0.1C specimens with mean austenite grain size of approximately 400 μm, which shows the kinetics of static transformation in this alloy.   As designed, the incubation times before the onset of isothermal transformation in this alloy are fairly long, and no static ferrite transformation occurred within 60 s above 600 °C, which is the holding period before compression as shown in **Fig. 2.2.1a**.   This indicates that the microstructure is 100% austenite at the onset of hot-compression under the present conditions.
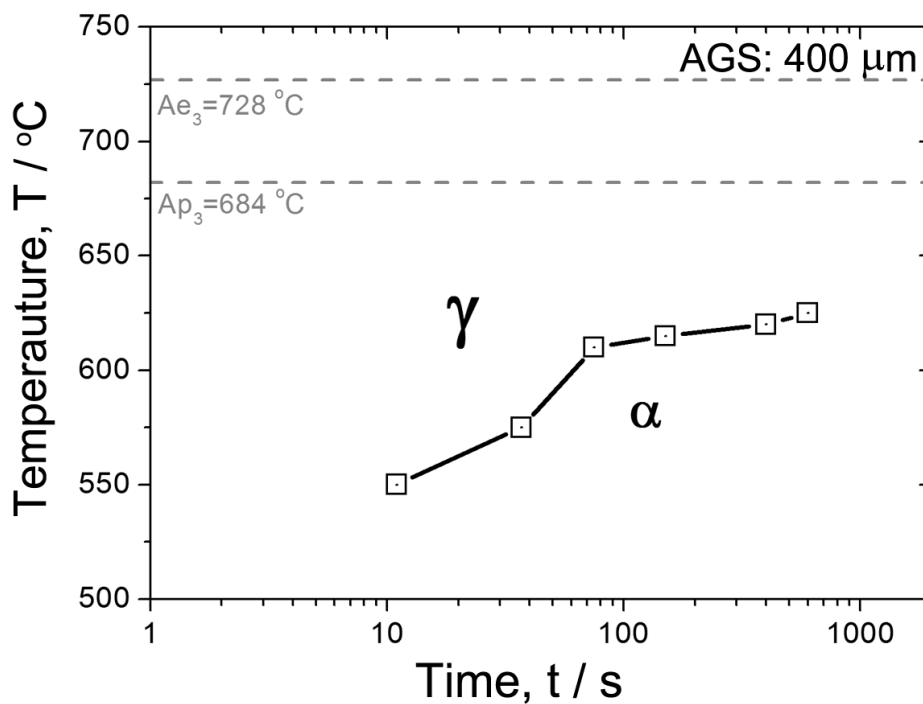

Fig. 2.2.2 Time-temperature-transformation (TTT) diagram of the 6Ni-0.1C steel obtained by dilatometry measurement.   Squares indicate the onset of isothermal transformation to ferrite at given temperatures.   The austenite grain size was around 400 μm.

2.2.3.2 Stress-strain behaviors

True stress-true strain curves of the specimens deformed to a true strain of 0.96 at different temperatures and strain rates in the way shown in **Fig. 2.2.1a** are shown in **Fig. 2.2.3**. As mentioned above, the specimens had microstructures of 100% austenite at the onset of hot-compression. The shape of the stress-strain curves can be classified into the following three types. Firstly, the curves deformed at high temperatures at all strain rates show typical shapes for the dynamic recrystallization (DRX) of austenite [24–26]. The flow stress increases with increasing strain until it reaches the maximum stress. After reaching the maximum stress, the flow stress decreases with increasing strain, and finally keeps a constant
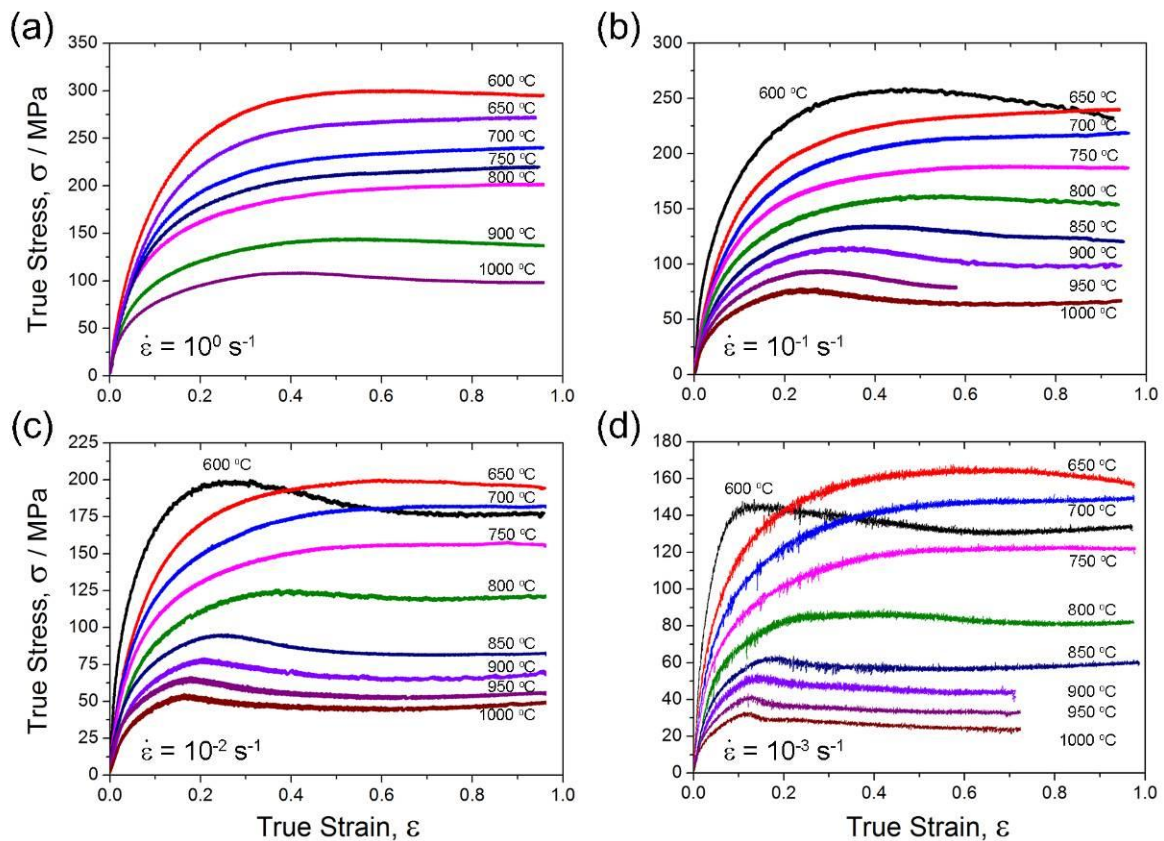

Fig. 2.2.3 True stress-true strain curves of the specimens deformed in the process shown in Fig. 2.1a at various deformation temperatures to a strain of 0.96 at strain rates of: (a) 10^0 s^{-1}, (b) 10^{-1} s^{-1}, (c) 10^{-2} s^{-1} and (d) 10^{-3} s^{-1}.

27

value. Secondly, the curves deformed at intermediate temperatures at all strain rates are similar to that of so-called dynamic recovery (DRV) type [30,31] exhibiting constant flow stress after initial strain-hardening. On the other hand, the stress-strain curves at low temperatures, especially at low strain rates, show significant softening after the maximum stress, and the shape is somehow similar to those of DRX of austenite at higher temperatures. Similar stress-strain curves have been reported in previous papers where the occurrence of dynamic transformation was claimed [6,32–34]. However, the occurrence of dynamic transformation cannot be confirmed only by the shape of the stress-strain curves now.

In order to determine the condition for the occurrence of dynamic transformation, the stress-strain behaviors at elevated temperature were systematically analyzed in detail. The
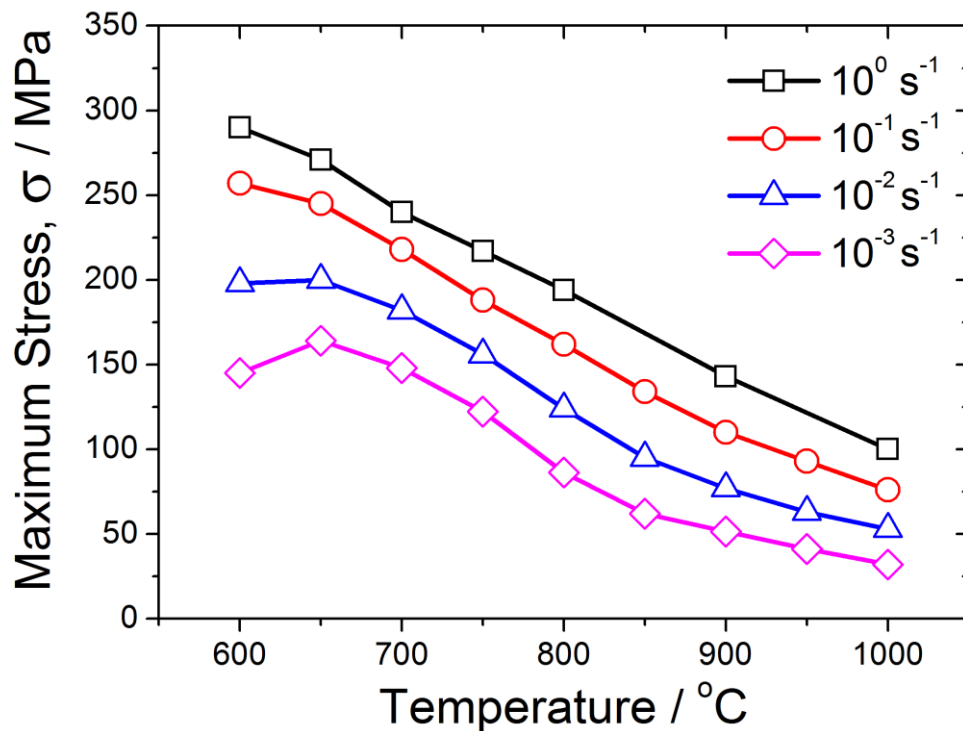

Fig. 2.2.4 The change in the maximum flow stress in the stress-strain curves at various strain rates as a function of deformation temperature; square: 10^0 s^{-1}, circle: 10^{-1} s^{-1}, triangle: 10^{-2} s^{-1} and diamond: 10^{-3} s^{-1}.

maximum stress values obtained from the stress-strain curves at different strain rates are summarized in **Fig. 2.2.4** as a function of the deformation temperature. In general, the maximum flow stress increases with decreasing deformation temperature and/or with increasing strain rate, which is a typical tendency during hot deformation of metals. However, at lower deformation temperatures at each strain rate, the maximum stress tends to decrease from extrapolation of the tendency. The softening (decrease in the maximum stress) at lower temperature is significant at strain rates of 10^{-2} s^{-1} and 10^{-3} s^{-1}, where longer time is taken in deformation.

The Zener-Hollomon parameter (Z), as expressed in **Eq. 2.2.1**, is known to unify the influence of deformation temperature and strain rate on high temperature deformation behaviors [6,24,30,35–38],

$$Z = \dot{\varepsilon} \cdot \exp(Q/RT) \qquad (2.2.1)$$

where $\dot{\varepsilon}$ is a strain rate, Q is a apparent activation energy for the high temperature deformation, R is the gas constant, and T is a absolute deformation temperature. It is also known that constitutive equations shown in **Eq. 2.2.2**, **Eq. 2.2.3** and **Eq. 2.2.4** are recognized between Z and flow stress (σ) in many cases of hot-deformation of metallic materials,

$$Z = A \cdot \sigma^n \qquad (2.2.2)$$

$$Z = A' \cdot \exp(\alpha \cdot \sigma) \qquad (2.2.3)$$

$$Z = A'' \cdot \sinh(\beta \cdot \sigma)^{n'} \qquad (2.2.4)$$

where *A, n, A', α, A'', β* and *n'* are material constants, and σ is a flow stress. Those equations were firstly introduced to describe creep phenomenon [39–43]. The power law (**Eq.2.2.2**) and the exponential law equations (**Eq.2.2.3**) are appropriate to interpret the deformation behaviors with low Z and high Z, respectively [39,42]. The hyperbolic-sine law (**Eq.2.2.4**),

meanwhile, can be applied for wide range of Z [39–43].

The maximum stresses at various deformation temperatures and strain rates shown in **Fig. 2.2.4** are plotted in **Fig. 2.2.5**, as a function of deformation temperature (**Figs. 2.2.5a** and **c**) and Z (**Figs. 2.2.5b** and **d**).   The apparent activation energies, Q, obtained from the slopes in **Figs. 2.2.5a** and **c** are *290 kJ mol^{-1}* for the power law (**Eq.2.2.2**) and *310 kJ mol^{-1}* for the
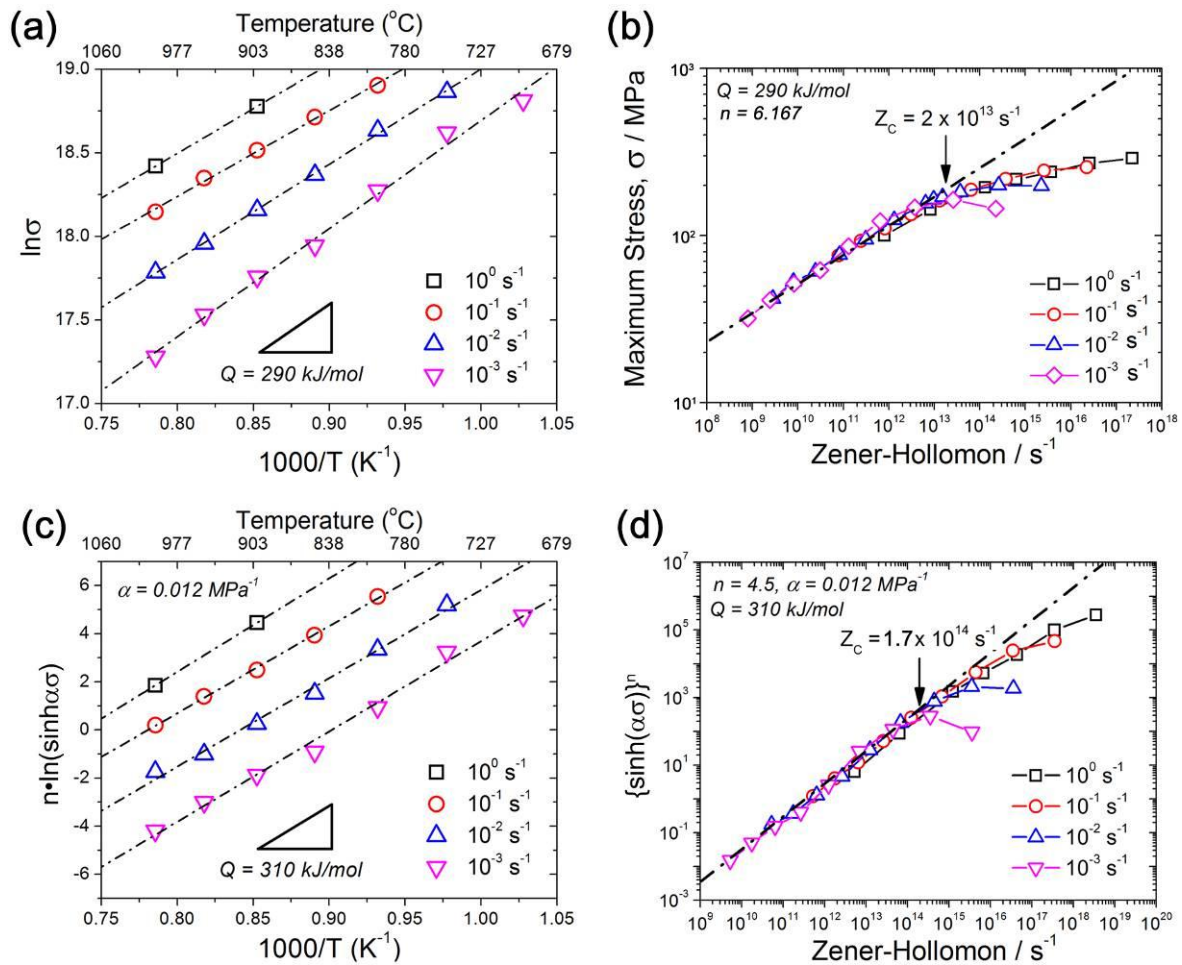
Fig. 2.2.5 Series of the maximum flow stress analyses using the power law (Eq. 2.2.2, (a), (b)) and the hyperbolic sine law (Eq. 2.2.4, (c), (d)).   (a) and (c) show the power-Arrhenius and the sinh-Arrhenius analyses, respectively, for different strain rates.   (b) and (d) display the maximum flow stress as a function of the Zener-Hollomon parameters obtained from Eq. 2.2.2 and Eq. 2.2.4 using different Q values.   The dash-dotted lines in (b) and (d) were fitted to the data at low Z, and extrapolated to the high Z region. Z_C (arrow) indicates the critical point at which the experimental data start to deviate from the dash-dotted line.

hyperbolic-sine law (**Eq.2.2.4**), respectively. The activation energy, *Q*, obtained from the power law is almost the same as the activation energy for self-diffusion of iron in austenite phase (*285 kJ mol^{-1}*) in pure iron [44]. Linear relationships between lnσ and ln$Z$ or $\{\sinh(\alpha\sigma)\}^n$ and ln$Z$, marked as dash-dotted lines in **Figs. 2.2.5b** and **d**, are recognized in the low Z region which indicates that the relationship shown in **Eq. 2.2.2** and **Eq. 2.2.4** stand well. Those lines for the low Z region in **Figs. 2.2.5b** and **d** are extrapolated to the region of high Z (dash-dotted lines). In the high Z region, however, experimentally determined values of σ in **Fig. 2.2.5b** and $\{\sinh(\alpha\sigma)\}^n$ in **Fig. 2.2.5d** are deviated from the dash-dotted line especially when strain rate is low. Depending on fitting equation, the deviation begins at a certain Z values (critical Z value, Z_C, hereafter) of approximately 2×10^{13} s^{-1} for the power law and 1.7×10^{14} s^{-1} for the hyperbolic-sine law, as indicated by the arrow in **Fig. 2.2.5b** and **d**. The deviation increases with increasing Z above Z_C. Deformation conditions above Z_C for the **Eq. 2.2.2** and **Eq. 2.2.4**, are listed in **Table 2.2.2**. It should be mentioned here that depending on the strain rate, the deviation trends from the extrapolated line are different.

The flow stress of ferrite in the present material was also investigated through the

Table 2.2.2 Deformation conditions above Z_C.

Strain rate	Deformation temperature, *T*	
	$Z_C = 2 \times 10^{13}$ s^{-1} in Eq. 2.2.2	$Z_C = 1.7 \times 10^{14}$ s^{-1} in Eq. 2.2.4
10^0 s^{-1}	*T* < 866 ℃	*T* < 865 ℃
10^{-1} s^{-1}	*T* < 786 ℃	*T* < 790 ℃
10^{-2} s^{-1}	*T* < 717 ℃	*T* < 725 ℃
10^{-3} s^{-1}	*T* < 656 ℃	*T* < 667 ℃

deformation procedure shown in **Fig. 2.2.1b**. **Figure 2.2.6** shows the true stress-true strain curves of ferrite at a strain rate of 10^{-2} s^{-1} at various temperatures ranging from 400 to 700 °C. The stress-strain behaviors of ferrite in **Fig. 2.2.6** exhibit a typical DRV type, where flow stress keeps a constant value after strain-hardening. As well as the case of the austenite deformation in **Fig. 2.2.3**, the maximum stress values of the stress-strain curves of ferrite increase with decreasing deformation temperature.

Figure 2.2.7a shows the maximum flow stress of austenite (open squares) and ferrite (open circles) deformed at a strain rate of 10^{-2} s^{-1} at various temperatures. The Ae$_3$ (728 °C) and the Ap$_3$ (684 °C) of the present material are also indicated in **Fig. 2.2.7a**. **Figure 2.2.7b** is an enlarged portion of **Fig. 2.2.7a** around Ae$_3$. The maximum flow stress of austenite increases with decreasing the deformation temperature. The dash-dotted curve was fitted to the maximum stress of austenite phase at temperatures ranging from 850 to 1000°C, and was
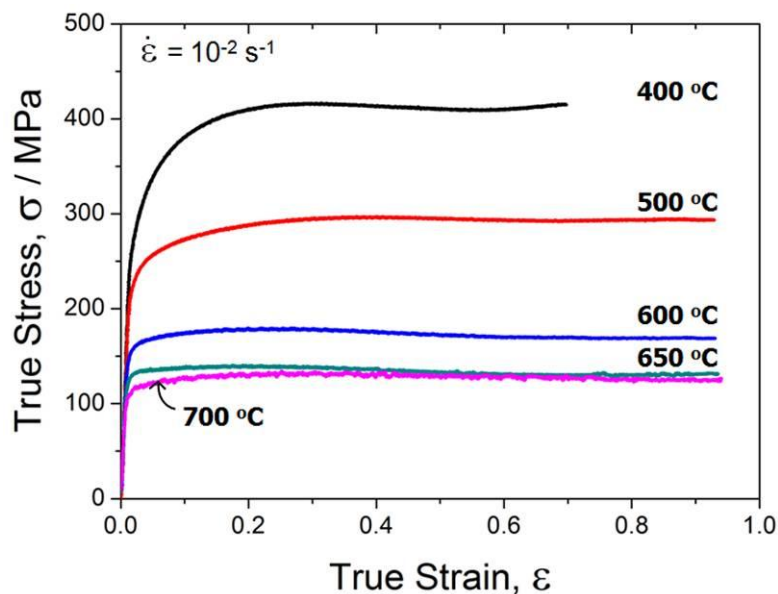
Fig. 2.2.6 True stress-true strain curves of ferrite in the 6Ni-0.1C steel deformed by the process shown in Fig. 2.2.1b to a strain of 0.96 at various deformation temperatures at a strain rate of 10^{-2} s^{-1}.
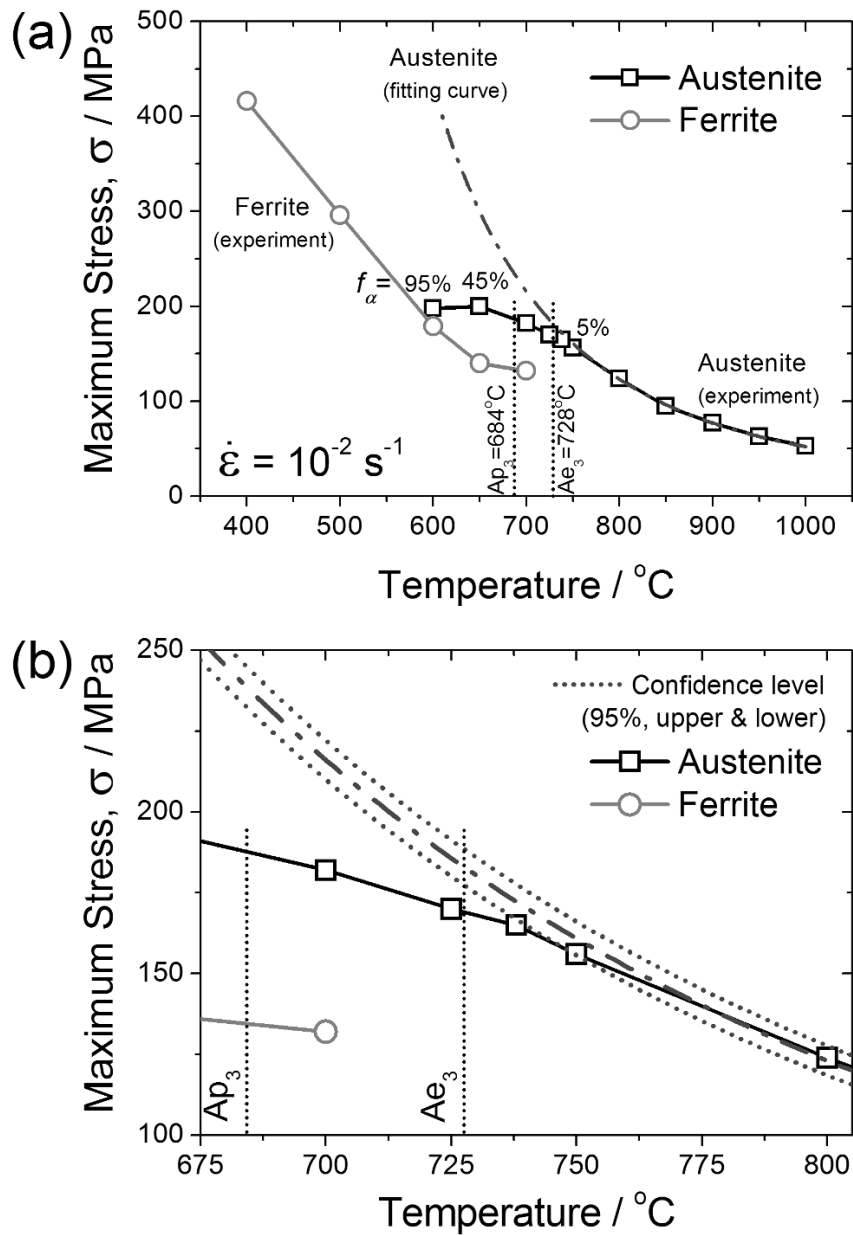
Fig. 2.2.7 (a) Maximum flow stress of austenite and ferrite in the 6Ni-0.1C steel as a function of deformation temperature at a strain rate of 10^{-2} s^{-1}, and (b) enlarged area of (a). Squares and circles indicate the maximum stress of austenite and ferrite, respectively. Dash-dotted curve is fitted to the data in the high temperature range from 850 to 1000 °C and extrapolated to the low temperature region. Dotted curves along the dash-dotted fitting curve in (b) indicate upper and lower 95% confidence intervals.

extrapolated to the lower temperature regime. The maximum flow stress of ferrite also increases with decreasing the deformation temperature, and it is much lower than that of austenite extrapolated from high temperature. The maximum stress of austenitized specimen experimentally obtained at temperatures below 750 ℃ tends to be lower than the expected stress of austenite indicated by the extrapolated dash-dotted line, and it approaches to the maximum stress of ferrite with decreasing deformation temperature. It should be noted that there is a trend of softening even above Ae$_3$, as indicated in **Fig 2.2.7b**. The fractions of ferrite (f_α,%) measured by microstructure observation are also shown in **Fig. 2.2.7a**. With decreasing the deformation temperature, the fraction of ferrite increases, and it comes close to 95% at 600 ℃.

2.2.3.3 Microstructural observation

Figure 2.2.8a and **b** show the IPF and GAM maps of the specimen statically transformed from austenite to ferrite (without deformation) which was firstly austenitized at 800 ℃ for 900 s (austenite grain size was approximately 15 μm), cooled down to 650 ℃ at a cooling rate of 30 ℃ s^{-1}, held at 650 ℃ for 60 s, and then subsequently water-quenched. The austenitization condition for the specimen in **Figure 2.2.8a** and **b** is different from **Fig. 2.2.1a**. This is because the kinetics of static ferrite transformation from the coarse grained (400 μm) austenite is too slow, and the fraction of ferrite is small even after holding for long
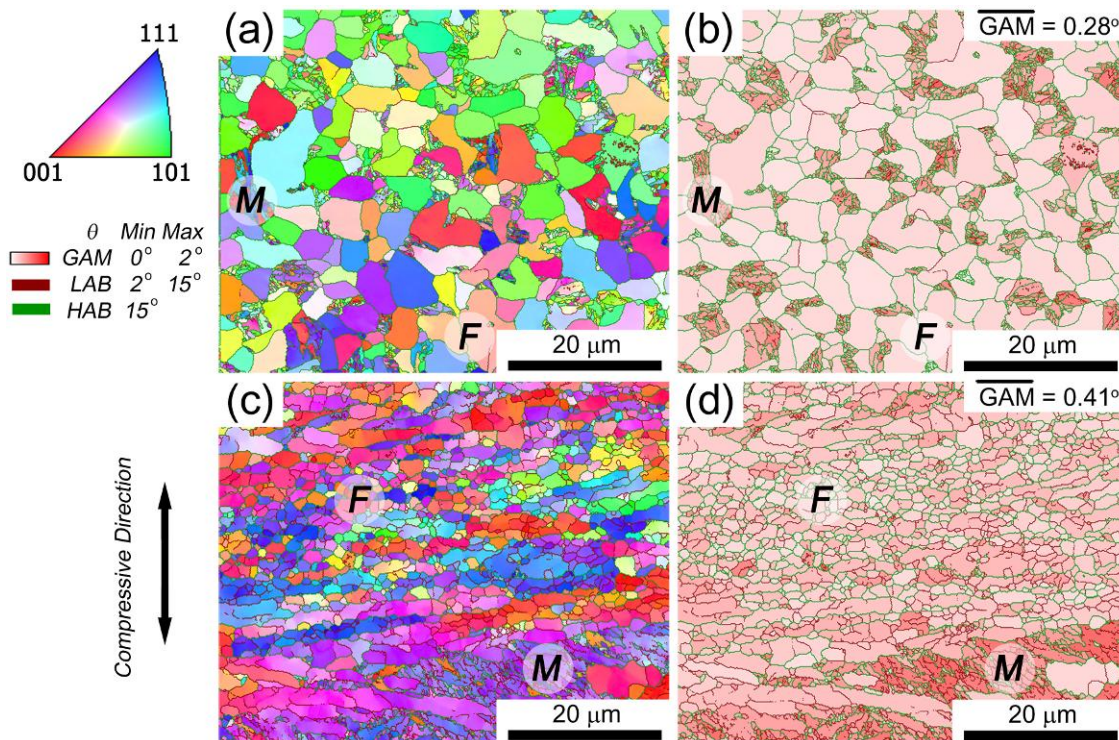
Fig. 2.2.8 Inverse pole figure (IPF) maps ((a), (c)) and corresponding grain average misorientation (GAM) maps ((b), (d)) obtained by EBSD measurements. (a), (b) the specimen isothermally held at 650 ℃ after austenitization at 800 ℃ for 900 s, and (c), (d) the specimen compressed to a strain of 0.96 at 650 ℃ at a strain rate of 10^{-1} s^{-1} after austenitization at 1200 ℃ for 180 s. F and M indicate the regions of ferrite and martensite, respectively. The low angle boundaries with misorientation of 2-15 ° and the high angle boundaries with misorientation above 15 ° are also drawn in red and green lines, respectively.

time at 650 ℃. Large fraction of retained austenite transforms to martensite during cooling, and it gives plastic deformation in adjacent ferrite grains to affect GAM data significantly. In order to avoid these, the specimen having fine prior austenite grain size was made through low-temperature austenitization only for **Fig. 2.2.8a** and **b**. It is naturally considered that the substructures within statically transformed ferrite obtained at an identical temperature are not affected by the prior austenite grain size. **Figure 2.2.8c** and **d** show the IPF and GAM maps of the specimen deformed to a strain of 0.96 at a strain rate of 10^{-1} s^{-1} at 650 ℃, and subsequently water cooled to room temperature. The colors in the IPF maps indicate the crystallographic orientation parallel to the compression direction at the measured point, according to the key stereographic triangle shown in the figure. Both ferrite and martensite phases (indicated by "F" and "M", respectively) are observed in **Figs. 2.2.8a** and **c**, and the coexistence of ferrite and martensite phases is also confirmed by OM and Vickers hardness test. The low angle boundaries with misorientation of 2-15 ° and the high angle boundaries with misorientation above 15 ° are also drawn in red and green lines, respectively. Most of the ferrite grains in **Fig. 2.2.8a** have no gradation of color within the grains, which means that there is little change in orientation. The degree of misorientation in each grain can be evaluated by GAM map, which is the average misorientation angle among all pairs of adjacent points in a given grain. The GAM map in **Fig. 2.2.8b** shows that most of ferrite grains have smaller GAM value. The average GAM of ferrite grains is approximately 0.28 °. These characteristics indicate that average misorientation within the ferrite grains statically formed is quite low. On the other hand, gradation of color in **Fig. 2.2.8c** is large compared with **Fig. 2.2.8a**. Average GAM of the ferrite grains in **Fig. 2.2.8d** is 0.41 °, which is obviously higher than that of the statically transformed ferrite (0.28 °). In addition, most of ferrite grains surrounded by high angle boundaries in **Fig. 2.2.8b** do not contain low angle

boundaries inside, with a probability of less than 10%. On the other hand, more than 50% of the ferrite grains surrounded by high angle boundaries in **Fig. 2.2.8d** contain low angle boundaries. It is noteworthy that the grain morphology in **Fig. 2.2.8c** is inhomogeneous, where fine equiaxed grains (~2 μm) and coarse grains elongated perpendicular to the compression direction exist together. The GAM map in **Fig. 2.2.8d** indicates that many of fine equiaxed ferrite grains have low GAM values less than 0.3 °, while most of coarse grains which are elongated perpendicular to the compression direction have high GAM values above 0.5 °.

Figure 2.2.9 is a TEM image of the specimen isothermally held at 650 ℃ without deformation after austenitization at 1200 ℃ for 180 s. The dislocation density within the ferrite grains is low, and dislocations are randomly distributed. **Figure 2.2.10a** and **b** are TEM image and corresponding boundary map of the specimen deformed to a strain of 0.96 at a strain rate of 10^{-1} s^{-1} at 650 ℃. The boundary map in **Fig. 2.2.10b** was obtained from Kikuchi-line diffraction pattern analysis in TEM. Coarse ferrite grains elongated perpendicular to the compression direction contain high density of dislocations. In addition, the ferrite grains surrounded by high angle boundaries contain some low angle boundaries.
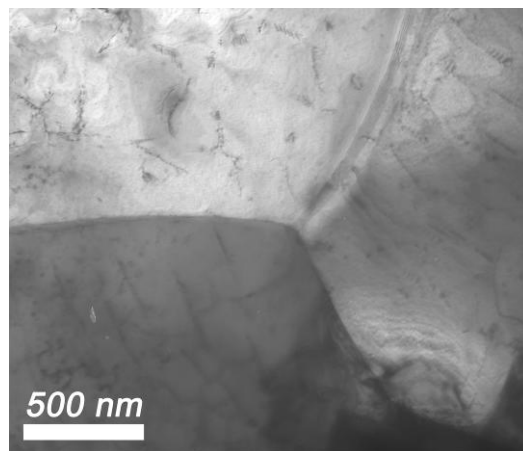
Fig. 2.2.9 TEM image of ferrite grains in the specimen isothermally held at 650 ℃ after austenitization.

Figure 2.2.10c is a high magnification TEM image around the area indicated by the arrow in **Fig. 2.2.10a**. A number of dislocations are accumulated at the corner of a coarse ferrite grain. Microstructural characteristics in **Fig. 2.2.8c, d** and **Fig. 2.2.10** represent typical microstructural features of deformed ferrite [45–47].
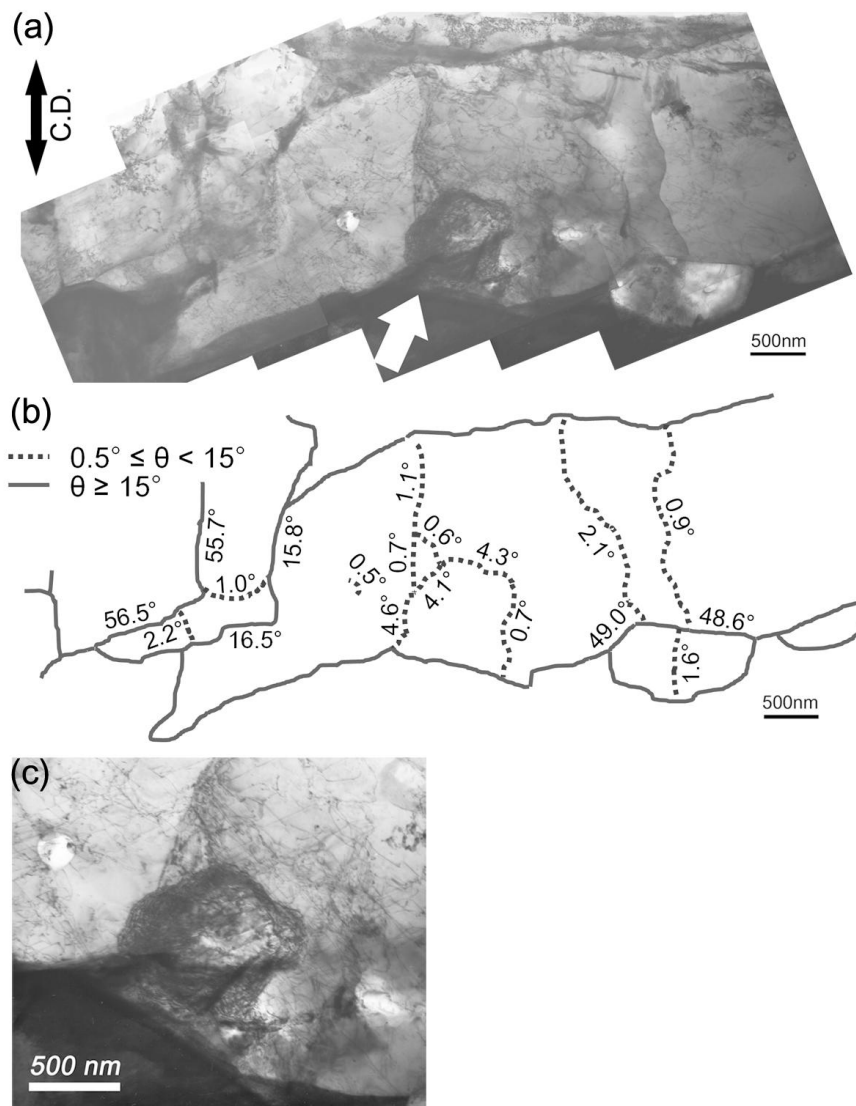
Fig. 2.2.10 TEM images of the specimen: (a) compressed to a strain of 0.96 at 650 ℃ at a strain rate of 10^{-1} s^{-1}, (b) misorientation map of (a) determined by Kikuchi pattern analysis in TEM (straight line and dotted one indicate high angle boundaries and low angle boundaries, respectively), and (c) enlarged image of the arrowed area in (a).

2.2.4 Discussions

In order to explore the origin of softening observed in the compression test, stress-strain behaviors were analyzed from various viewpoints. Here, the reasons why maximum stresses of each stress-strain curve for austenite shown in **Fig. 2.2.7** decreases above Z_C will be discussed.

One of the possible reasons for softening of austenite during deformation is adiabatic heating during compression. The maximum stress of the specimen (austenite) deformed at a strain rate of 10^{-2} s^{-1} at 650 °C is approximately 200 MPa in **Fig. 2.2.7a**. This maximum stress is significantly lower than the stress expected from the extrapolated curve (about 300 MPa). Supposing that there is no ferrite transformation during deformation, an adiabatic heating of about 60 °C would be necessary to decrease the flow stress of 100 MPa at this strain rate. Because the temperature fluctuation of the specimen recorded by the thermocouple welded to the specimen was less than 3 °C during deformation, the adiabatic heating during deformation could not be the reason for the softening during austenite deformation.

Wang *et al.* [31] revealed through uniaxial compression tests at intercritical temperature range that maximum stresses in the deformation of dual phase (austenite and ferrite) structures in plain carbon steels (Fe-0.5Mn-0.3Si-xC; $0.1 \leq x \leq 0.3$) decreased with increasing ferrite fraction. As shown in **Fig. 2.2.7a**, the fraction of ferrite in the deformed specimen is increased with decreasing deformation temperature, and the softening tendency observed through the stress-strain analyses corresponds with the increase in the fraction of ferrite. Consequently, it is concluded that the softening shown in **Fig. 2.2.4**, **Fig. 2.2.5** and **Fig. 2.2.7** is attributable to the ferrite transformation from austenite during deformation, i.e.

dynamic ferrite transformation.

The microstructures of the specimens which show softening in flow stress represent typical microstructural features of deformed ferrite [45–47] as shown in **Fig. 2.2.8c** and **d** and **Fig. 2.2.10**. The ferrite grains dynamically transformed at a certain stage of compression are deformed further in subsequent compression, resulting in the development of deformed ferrite microstructures. Accordingly, the microstructural observation also confirmed that the softening of flow stress corresponds with the occurrence of dynamic transformation.

As mentioned above, the softening in **Figs. 2.2.5b** and **d** shows different trends depending on strain rate, which affects the kinetics of dynamic transformation. When strain rate is slow, i.e. compression is applied for a long period, the material has much time to transform from austenite to ferrite, so that the softening becomes more significant. When strain rate is fast, time for transformation is limited, so that the softening becomes small and maximum stress is close to the fitted dash-dotted lines at the same Z value in **Fig. 2.2.5b** and **d**. At the same time, however, higher strain rate would increase the density of accumulated dislocations, leading to more acceleration of transformation kinetics, which suggests that the effect of strain rate on dynamic transformation is not so simple.

Plastic deformation on austenite generates numerous kinds of defects, which could act as nucleation site of ferrite, such as shear bands, deformation bands and dislocation substructures, etc. The increase in the driving force and the increase in the number of nucleation site by plastic deformation of austenite accelerate the kinetics of ferrite transformation. In **Fig. 2.2.7a**, the fraction of ferrite in the specimen deformed at a strain rate of 10^{-2} s^{-1} to a strain of 0.96 at 650 $^{\circ}$C is 45%. Total period for holding (60 s) and deformation (92 s) at 650 ℃ after austenitization is 152 s, while the isothermal ferrite transformation does not occur even after holding for 2000 s at 650 ℃ as displayed in **Fig.**

2.2.2. This clearly indicates that plastic deformation of austenite accelerates the ferrite transformation significantly.

It is noteworthy that the dynamic transformation seems to occur even above Ae_3 temperature, as was shown in **Fig.2.2.7b** and **Table 2.2.2**. Several research groups have suggested the possibility of the occurrence of dynamic transformation above Ae_3 [2,3,6,12,13,17,18,20,22], and it will be simulated and discussed in the next section (Chapter 2.3).

2.2.5 Summary

The occurrence of the dynamic transformation in a Fe-6Ni-0.1C alloy has been systematically investigated by analyzing the stress-strain curves and observing the microstructures. The major results are summarized as follows:

1. True stress-true strain curves of austenite were obtained during uniaxial compression at various strain rates ranging from 10^{-3} s^{-1} to 10^{0} s^{-1} to a strain of 0.96 at various temperatures ranging from 600 to 1000 ℃. The softening of the maximum flow stresses of austenite, which is different from that owing to dynamic recrystallization of austenite, was observed under certain deformation conditions.

2. With increasing Zener-Hollomon parameter of austenite (Z), the softening was greatly enhanced. The critical Z values (Z_C) for the onset of softening determined by the power law and the hyperbolic-sine law were $Z_C = 2 \times 10^{13}$ s^{-1} and 1.7×10^{14} s^{-1} using an apparent activation energy of $Q = 290$ kJ mol^{-1} and 310 kJ mol^{-1}, respectively.

3. The tendency of the softening of austenite corresponded with the fraction of ferrite observed in the microstructure. With decreasing deformation temperature, i.e., increasing Z value, the fraction of ferrite increased and the degree of softening increased.

4. Microstructure observations revealed that dynamically transformed ferrite exhibited characteristics of deformation microstructure, such as larger misorientation, existence of sub-boundaries, and a number of dislocations within the grains.

5. It can be concluded from the present experiments that dynamic transformation from austenite to ferrite during hot-deformation certainly occurs under high Z deformation conditions above the Z_C. The present study clearly shows that the occurrence of the dynamic transformation can be confirmed from stress-strain analysis of the material.

2.3 Occurrence of dynamic transformation above Ae_3

2.3.1 Introduction

In the former section, it was shown that dynamic transformation occurred under the certain deformation conditions where Zener-Hollomon parameter was higher than the critical value, $Z_C = 1.7 \times 10^{14}$ s^{-1}, $Q = 310$ kJ mol^{-1}.   The maximum temperature under this condition is dependent on a given strain rate as shown in **Table 2.2.2**.   For example, at a strain rate of 10^{-1} s^{-1}, it is predicted that dynamic transformation can occur at temperature up to 790 ℃ although the highest temperature is higher than Ae_3, 728 ℃, in the 6Ni-0.1C steel used in this study.   Therefore, it is necessary to confirm whether dynamic transformation surely occurs at temperatures above Ae_3 or not.

In this section, the author studies the occurrence of dynamic transformation at a wide temperature range including the temperatures above Ae_3 through stress-strain curve analysis, microstructure observation and Vickers hardness test.   The validity of Ae_3 temperature, 728 ℃, calculated by Thermo-Calc is also examined.   Finally, the author discusses the reason why dynamic transformation can occur even above Ae_3.

2.3.2 Experimental procedure

The material used in the present study is the same alloy used in the previous section as shown in **Table 2.2.1**. The Ae$_3$ and Ap$_3$ of the 6Ni-0.1C steel were calculated to be 728 ℃ and 684 ℃ by Thermo-Calc software, as mentioned in the previous section. In order to investigate stress-strain behaviors of both austenite and ferrite phases as described in Chapter 2.2.2.3, two series of specimens were prepared by different cooling procedures after the homogenization treatment, i.e. water-cooling and furnace-cooling: the former (water-cooled one) was provided for an austenite deformation, while the latter (furnace-cooled one) for a ferrite deformation. The detailed information about preparation of specimens is identical to the description written in Chapter 2.2.2.3. The details of the thermomechanical tests are described below. **Figures 2.3.1a** and **b** show the procedures for the hot-compression of austenite and ferrite, respectively. In the case of austenite deformation (**Fig. 2.3.1a**), the specimens having martensite starting microstructure were firstly austenitized at 800 ℃ for 180 s to obtain fine austenite with an average grain size of approximately 15 μm. The austenitized specimens were cooled by N$_2$ gas at a cooling rate of 30 ℃ s^{-1} to the deformation temperature ranging from 600 to 780 ℃, and held isothermally for 10 s (at temperature of
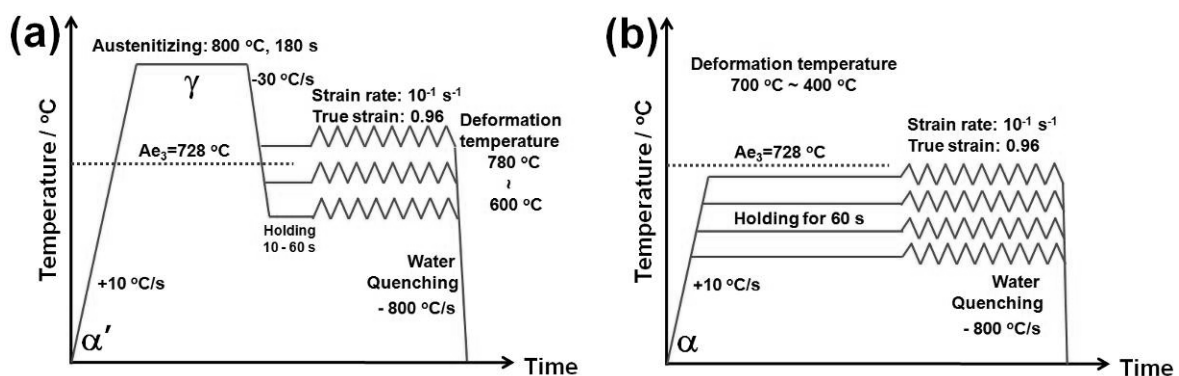

Fig. 2.3.1 Schematic illustrations of the thermomechanical processes in compression deformation of (a) austenitized specimens and (b) ferrite specimens.

44

600 ℃) or 60 s (at temperatures ranging from 650 to 780 ℃) before compression for making temperature distribution in the specimens homogenous. Hereafter, these specimens are referred to as 'austenitized specimens.' The holding time for 60 s at temperatures ranging from 650 to 780 ℃ is short enough to avoid isothermal (static) transformation to ferrite till applying deformation. In contrast, the holding time was 10 s in the case of 600 ℃ deformation because isothermal transformation is initiated around 10 s at this temperature. The fraction of isothermally transformed ferrite during 10 s holding at 600 ℃ was 5% in metallographic observation, and it was considered that such a small fraction of ferrite did not affect stress-strain curves so much. On the other hand, in order to obtain stress-strain curves of ferrite (**Fig. 2.3.1b**), the specimens with ferrite and small portion of pearlite were heated directly to the deformation temperatures ranging from 400 to 700 ℃, and kept for 60 s. Hereafter, these specimens are referred to as 'ferrite specimens.' After two series of specimens ('austenitized specimens' and 'ferrite specimens') were kept at deformation temperature, uniaxial compression was applied at a strain rate of 10^{-1} s^{-1} to a strain of 0.96 (60% reduction in height). Deformed specimens were immediately cooled by water-injection, at a cooling rate of approximately 800 ℃ s^{-1}.

Microstructural observation was carried out by OM, and EBSD in SEM. The detailed description for microstructural observation is identical with that written in the previous section. Vickers hardness test was also carried out. The test load was 980 mN, and the duration time was 10 s.

2.3.3 Results

2.3.3.1 Stress-strain behaviors

True stress-true strain curves of two series of specimens deformed to a strain of 0.96 at a strain rate of 10^{-1} s^{-1} at different temperatures are shown in **Fig. 2.3.2**.   In **Fig. 2.3.2a**, the shape of the stress-strain curves of the austenitized specimens can be classified into the following three kinds, as was shown in the previous section; the type of DRX of austenite at higher temperature [24,30,31], the shape of DRV of austenite at intermediate temperatures [24,31] and the form of dynamic transformation showing dynamic softening [6,32–34].   As pointed in the previous section, however, it cannot be confirmed the occurrence of dynamic transformation only by the shape of the stress-strain curves.   The maximum stress value of the stress-strain curves of the austenitized specimens increases with decreasing the deformation temperature, but it is lower at temperature of 600 ℃ than that at 650 ℃. **Figure 2.3.2b,** on the other hand, shows that the stress- strain curves of the ferrite specimens exhibit typical DRV types, where a flow stress keeps a constant value after initial strain-
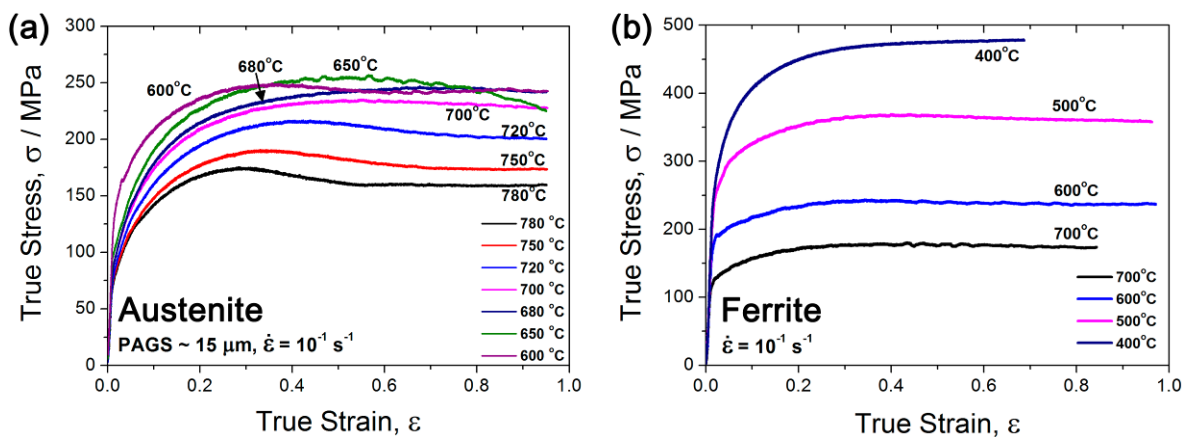

Fig. 2.3.2 True stress-true strain curves of two series of specimens deformed in the processes shown in Fig. 2.3.1 at various deformation temperatures at a strain rate of 10^{-1} s^{-1}.   (a) Austenitized specimens.   (b) Ferrite specimens.

hardening [45,48]. As well as the case of the austenite deformation in **Fig. 2.3.2a**, the maximum stress value of the stress-strain curves of the ferrite specimens increases with decreasing deformation temperature.

In order to determine the occurrence of dynamic transformation, as was done in the previous section, the maximum stress values obtained from the stress-strain curves of the specimens are summarized as a function of deformation temperature in **Fig. 2.3.3a**. **Figure 2.3.3b** is an enlarged portion of **Fig. 2.3.3a** around Ae$_3$. The Ae$_3$ (728 ℃) and the Ap$_3$ (684 ℃) of the present material are also indicated. The maximum stresses of the austenitized specimens deformed at high temperatures ranging from 800 to 1000℃ are taken from the data in the previous section with a different austenite grain size because the maximum stress is not affected by the prior austenite grain size. With decreasing the deformation temperature, the maximum flow stresses of the austenitized specimens and those of the ferrite specimens increase, but the flow stress of the austenitized specimen deformed at
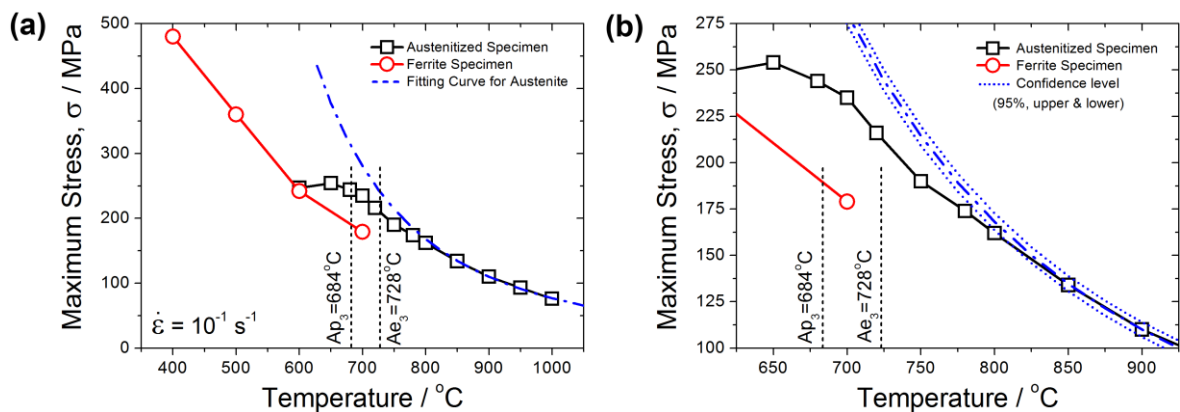
Fig. 2.3.3 (a) The maximum flow stresses of the austenitized specimens (squares) and those of the ferrite specimens (circles) as a function of deformation temperature, deformed at a strain rate of 10^{-1} s^{-1}. (b) Enlarged area around Ae$_3$ of (a). Dash-dotted curve is obtained through fitting using Eq. 2.3.1 for the maximum stress values of the austenitized specimens at temperatures ranging from 900 to 1000 ℃, and it is extrapolated to the low temperature region. The 95% confidence levels (upper and lower) for the fitted curve of the fitted curve are marked as dotted curves along the dash-dotted fitting curve in (b).

600 °C is lower than that at 650 °C, and it is close to the flow stress of the ferrite specimen.

It is well known that the flow stress of materials at elevated temperatures and Zener-Hollomon parameter (Z) have a following relationship [40,49,50]:

$$Z = \dot{\varepsilon} \cdot \exp(Q/RT) = A \cdot \sinh(\alpha \cdot \sigma)^n \qquad (2.3.1)$$

where $\dot{\varepsilon}$ is strain rate, Q is apparent activation energy for high temperature deformation, R is gas constant, A, α and n are material constants. The dash-dotted curve in **Fig. 2.3.3** was fitted by using **Eq. 2.3.1** for the maximum stresses of the specimens austenitized at high temperatures ranging from 900 to 1000 °C where dynamic recrystallization of austenite took place. This fitted curve is extrapolated to the lower temperature region. The 95% confidence levels (upper and lower) are marked as dotted curves along the dash-dotted fitting curve in **Fig. 2.3.3b**. The maximum flow stress of the austenitized specimens at low temperatures tends to be lower than the extrapolated stress of austenite, and it approaches to the maximum stress of ferrite with decreasing the deformation temperature. Here, it should be noted that the deviation of the experimentally obtained flow stress from the fitted curve is clearly observed at temperatures above Ae$_3$ in **Fig 2.3.3b**. Since the stress values used for fitting are the peak stresses in the DRX-type curves of austenite at higher temperatures, the stress deviation above Ae$_3$ in **Fig. 2.3.3b** is attributed to another softening mechanism. As shown in the previous section, this softening is thought to be originated from the occurrence of dynamic transformation even above Ae$_3$.

2.3.3.2 Microstructural observation and Vickers hardness test

The representative specimen was chosen to observe microstructural features using EBSD. **Figures 2.3.4a** and **b** show an image quality map and an inverse pole figure (IPF) map obtained from EBSD measurement for the austenitized specimen deformed to a strain of 0.96 at a strain rate of 10^{-1} s^{-1} at 750 °C, which is above Ae$_3$. The microstructure consists of ferrite and martensite, indicated by "F" and "M", respectively. The martensite was transformed from austenite retained at the completion of compression. The color in the IPF map represents the crystallographic orientation at the measured point, which is parallel to the compression direction, according to the key stereographic triangle shown in the upper corner in **Fig. 2.3.4**. The black and white lines represent high angle boundaries with misorientation (θ) larger than 15 °, and low angle boundaries with misorientation 2 ° $\leq \theta <$ 15 °, respectively. The mean grain average misorientation (GAM), which is the average
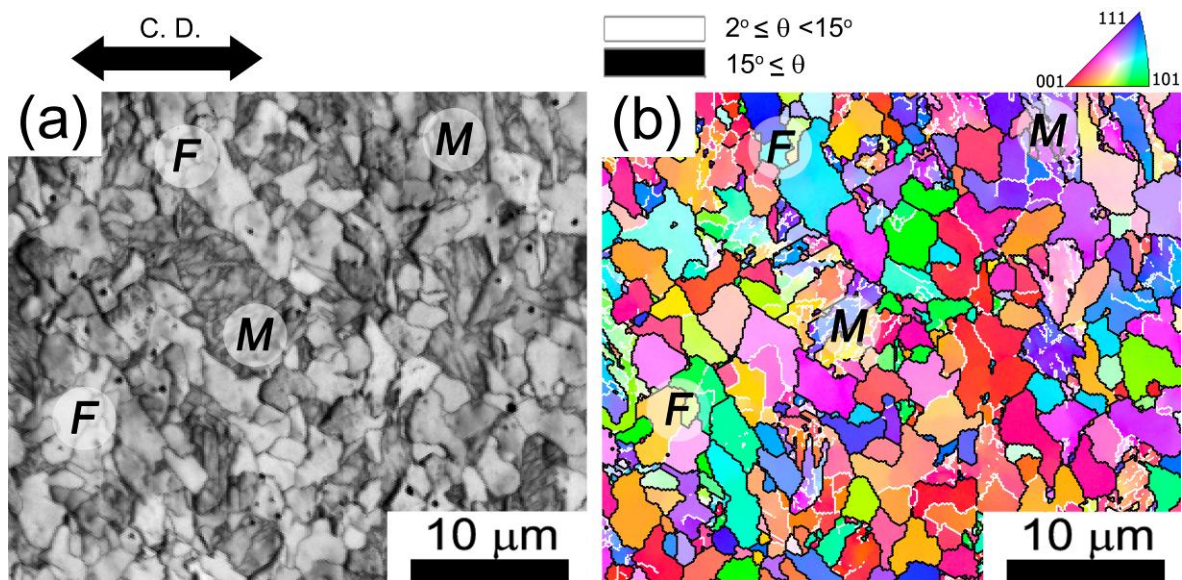

Fig. 2.3.4 Image quality map (a) and inverse pole figure map (b) obtained from EBSD measurement of the austenitized specimen deformed to a strain of 0.96 at a strain rate of 10^{-1} s^{-1} at 750 °C. **F** and **M** indicate ferrite and martensite, respectively. Compression direction is parallel to the horizontal axis in the images.

misorientation angle among all pairs of adjacent points of EBSD measurement in each grain [23,29], for the ferrite grains is 0.38 °. The GAM value for the ferrite grains in this specimen is much higher than that for isothermally transformed ferrite grains (0.28 ° in **Fig. 2.2.8b**).   This means that the ferrite grains in **Fig. 2.3.4** involve higher misorientation, which corresponds to higher density of dislocations, than the statically transformed ferrite.   In addition, a number of low angle grain boundaries (white boundaries) are observed within the ferrite grains in **Fig. 2.3.4b**. The high mean GAM value and large number of low angle boundaries in the ferrite grains are typical features of deformed microstructures of ferrite [45–47]. Those deformation features of the ferrite grains in the specimen deformed at temperature above Ae_3 is one of the representative evidences for the occurrence of dynamic transformation above Ae_3, because the dynamically transformed ferrite grains formed at a certain stage of compression are deformed in subsequent compression, resulting in the development of deformation microstructures in the ferrite grains.   The detailed information of microstructure of the austenitized specimens deformed at different temperatures will be analyzed in Chapter 4.3.

The changes in the fraction of ferrite and Vickers hardness in the specimens deformed at various temperatures are shown in **Fig. 2.3.5a**, and its correlation between the hardness values and the fraction of ferrite is shown in **Fig. 2.3.5b**.   Square and circle in **Fig. 2.3.5a** indicate the fraction of ferrite and the hardness value, respectively, as a function of deformation temperature. Ae_3 (728 ℃) and Ap_3 (684 ℃) of the present material are also indicated.   With the increase in deformation temperature, fraction of ferrite decreases, but hardness values of the specimens increase due to the increase in the fraction of martensite. The tendency of the increase in hardness values meets the hardness of 100% martensite (398 Hv) at temperature of 806 ℃.   It is noteworthy that this temperature (806 ℃) is close to the
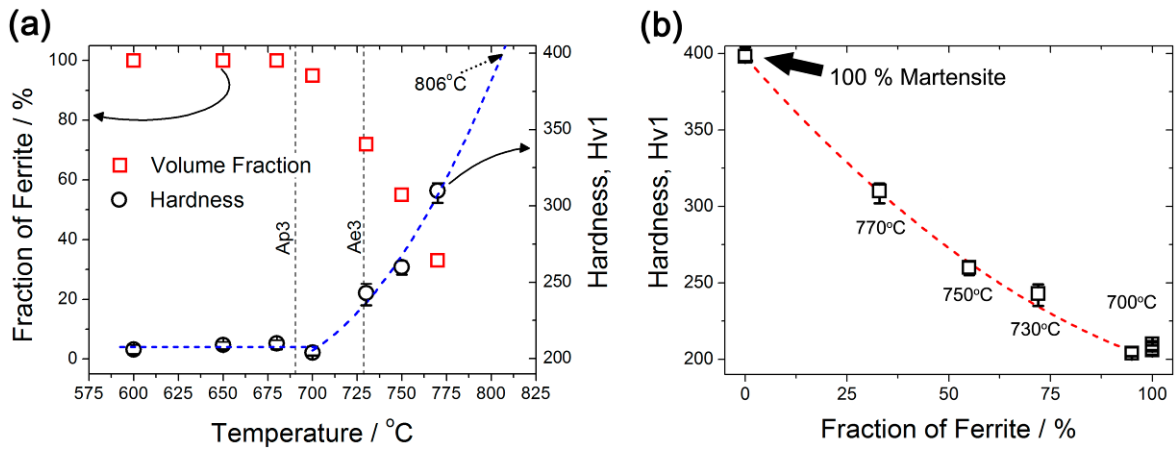
Fig. 2.3.5 (a) Changes in the fraction of ferrite and the Vickers hardness as a function of deformation temperature. Ae_3 (728 ℃) and Ap_3 (684 ℃) of the present material are indicated. The increase in hardness values meets the hardness of 100% martensite (398 Hv) at temperature of 806 ℃. (b) Comparison between the fraction of ferrite and the Vickers hardness.

upper limit temperature (790 ℃) predicted for the occurrence dynamic transformation by $Z = Z_C$ in the previous section.

51

2.3.4 Discussions

2.3.4.1 Validation of Ae$_3$

Even though the stress analysis in **Fig. 2.3.3**, the microstructural observation in **Fig. 2.3.4**, the changes in ferrite fraction and hardness in **Fig. 2.3.5** all suggest that dynamic transformation occurred at 750 ℃, i.e. above Ae$_3$, it is still possible that the ferrite transforms from deformed austenite during cooling procedure, or the Ae$_3$ calculated by Thermo-Calc software is lower than the actual Ae$_3$ of the present alloy. **Figures 2.3.6a** and **b** are optical microscope images of the austenitized specimens deformed at 750 ℃ to a strain of (a) $\varepsilon = 0.33$ and (b) $\varepsilon = 0.96$. The volume fraction of ferrite increases from 15% to 55% with the increase in strain from 0.33 to 0.96. Supposing that dynamic transformation did not occur during hot-compression, the observed ferrite in **Figs. 2.3.6a** and **b** formed statically after compression. The flow stress, which corresponds to the density of lattice defects (especially dislocations), at a strain of 0.96 is lower than that at a strain of 0.33 in **Fig. 2.3.2a**. Under this circumstance, the volume fraction of ferrite formed statically during cooling procedure in
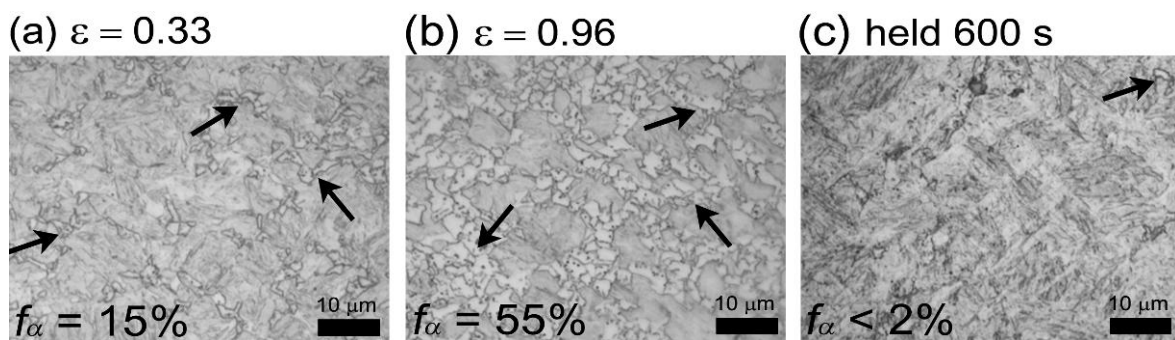
Fig. 2.3.6 Optical microscope images of the austenitized specimens deformed at 750 ℃ at a strain rate of 10^{-1} s^{-1} to different strains. (a) $\varepsilon = 0.33$ and (b) $\varepsilon = 0.96$. (c) The austenitized specimen deformed at 750 ℃ to a strain of 0.96, and subsequently held at the same temperature (750 ℃) for 600 s after the deformation. Arrows indicate ferrite grains. Compression direction is parallel to the vertical axis in the images.

the specimen deformed to a strain of 0.96 should be smaller than that in the specimen deformed to 0.33, because the density of lattice defects in austenite that can accelerate ferrite transformation is considered to be rather lower at a strain of 0.96 than at a strain of 0.33. As a result, it is likely that the observed ferrite grains formed, not during cooling (i.e., by static transformation), but during deformation (i.e., by dynamic transformation), and the mechanism of softening of the flow stress observed in the austenitized specimens above Ae_3 in **Fig. 2.3.2a** and **Fig. 2.3.3** is attributed to dynamic transformation.

Figure 2.3.6c is an optical microscope image of the specimen deformed at 750 ℃ to a strain of 0.96, and subsequently held at the same temperature (750 ℃) for 600 s without loading after deformation. Volume fraction of ferrite in **Fig. 2.3.6c** is less than 2% and decreases significantly compared with **Fig. 2.3.6b**. This indicates that the dynamically transformed ferrite transformed reversely to austenite during static holding at 750 ℃ after deformation. As a result, it can be concluded that the deformation temperature, 750 ℃, is surely above Ae_3. These experimental results clearly confirm that dynamic transformation occurred even above Ae_3.

2.3.4.2 Change in free energy for dynamic transformation

It was demonstrated that ferrite can be formed dynamically even above Ae_3. The occurrence of dynamic transformation at temperatures above Ae_3 has been reported by other researchers [3,12,13,16–19,51], and it has been thought that the dynamic transformation above Ae_3 is owing to the stored energy in the plastically deformed austenite. The free energy change of system during ferrite transformation from austenite without deformation (J mol^{-1}) can be expressed as follows,

$$\Delta G = -V^{\gamma \to \alpha} \Delta G_{Chem} + A\lambda + V^{\gamma \to \alpha} \Delta G_{S} \qquad (2.3.2)$$

where $V^{\gamma \to \alpha}$ is mole fraction of austenite transformed ferrite, ΔG_{Chem} is a chemical driving force per mole (J mol^{-1}), A is an interface per mole (m^2 mol^{-1}), λ is an interface energy per area (J m^{-2}), ΔG_{S} is a misfit strain energy per mole (J mol^{-1}). When austenite is plastically deformed, a stored energy, $-V^{\gamma \to \alpha} \Delta G_{Def}$, is added into **Eq. 2.3.2** as the free energy change of dynamic transformation. The stored energy of austenite per mole, ΔG_{Def}, (J mol^{-1}) can be calculated by a following formula,

$$\Delta G_{Def} = \mu \rho b^2 V_m \qquad (2.3.3)$$

where μ is a shear modulus (Pa), ρ is a dislocation density (m^{-2}), b is the magnitude of Burgers vector (m), V_m is a molar volume of austenite (m^3 mol^{-1}). Ae$_3$ curves in a phase diagram of Fe-6Ni-xC system can be drawn using Thermo-Calc software with different extra
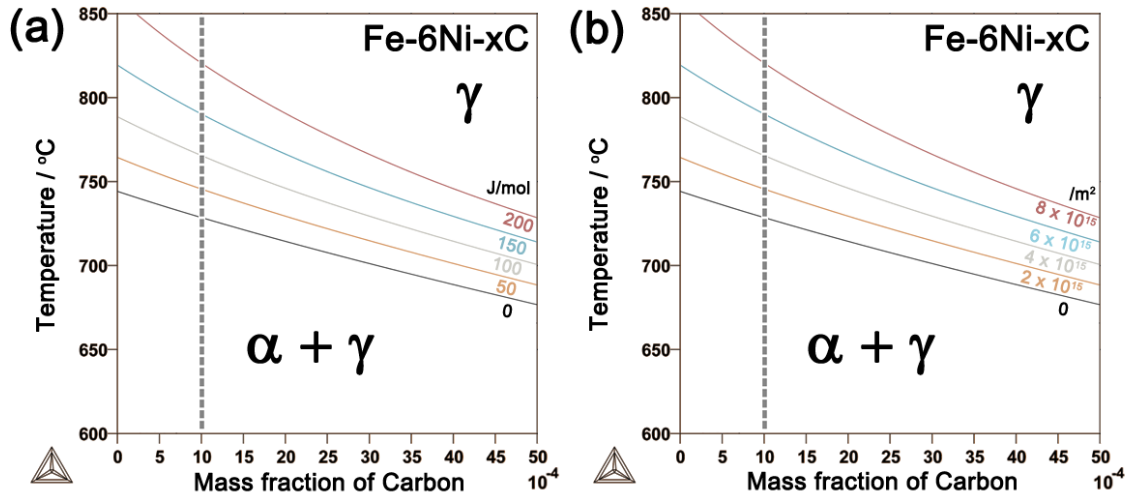

Fig. 2.3.7 Change in Ae$_3$ curves with different amount of (a) extra energy (J mol^{-1}) and (b) corresponding dislocation density (m^{-2}) of austenite in the phase diagram of Fe-6Ni-xC ($0 \le x < 0.5$ wt .(%). Dashed line marks the position of 0.1 wt.% C used in this study. (b) Dislocation density was calculated by Eq. 2.3.3.

energies as shown in **Fig. 2.3.7**. Ae_3 increases with the increase in an extra energy in austenite.

It is well known that flow stress of deformed austenite is proportional to the square root of average dislocation density as following equation [52,53],

$$\Delta\sigma = M\alpha\mu b\rho^{1/2} \qquad (2.3.4)$$

where M is the Taylor factor of polycrystalline austenite, and α is a numerical constant. Thus, the average dislocation density during deformation can be estimated from the flow stress by the use of **Fig. 2.3.2a**. For example, the flow stress of the austenitized specimen deformed at 750 °C at a strain of 0.33 is around 190 MPa. Since it was contributed from several parameters, such as friction stress including elastic term, strengthening owing to pre-existing dislocations, grain boundaries or solid solutions, etc., yield stress ($\sigma_{0.2\%}^{yield}$ = 77 MPa) is subtracted from 190 MPa to be 113 MPa. The increase in the flow stress of 113 MPa corresponds to the dislocation density to be 3.4×10^{14} m^{-2} by **Eq. 2.3.4** with constants of M = 3.11, α = 0.15, μ = 51 GPa, b = 0.258 nm, and it is equivalent to the stored energy of 8.5 J mol^{-1} by **Eq. 2.3.3**. However, the extra energy required to initiate ferrite transformation in the deformed austenite at 750 °C is around 50 J mol^{-1}, which is much larger than the calculated one (8.5 J mol^{-1}).

There are other candidates that raise energy state of austenite, such as an elastic energy under loaded state, grain boundary energy of austenite, and so on. Elastic energy under loaded state, U, can be expressed as a following equation [53],

$$U = \frac{\sigma^2}{2E} = \frac{\sigma^2}{2\{2\mu(1+\nu)\}} \quad \text{(J m}^{-3}\text{)} \qquad (2.3.5)$$

where E is an elastic modulus of austenite, ν is a poisson's ratio of austenite to be 0.31.

The elastic energy at a strain of 0.33 (190 MPa) is calculated to be 139 kJ m^{-3}, equal to be 0.985 J mol^{-1}. Additionally, grain boundary energy of austenite per square meter is known as 0.756 J m^{-2} [54], and it is converted to be 1.097 J mol^{-1} when mean grain size of austenite is 15 μm. When austenite grains are plastically deformed, grain boundary area of austenite is increased. It is reported that grain boundary area of austenite deformed to a strain of 0.96 is 1.57 times higher than that of undeformed austenite [55]. In this case, the austenite grain boundary energy is increased to be 1.722 J mol^{-1}, but it is still much smaller than 50 J mol^{-1}.

Some researchers proposed the heterogeneity of dislocation distribution in austenite, which increases a stored energy at local area, resulting in raising the local driving force for dynamic transformation much more than the situation assuming homogeneously distributed dislocations [12,13,16–19,53,56–58]. Hurley *et al.* [59] showed a deformation substructure of the Ni-30 wt.% Fe which performed a similar deformation behavior to the austenite in low carbon steels due to similar stacking fault energy. They proposed that the regions where the degree of inhomogeneous deformation was high, such as micro bands, grain boundaries, were the favorable nucleation site for dynamic recrystallization of austenite. It could be thought that such sites are also preferred nucleation sites for ferrite transformation. Therefore, the inhomogeneity of dislocation distribution should be taken into account for the occurrence of dynamic transformation above Ae$_3$.

Supposing dynamic transformation occurs due to an inhomogeneity of dislocation distribution, large numbers of dislocations are consumed by the formation of ferrite so that the free energy of austenite is significantly decreased. It should be explained how large fraction of ferrite (55% in **Fig. 2.3.6**) was kept even after mean value of stored energy of austenite was lowered. **Figure 2.3.8** exhibits schematic illustrations of dynamic transformation from austenite to ferrite under an assumption of heterogeneous distribution of

dislocations. The upper parts of each image show both austenite (hexagons) and ferrite (circles) grains. The background colors of grains represent average stored energies caused by deformation in each phase. The local energy distributions in both austenite (solid lines) and ferrite (dashed lines) grains along two cross lines (left and right hand sides) in the upper parts are displayed at the lower parts with two relative energy levels, marked as E_{Ini} and E_{Cri},

Fig. 2.3.8 Schematic illustrations showing dynamic transformation at temperature above Ae₃. The upper part of each image (a-c) shows both austenite (hexagons) and ferrite (circles), respectively. The colors of both austenite and ferrite grains indicate mean stored energies. The local energy distributions of both austenite (solid lines) and ferrite (dashed lines) grains in two cross sections (left and right hand sides) are displayed at the lower part. Two relative energy levels are marked as E_{Ini} and E_{Cri}. E_{Ini} indicate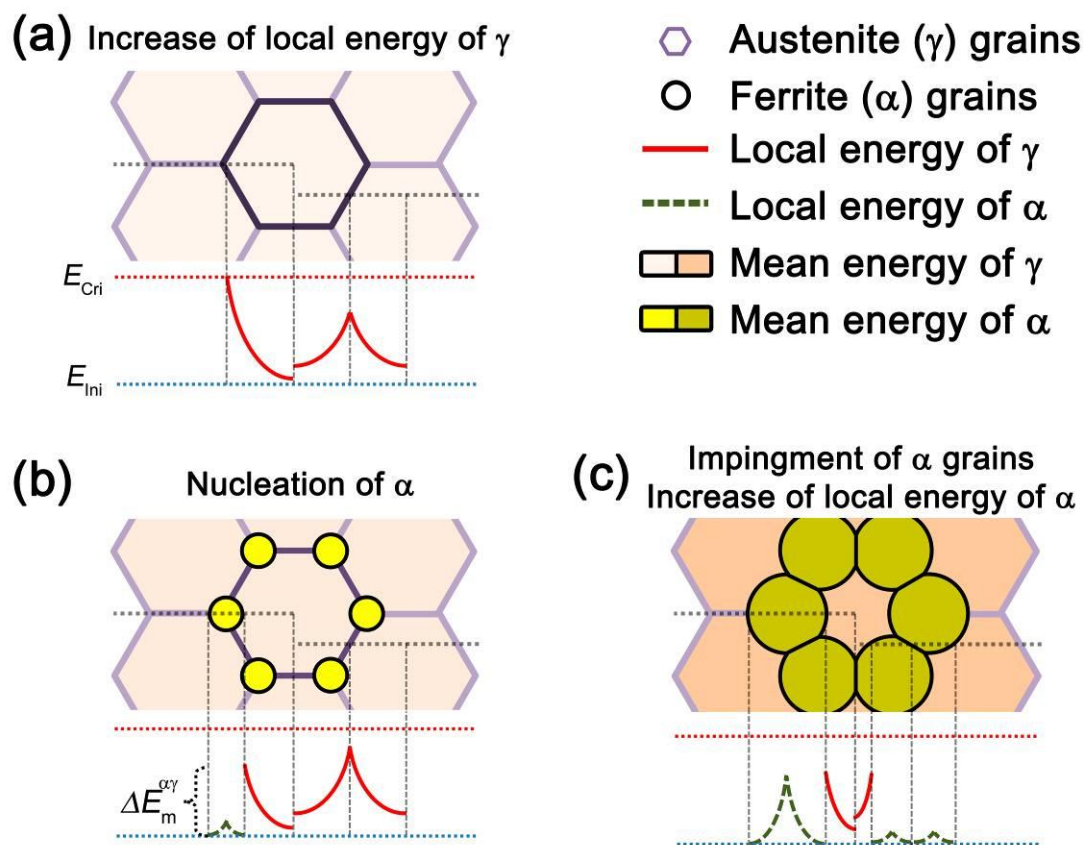s an initial energy level of newly-formed grains, and E_{Cri} represents a critical level for transformation. $\Delta E_m^{\alpha\gamma}$ is a driving force for interphase boundary migration between austenite and ferrite

57

where E_{Ini} indicates an initial energy level of undeformed grains, and E_{Cri} represents a critical level for transformation. Here, 'the local energy' is not limited only by *a stored energy of austenite*, but also includes *elastic energy originated by an external stress, grain boundary energy, etc*. (a) When deformation of austenite proceeds, the energy level of austenite rises and it reaches to a critical level for the formation of ferrite in the vicinity of austenite grain boundary edges or corners. (b) Ferrite grains are dynamically formed at which local energy of austenite reaches to the critical level. Those ferrite grains grow into austenite grains interior or along austenite grain boundaries at fast growth rate due to existing defects, such as dislocations, vacancies, and so on [55,60,61]. Driving force for interphase boundary migration between austenite and ferrite ($\Delta E_m^{\alpha\gamma}$) is originated from energy difference between newly formed ferrite and deformed austenite [60]. Those growing ferrite grains are simultaneously deformed so that the ferrite in the original nucleated location near prior austenite grain boundaries is deformed for relatively longer period compared to the ferrite in the vicinity of interphase growing boundary, resulting in the increase of mean energy of ferrite. (c) Growth of ferrite grains are maintained, and those impinge to each other. At the same time, average energy levels of ferrite and retained austenite grains rise. It could be thought that such an assistance of the ferrite growth owing to heterogeneous distribution of energy level in austenite makes it possible for large fraction of ferrite grains to be kept at temperature above Ae_3.

2.3.5 Summary

The author confirmed that dynamic transformation certainly occurred at temperature above Ae_3 in the 6Ni-0.1C steel.　The major results are summarized as follows:

1. Stress-strain analysis showed that softening of the maximum stress of the austenitized specimen occurred at temperature above Ae_3.　With increasing deformation temperature, the fraction of ferrite decreased and the degree of softening also decreased even above Ae_3.

2. Microstructural observation in the specimen deformed at 750 ℃ (Ae_3 = 728 ℃) showed deformation microstructures of ferrite.　Reverse transformation from ferrite to austenite took place at this temperature during subsequent holding after deformation.

3. The growth of ferrite grains under deformation condition was qualitatively explained with an assumption that energy level in grains was heterogeneously distributed with grains.　The driving force for interphase boundary migration between austenite and ferrite was originated from energy difference between newly formed ferrite and deformed austenite.

4. It can be concluded from the present experiments that dynamic transformation from austenite to ferrite during hot-deformation certainly occurs under high Z deformation conditions above the Z_C predicted in the previous section.

2.4 Conclusions

In the Chapter 2, the occurrence of dynamic transformation in the 6Ni-0.1C steel was systematically investigated at various strain rates and temperatures by analyzing the stress-strain curves and observing the microstructures. The softening of the maximum flow stresses resulting from the occurrence of dynamic transformation was observed under the certain deformation conditions which correspond to the critical Zener-Hollomon parameter (Z) of austenite. Microstructure observations revealed that dynamically transformed ferrite exhibited characteristics of deformation microstructure of ferrite, such as larger misorientation, existence of sub-boundaries, and a number of dislocations.

The softening of the maximum stress due to the occurrence of dynamic transformation happened even at temperatures above Ae_3. With increasing deformation temperature, the fraction of ferrite decreased and the degree of softening also decreased. The growth of ferrite grains during deformation was qualitatively explained under an assumption that energy distribution in austenite was heterogeneous within austenite grains.

Based on the study in Chapter 2, it can be concluded that dynamic transformation from austenite to ferrite during hot-deformation certainly occurs where the Z value of deformation condition is higher than the critical Z value, even if deformation temperature is higher than Ae_3.

2.5 References

[1] H. Yada, Y. Matsumura, and K. Nakajima, "Ferritic steel having ultra-fine grains and a method for producing the same," U.S. Patent US 446684221-Aug-1984.

[2] Y. Matsumura and H. Yada, "Evolution deformation of ultrafine-grained ferrite in hot successive deformation," *Transactions ISIJ*, vol. 27, pp. 492–498, 1987.

[3] S. W. Lee, D. H. Seo, and W. Y. Choo, "Study of ferrite refinement using heavy deformation in plain low carbon steels," *Korean Journal of Metals and Materials*, vol. 36, pp. 1966–1973, 1998.

[4] P. Hodgson, M. R. Hickson, and R. K. Gibbs, "Ultrafine ferrite in low carbon steel," *Scripta Materialia*, vol. 40, pp. 1179–1184, 1999.

[5] P. J. Hurley, P. D. Hodgson, and B. C. Muddle, "Analysis and characterisation of ultra-fine ferrite produced during a new steel strip rolling process," *Scripta Materialia*, vol. 40, pp. 433–438, 1999.

[6] H. Yada, C.-M. Li, and H. Yamagata, "Dynamic $\gamma \rightarrow \alpha$ transformation during hot deformation in iron-nickel-carbon alloys," *ISIJ international*, vol. 40, pp. 200–206, 2000.

[7] R. Priestner and A. K. Ibraheem, "Processing of steel for ultrafine ferrite grain structures," *Materials Science and Technology*, vol. 16, pp. 1267–1272, 2000.

[8] Y. Choi, W. Y. Choo, and D. Kwon, "Analysis of mechanical property distribution in multiphase ultra-fine-grained steels by nanoindentation," *Scripta Materialia*, vol. 45, pp. 1401–1406, 2001.

[9] J.-K. Choi, D.-H. Seo, J.-S. Lee, K.-K. Um, and W.-Y. Choo, "Formation of ultrafine ferrite by strain-induced dynamic transformation in plain low carbon steel," *ISIJ International*, vol. 43, pp. 746–754, 2003.

[10] S. C. Hong, S. H. Lim, H. S. Hong, K. J. Lee, D. H. Shin, and K. S. Lee, "Effects of Nb on strain induced ferrite transformation in C-Mn steel," *Materials Science and Engineering A*, vol. 355, pp. 241–248, 2003.

[11] S. C. Hong, S. H. Lim, K. J. Lee, D. H. Shin, and K. S. Lee, "Effect of undercooling of austenite on strain induced ferrite transformation behavior.," *ISIJ International*, vol. 43, pp. 394–399, 2003.

[12] M. Tong, J. Ni, Y. Zhang, D. Li, and Y. Li, "Temporal oscillatory behavior in deformation induced ferrite transformation in an Fe–C binary system," *Scripta Materialia*, vol. 50, pp. 909–913, 2004.

[13] M. Tong, D. Li, Y. Li, J. Ni, and Y. Zhang, "Monte carlo-method simulation of the deformation-induced ferrite transformation in the Fe-C system," *Metallurgical and Materials Transactions A*, vol. 35, pp. 1565–1577, 2004.

[14] H. Beladi, G. Kelly, A. Shokouhi, and P. Hodgson, "Effect of thermomechanical parameters on the critical strain for ultrafine ferrite formation through hot torsion testing," *Materials Science and Engineering A*, vol. 367, pp. 152–161, 2004.

[15] H. Beladi, G. L. Kelly, and P. D. Hodgson, "Ultrafine grained structure formation in steels using dynamic strain induced transformation processing," *International Materials Reviews*, vol. 52, pp. 14–28, 2007.

[16] X. Sun, H. Luo, H. Dong, Q. Liu, and Y. Weng, "Microstructural evolution and kinetics for post-dynamic transformation in a plain low carbon steel," *ISIJ International*, vol. 48, pp. 994–1000, 2008.

[17] C. Zheng, D. Li, S. Lu, and Y. Li, "On the ferrite refinement during the dynamic strain-induced transformation: A cellular automaton modeling," *Scripta Materialia*, vol. 58, pp. 838–841, 2008.

[18] C. Zheng, N. Xiao, L. Hao, D. Li, and Y. Li, "Numerical simulation of dynamic strain-induced austenite–ferrite transformation in a low carbon steel," *Acta Materialia*, vol. 57, pp. 2956–2968, 2009.

[19] V. V Basabe and J. J. Jonas, "The ferrite transformation in hot deformed 0.036 % Nb austenite at temperatures above the Ae 3," *ISIJ international*, vol. 50, pp. 1185–1192, 2010.

[20] V. V Basabe, J. J. Jonas, and H. Mahjoubi, "Dynamic transformation of a low carbon steel at temperatures above the Ae3," *ISIJ international*, vol. 51, pp. 612–618, 2011.

[21] J. J. Jonas and V. V. Basabe, "Ferrite formation above the Ae3 in a medium-carbon steel," *Solid State Phenomena*, vol. 172–174, pp. 372–377, 2011.

[22] J. J. Jonas and V. V Basabe, "The transformation of hot deformed austenite above the Ae3," in *THERMEC'2011*, 2011, p. 596.

[23] Y. M. Kim, T.-H. Ahn, K. K. Park, K. H. Oh, and H. N. Han, "Identification of dynamic ferrite formed during the deformation of super-cooled austenite by image-based analysis of an EBSD map," *Metals and Materials International*, vol. 17, pp. 181–186, 2011.

[24] T. Sakai and J. Jonas, "Overview no. 35 Dynamic recrystallization: Mechanical and microstructural considerations," *Acta Metallurgica*, vol. 32, pp. 189–209, 1984.

[25] E. Poliak and J. Jonas, "A one-parmenter approach to determining the critical conditions for the initiation of dynamic recrystallization," *Acta Materialia*, vol. 44, pp. 127–136, 1996.

[26] S. Kim and Y. Yoo, "Dynamic recrystallization behavior of AISI 304 stainless steel," *Materials Science and Engineering A*, vol. 311, pp. 108–113, 2001.

[27] H. Beladi, I. B. Timokhina, S. Mukherjee, and P. D. Hodgson, "Ultrafine ferrite formation through isothermal static phase transformation," *Acta Materialia*, vol. 59, pp. 4186–4196, 2011.

[28] J. Kang, B. Bacroix, H. Regle, K. Oh, and H. Lee, "Effect of deformation mode and grain orientation on misorientation development in a body-centered cubic steel," *Acta Materialia*, vol. 55, pp. 4935–4946, 2007.

[29] R. Yoda, T. Yokomaku, and N. Tsuji, "Plastic deformation and creep damage evaluations of type 316 austenitic stainless steels by EBSD," *Materials Characterization*, vol. 61, pp. 913–922, 2010.

[30] C. M. Sellars, "The kinetics of softening processes during hot working of austenite," *Czechoslovak Journal of Physics*, vol. 35, pp. 239–248, 1985.

[31] R. Wang and T. Lei, "Deformation and restoration behaviour of ferrite-austenite two-phase structures," *Materials Science and Engineering A*, vol. 165, pp. 19–27, 1993.

[32] Y. Weng, X. Sun, H. Dong, and others, "Overview on the theory of deformation induced ferrite transformation," in *Symp Ultrafine Grain Struct (ISUG2005), Beijing: Metallurgical Industry Press*, 2005, vol. 2, pp. 9–15.

[33] S. Y. Ok and J. K. Park, "Dynamic austenite-to-ferrite transformation behavior of plain low carbon steel within (α+γ) 2-phase field at low strain rate," *Scripta Materialia*, vol. 52, pp. 1111–1116, 2005.

[34] J.-Y. An, Y. Kwon, D.-L. Lee, I.-S. Kim, and Y.-C. Yoo, "Modeling of flow stress and microstructural variations in strain induced dynamic transformation of low carbon steel by hot torsion deformation," *Korean Journal of Metals and Materials*, vol. 43, pp. 740–743, 2005.

[35] C. Zener and J. H. Hollomon, "Effect of strain rate upon plastic flow of steel," *Journal of Applied Physics*, vol. 15, p. 22, 1944.

[36] C. Roucoules, M. Pietrzyk, and P. Hodgson, "Analysis of work hardening and recrystallization during the hot working of steel using a statistically based internal variable model," *Materials Science and Engineering A*, vol. 339, pp. 1–9, 2003.

[37] L. Longfei, Y. Wangyue, and S. Zuqing, "Dynamic recrystallization of ferrite in a low-carbon steel," *Metallurgical and Materials Transactions A*, vol. 37, pp. 609–619, 2006.

[38] T. Csanádi, N. Q. Chinh, J. Gubicza, and T. G. Langdon, "Plastic behavior of fcc metals over a wide range of strain: Macroscopic and microscopic descriptions and their relationship," *Acta Materialia*, vol. 59, pp. 2385–2391, 2011.

[39]   J. J. Jonas, C. M. Sellars, and W. J. M. Tegart, "Strength and structure under hot-working conditions," *Metallurgical Reviews*, vol. 14, pp. 1–24, 1969.

[40]   A. Cingara and H. J. McQueen, "New method for determining sinh constitutive constants for high temperature deformation of 300 austenitic steels," *Journal of Materials Processing Technology*, vol. 36, pp. 17–30, 1992.

[41]   H. J. McQueen and W. Blum, "Dynamic recovery: sufficient mechanism in the hot deformation of Al (<99.99)," *Materials Science and Engineering A*, vol. 290, pp. 95–107, 2000.

[42]   C. A. C. Imbert and H. J. McQueen, "Peak strength, strain hardening and dynamic restoration of A2 and M2 tool steels in hot deformation," *Materials Science and Engineering A*, vol. 313, pp. 88–103, 2001.

[43]   H. J. McQueen and N. D. Ryan, "Constitutive analysis in hot working," *Materials Science and Engineering A*, vol. 322, pp. 43–63, 2002.

[44]   T. Heumann and R. Imm, "Self-diffusion and isotope effect in γ-iron," *Journal of Physics and Chemistry of Solids*, vol. 29, pp. 1613–1621, 1968.

[45]   G. Glover and C. M. Sellars, "Recovery and recrystallization during high temperature deformation of α-iron," *Metallurgical Transactions*, vol. 4, pp. 765–775, 1973.

[46]   R. Wang and T. Lei, "Role of interface in nucleation of dynamic recrystallization of austenite," *Scripta Metallurgica et Materialia*, vol. 28, pp. 725–728, 1993.

[47]   N. Tsuji, Y. Matsubara, and Y. Saito, "Dynamic recrystallization of ferrite in interstitial free steel," *Scripta Materialia*, vol. 37, pp. 477–484, 1997.

[48]   N. Tsuji, Y. Matsubara, Y. Saito, and T. Maki, "Occurrence of dynamic recrystallization in ferritic iron," *Journal of Japan Institute of Metals*, vol. 62, pp. 967–976, 1998.

[49]   A. Z. Hanzaki, R. Pandi, P. D. Hodgson, and S. Yue, "Continuous cooling deformation testing of steels," *Metallurgical Transactions A*, vol. 24, pp. 2657–2665, 1993.

[50]   J. M. Cabrera, A. A. Omar, J. M. Prado, and J. J. Jonas, "Modeling the flow behavior of a medium carbon microalloyed steel under hot working conditions," *Metallurgical and Materials Transactions A*, vol. 28, pp. 2233–2244, 1997.

[51]   H. Dong and X. Sun, "Deformation induced ferrite transformation in low carbon steels," *Current Opinion in Solid State and Materials Science*, vol. 9, pp. 269–276, 2005.

[52]   J. E. Bailey and P. B. Hirsch, "The recrystallization process in some polycrystalline metals," *Proceedings of the Royal Society A: Mathematical, Physical and Engineering Sciences*, vol. 267, pp. 11–30, 1962.

[53] H. Mughrabi, "A two-parameter description of heterogeneous dislocation distributions in deformed metal crystals," *Materials Science and Engineering*, vol. 85, pp. 15–31, 1987.

[54] D. A. Porter and K. E. Easterling, *Phase Transformations in Metals and Alloys*, 2nd ed. London: Chapman & Hall, 1992.

[55] A. Hiramatsu and M. Umemoto, "Computer modelling of phase transformation from work-hardened austenite," *ISIJ International*, vol. 32, pp. 306–315, 1992.

[56] H. Mughrabi, "Dislocation wall and cell structures and long-range internal stresses in deformed metal crystals," *Acta Metallurgica*, vol. 31, pp. 1367–1379, 1983.

[57] T. Ungár, H. Biermann, and H. Mughrabi, "Dislocation distributions as seen by X-ray line profiles," *Materials Science and Engineering A*, vol. 164, pp. 175–179, 1993.

[58] T. Ohashi, R. I. Barabash, J. W. L. Pang, G. E. Ice, and O. M. Barabash, "X-ray microdiffraction and strain gradient crystal plasticity studies of geometrically necessary dislocations near a Ni bicrystal grain boundary," *International Journal of Plasticity*, vol. 25, pp. 920–941, 2009.

[59] P. Hurley, P. D. Hodgson, and B. C. Muddle, "A study of deformation substructures in austenite using a model Ni–30 wt.% Fe alloy," *Scripta Materialia*, vol. 45, pp. 25–32, 2001.

[60] D. G. Cram, H. S. Zurob, Y. J. M. Brechet, and C. R. Hutchinson, "Modelling discontinuous dynamic recrystallization using a physically based model for nucleation," *Acta Materialia*, vol. 57, pp. 5218–5228, 2009.

[61] R. Wei, K. Kanno, and M. Enomoto, "Alloying element partition and growth kinetics of proeutectoid ferrite in hot-deformed Fe-0.1C-3Mn-1.5Si austenite," *Metallurgical and Materials Transactions A*, vol. 42, pp. 2189–2198, 2011.

CHAPTER 3

KINETICS OF DYNAMIC TRANSFORMATION

3.1 Introduction

In the previous chapter, it was confirmed through stress-strain curve analysis that dynamic transformation in the 6Ni-0.1C steel certainly occurred. In general, the peak stress during deformation of austenite is regarded as the signal that the fraction of dynamically recrystallized austenite begins to increase significantly. The transformation from strain-hardened austenite to newly formed ferrite having low dislocation density results in the dynamic softening of flow stress [1–3]. It is well known that onset of dynamic recrystallization (DRX) of austenite is a function of prior austenite grain size, strain rate, temperature, precipitates, and so on [1,3]. Onset of ferrite transformation is also expected to be a function of prior austenite grain size since austenite grain boundaries act as the preferential nucleation sites for ferrite transformation [4–8]. Those two different phenomena have a common aspect that kinetics of each phenomenon is significantly influenced by austenite grain size. It was reported that the fraction of dynamically transformed ferrite at a given strain increased with decreasing austenite grain size [9–11]. In addition, with increasing strain, the fraction of ferrite increased but the flow stress decreased, similar to the dynamic softening due to DRX of austenite [10,12]. As ferrite is softer than austenite at elevated temperature, a change in the fraction of ferrite during deformation has an effect on a stress-strain curve as shown in previous Chapter 2 and following references. [10–16]. However, there is no quantitative study about the correlation between stress-strain curve and kinetics of dynamic transformation. The purpose of this chapter is to confirm

how flow stress is influenced by the kinetics of dynamic transformation.

Chapter 3 consists of two sections.   In the first section, the effect of austenite grain size on the onset of dynamic transformation is studied.   In addition, the correlation between the degree of dynamic softening of flow stress and the change in fraction in dynamically transformed ferrite is examined, too.   In the second section, the kinetics of dynamic transformation is discussed in detail.

3.2. Effect of austenite grain size on the onset of dynamic transformation

3.2.1 Experimental procedure

The material used in the present study is the Fe-6Ni-0.1C alloy (wt.%) having the same composition as that used in Chapter 2. **Figure 3.2.1** shows a schematic illustration of the thermomechanical process. In order to know the effect of austenite grain size (AGS) on the onset of dynamic transformation, different austenitization temperatures were chosen to change in the size of austenite grain. After austenitization for 180 s at different temperatures ranging from 800 to 1200 ℃, specimens were cooled by N_2 gas at a cooling rate of 30 ℃ s^{-1} to the deformation temperature, 750 ℃, and held isothermally for 60 s before compression for making temperature distribution in the specimens homogenous. Uniaxial
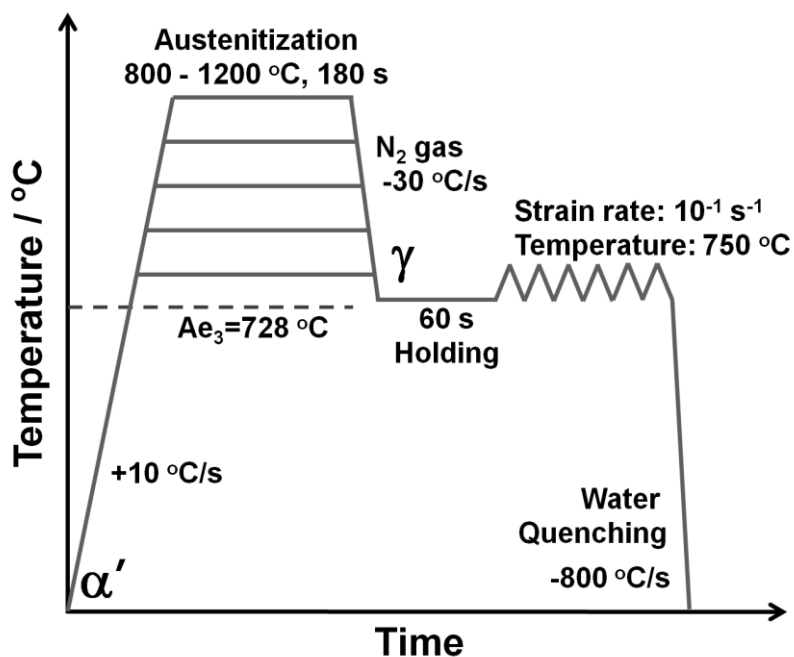

Fig. 3.2.1 Schematic illustration of the thermomechanical processes in compression deformation of austenite.

compression was applied to a strain of 0.96 (60% reduction in height) at a strain rate of 10^{-1} s^{-1}.   Deformed specimens were immediately cooled by water-injection, at a cooling rate of approximately 800 ℃ s^{-1}.   The cross-sections parallel to the compression axis of the water-quenched specimens were observed by optical microscopy (OM) after etching by 3% nital solution.   The fraction of ferrite was measured from OM image.

3.2.2 Results and discussions

Figure 3.2.2 shows the effect of austenitization temperature on the mean AGS.   As the austenitization temperature becomes high, the mean AGS rises.   As austenite grain boundaries are known as the preferred nucleation sites for ferrite transformation, higher density of nucleation sites is expected when the AGS is finer.
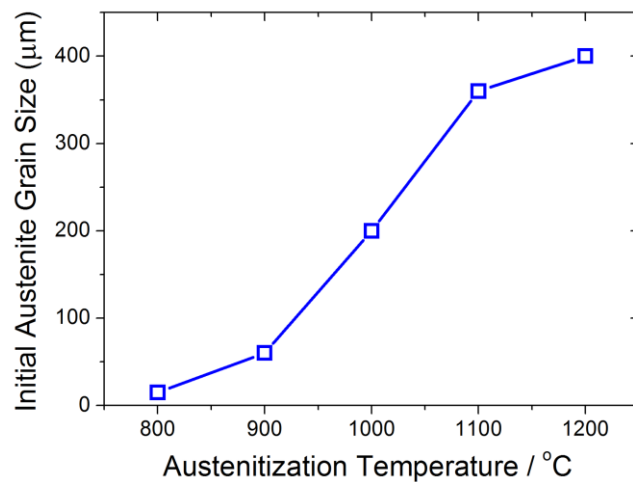

Fig. 3.2.2 The change in the austenite grain size as a function of austenitization temperature. Austenitization period at given temperatures was 180 s.

Figure 3.2.3 shows stress-strain curves of the specimens with various AGSs deformed at a strain rate of 10^{-1} s^{-1} to a strain of 0.96 at 750 ℃.   The various stress and strain values obtained from those curves are summarized in **Table 3.2.1**.   When the specimen has an AGS coarser than 360 μm, the stress-strain curve shows monotonous strain-hardening without any softening.   In contrast, the stress-strain curves of specimens with the AGS finer than 360 μm exhibit dynamic softening where the flow stress reaches to the maximum (peak stress) and then decreases with increasing strain, which is similar to typical stress-strain curves for dynamic recrystallization (DRX) of austenite or dynamic ferrite transformation [1,2,17].   It was confirmed that the softening at the given deformation condition is mainly attributed to
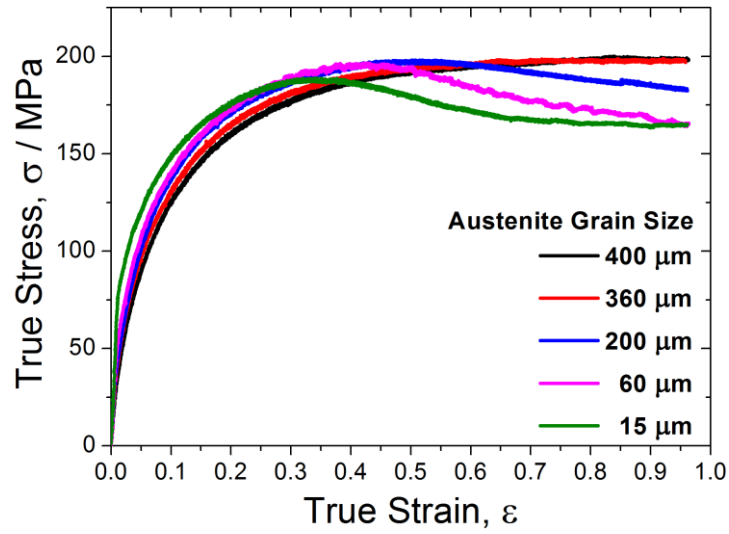
Fig. 3.2.3 True stress-true strain curves of the specimens with various austenite grain sizes (400, 360, 200, 60 and 15 μm) deformed at 750 °C at a strain rate of 10^{-1} s^{-1} to a strain of 0.96.

dynamic transformation rather than DRX of austenite, as shown in the previous Chapter 2. As the AGS decreases, the strain corresponding to the maximum stress (the maximum strain, ε_m) and the critical strain (ε_c), where dynamic transformation is initiated, decreases (**Table 3.2.1**). Here, the critical strain (ε_c) is determined by a second-order differential form of stress-strain curves when $\partial(\partial\theta/\partial\sigma)/\partial\sigma = 0$, as shown in **Fig. 3.2.4** [17,18]. Such an acceleration of the onset of dynamic softening by refinement of austenite grains has been observed in DRX of austenite [1,2,17] and dynamic transformation below Ae$_3$ [10,12]. The onset of DRX of austenite has been empirically described as a function of AGS, as follows [1,3]

$$\varepsilon_m = k \cdot D_\gamma^t \qquad (3.2.1)$$

where ε_m is a maximum strain, D_γ is a AGS, k and t are constants. The k is dependent on strain rate and deformation temperature. **Equation 3.2.1** was adopted for the
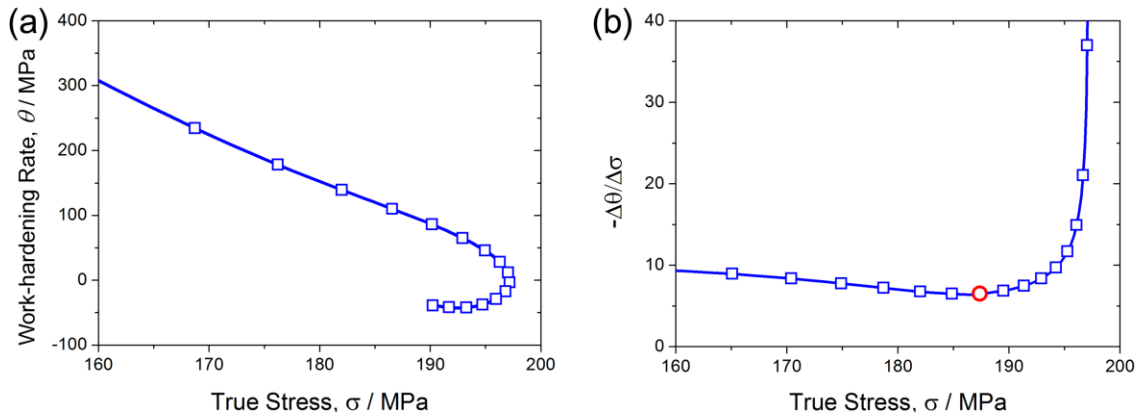
71

Fig. 3.2.4 An example of the determination procedure of the critical strain (ε_c) in a specimen having austenite grain size of 200 μm [17,18].   (a) Work-hardening rate defined as the first-order differential form ($\theta \equiv \partial\sigma/\partial\varepsilon$) of true stress-strain curve in Fig. 3.2.3 and (b) the second-order differential form as a function of true stress.   The open circle in (b) indicates the $\partial(\partial\theta/\partial\sigma)/\partial\sigma$ equals to zero.

Table 3.2.1 Austenite grain sizes of the specimens austenitized at various temperatures, and their data values obtained from Fig. 3.2.2 and Fig. 3.2.3. $\sigma_{0.96}$, σ_{sat} and $\Delta\sigma$ represent the flow stress at a strain of 0.96, the saturated stress fitted by Eq. 3.2.1 and the difference between σ_{sat} and $\sigma_{0.96}$, respectively. ε_m is the strain that corresponds to the maximum flow stress and ε_c is the critical strain which is determined through second-order differential form of stress-strain curves [17,18].

Austenitization temperature (°C)	Austenite grain size (μm)	True stress at $\varepsilon = 0.96$, σ (MPa)			True strain, ε		Ferrite fraction at $\varepsilon = 0.96$ (%)
		$\sigma_{0.96}$	σ_{sat}	$\Delta\sigma$	ε_m	ε_c	
1200	400	198	199	1	0.94	-	5
1100	360	193	204	11	0.64	0.52	15
1000	200	183	199	16	0.53	0.40	20
900	60	167	198	31	0.43	0.32	50
800	15	165	200	35	0.34	0.26	55

onset of dynamic transformation in the present study.   The values of k and t are determined to be 0.2 and 0.192, respectively.

Figures 3.2.5a and **b** show the flow stress at a strain of 0.96 ($\sigma_{0.96}$) obtained from **Fig. 3.2.3** and the ferrite fraction measured by optical microscopy in the specimens deformed to a strain of 0.96, respectively, as a function of AGS.   As the AGS decreases, the flow stress ($\sigma_{0.96}$) decreases monotonously, and the fraction of ferrite increases.   It is obvious from **Fig. 3.2.5** that the ferrite fraction has a certain correlation with the decrease in the flow stress. Quantification of the decrease in the flow stress in **Fig. 3.2.5** can be formulized using the saturated stress (σ_{sat}), where the work-hardening rate is balanced with the dynamic recovery rate [2,19–21], as follows,

$$\sigma = \sigma_0 + \sigma_{sat}\left[1 - \exp\left(-k \cdot \varepsilon\right)\right]^d$$

$$\sigma_{sat} = (\sigma - \sigma_0)\left[1 - \exp\left(-k \cdot \varepsilon\right)\right]^{-d}$$

(3.2.2)

where σ_0 is an yield stress of the material, σ_{sat} is a saturated stress at large strain, k is a constant depending on deformation conditions, ε is a true strain and d is a constant around 0.5.
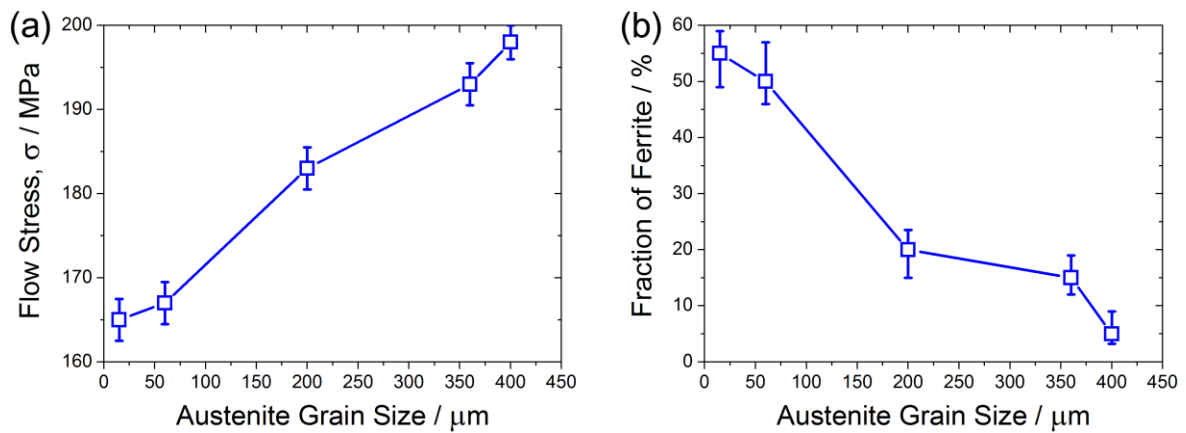

Fig. 3.2.5 Effect of the austenite grain size on (a) the flow stress and (b) the fraction of dynamically transformed ferrite at a strain of 0.96.

The difference between the fitted saturated stress (σ_{sat}) and the flow stress at a strain of 0.96 ($\sigma_{0.96}$) is represented as $\Delta\sigma$ in **Table 3.2.1** and **Fig. 3.2.6** for different AGSs. It is found from **Fig. 3.2.6** and **Table 3.2.1** that the fraction of ferrite monotonously increases with increasing $\Delta\sigma$. Therefore, it would be possible to predict the kinetics of dynamic transformation, which is shown in the following section by using the change in flow stress during deformation.
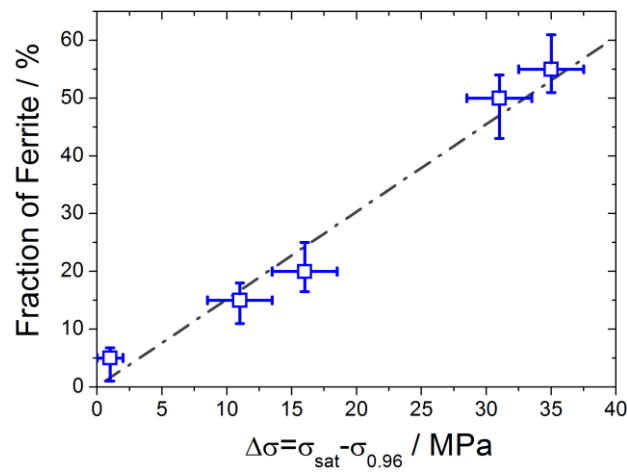

Fig. 3.2.6 Comparison between the fraction of ferrite and the difference of stresses, $\Delta\sigma = \sigma_{sat} - \sigma_{0.96}$, at a strain of 0.96.

3.2.3 Summary

The effect of austenite grain size on the kinetics of dynamic transformation was studied in this section and following conclusions are derived:

1. The onset of dynamic transformation was accelerated by refinement of austenite grain size, similar to static transformation, which might be due to high density of austenite grain boundary which is known as the preferred nucleation site for ferrite transformation.

2. The decrease in flow stress was correlated with the increase in the fraction of dynamically transformed ferrite. Fraction of ferrite increased proportionally with decreasing flow stress at a certain strain.

3.3. Kinetics of dynamic transformation determined by dynamic softening of flow stress during deformation

3.3.1 Introduction

It was confirmed in the previous section that the increase in the stress difference ($\Delta\sigma$) between the saturated stress (σ_{sat}) and the flow stress at a strain of 0.96 ($\sigma_{0.96}$) was proportional to the increase in the fraction of dynamically transformed ferrite. This indicates that stress-strain curve could be converted to the fraction of dynamically transformed ferrite during deformation. In order to reveal characteristics of kinetics in dynamic transformation, two different deformation conditions that show a saturation of flow stress at large strain are chosen.

3.3.2 Experimental procedure

The material used in the present study is the same as that used in Chapter 2. The details of the deformation conditions of two series of experiments are shown in **Table. 3.3.1.** **Figure 3.3.1** shows the thermomechanical processes of two series of experiments. In the case of series 1 shown in **Fig. 3.3.1a**, after austenitization treatment at 800 ℃ for 180 s, the specimens with fine AGS of 15 μm were cooled by N_2 gas at a cooling rate of 30 ℃ s^{-1} to the deformation temperature, 750 ℃, and held isothermally for 60 s. Uniaxial compression was then applied at a strain rate of 10^{-1} s^{-1} to different strains. In the case of series 2 shown in **Fig. 3.3.1b**, on the other hand, specimens were austenitized at 1200 ℃ for 180 s to make

Table 3.3.1 Deformation conditions for two series of experiments

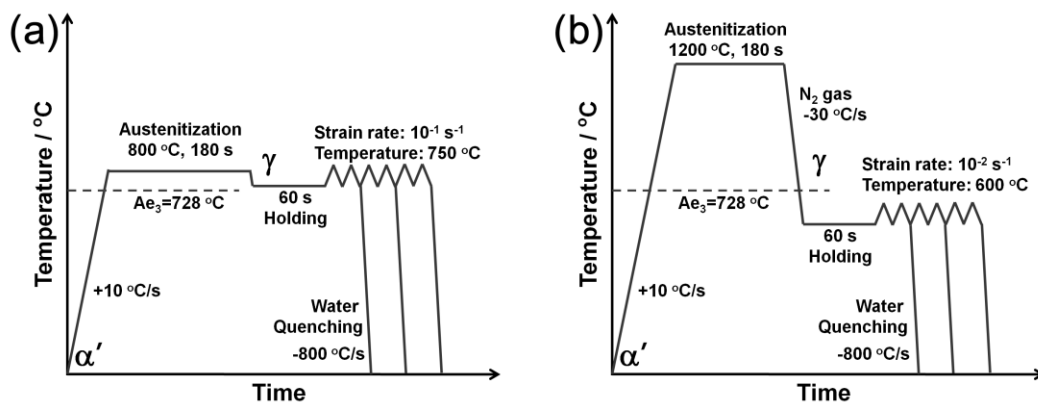| Conditions	Austenitization temperature	Austenite grain size	Deformation temperature	Strain rate
Series 1	800 ℃	15 μm	750 ℃	10^{-1} s^{-1}
Series 2	1200 ℃	400 μm	600 ℃	10^{-2} s^{-1}

Fig. 3.3.1 Schematic illustrations of the thermomechanical processes in compression deformation of austenite.

coarse AGS of 400 μm.　 The specimens were cooled to the deformation temperature, 600 ℃ by N_2 gas at a cooling rate of 30 ℃ s^{-1}, and isothermally held for 60 s before compression. Uniaxial compression was applied at a strain rate of 10^{-2} s^{-1} to different strains.　 Deformed specimens of two series of experiments were immediately cooled by water-injection, at a cooling rate of approximately 800 ℃ s^{-1}.　 The cross-sections parallel to the compression axis of the water-quenched specimens were observed by optical microscopy (OM) after etched by 3% nital solution to measure the fraction of ferrite.

3.3.3 Results

3.3.3.1 Kinetics of dynamic transformation in specimens having fine austenite grain size deformed at a fast strain rate at temperature above Ae$_3$

Figure 3.3.2a shows the representative stress-strain curve of the specimen, whose thermomechanical process are shown in **Fig. 3.3.1a** (series 1), deformed at a strain rate of 10^{-1} s^{-1} to various strains at 750 °C. Flow stress is initially increased, then gradually decreased, and finally kept almost constant stress. Markers on the stress-strain curve in **Fig. 3.3.2a** indicate the moment where deformation was interrupted, and the strains of square, circle, triangle, diamond and hexagon are 0.18, 0.33, 0.41, 0.76 and 0.96, respectively. In order to compare the dynamic softening in flow stress with the fraction of ferrite systematically, ferrite fraction in each specimen of which compression was interrupted at different strains was measured. The change in the fraction of ferrite as a function of strain is displayed in **Fig. 3.3.2b**. It is clearly seen that with increasing strain, fraction of ferrite is
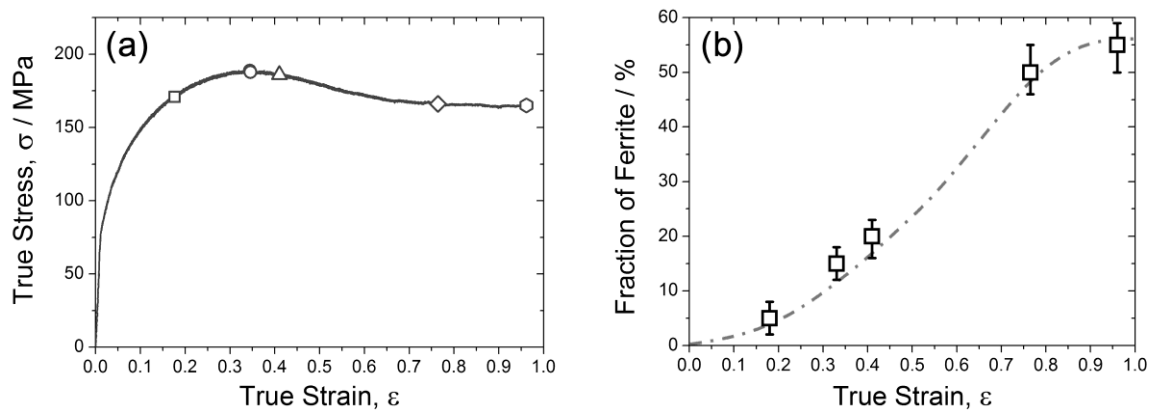

Fig. 3.3.2 (a) Stress-strain curve of the specimen deformed at a strain rate of 10^{-1} s^{-1} to different strains at 750 °C (series 1 in Table 3.3.1). Square, circle, triangle, diamond and hexagon symbols indicate true strains of 0.18, 0.33, 0.41, 0.76 and 0.96, respectively. (b) Change in ferrite fraction as a function of strain.

gradually increased.

It has been confirmed in the previous section that the change in flow stress has a linear correlation with the increase in the fraction of ferrite. In order to estimate the change in flow stress, the stress-strain curve in **Fig. 3.3.2a** was fitted by using **Eq. 3.2.2**, in a strain range from 0.02 to 0.18, and was extrapolated to large strain region as shown in **Fig. 3.3.3a**. Fitting parameters for **Eq. 3.2.2** are shown in **Table 3.3.2**.

The solid curve in **Fig. 3.3.3a** is the stress-strain curve shown in **Fig. 3.3.2a**, and the dash-dotted curve is a result obtained from **Eq. 3.2.2**. The dashed curve in **Fig. 3.3.3a**

Table 3.3.2 Fitting parameters of Eq. 3.2.2.

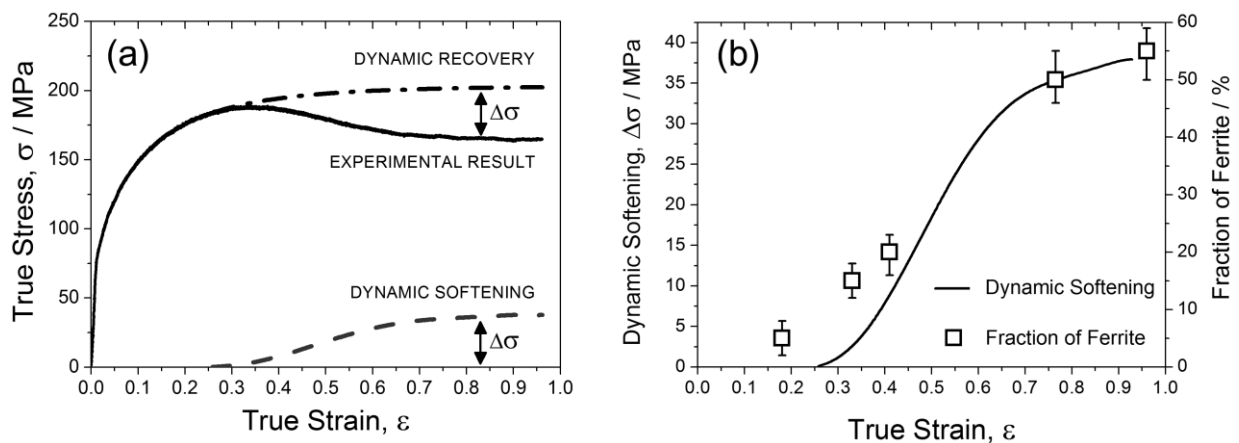| σ_0	σ_{sat}	k	d
9 MPa	200 MPa	6.58	0.49

Fig. 3.3.3 (a) Experimentally obtained stress-strain curve shown in Fig. 3.3.2a (solid line), the dynamic recovery type curve predicted by Eq. 3.2.2 (dash-dotted line) and the difference between two previous curves corresponding to the dynamic softening, $\Delta\sigma$ (dashed line). (b) Change in dynamic softening determined in (a) (solid line) and the fraction of dynamically transformed ferrite (squares) shown in Fig. 3.3.2b, as a function of strain.

represents the amount of dynamic softening ($\Delta\sigma$), corresponding to the difference between the dash-dotted curve and the experimentally obtained curve, and it is displayed again in **Fig. 3.3.3b** as the solid curve in order to compare it with the fraction of ferrite. The scales of two vertical axes in **Fig. 3.3.3b** are normalized each other, in order words, the maximum stress of dynamic softening of the vertical axis on left-hand side was set to the maximum ferrite fraction of the vertical axis on right-hand side. The dynamic softening ($\Delta\sigma$) in **Fig. 3.3.3** is initiated at a strain of 0.25 which is close to the critical strain of stress-strain curve as shown in **Table 3.2.2**, and it starts to saturate at a strain of 0.8 approximately. **Fig. 3.3.5b** distinctly shows that the change in the fraction of ferrite is corresponded to that of dynamic softening, even though the ferrite fraction is somewhat deviated from the dynamic softening curve at low strain.

3.3.3.2 Kinetics of dynamic transformation in specimens having coarse austenite grain size deformed at a slow strain rate at temperature below Ae_3

Figure 3.3.4a shows the representative stress-strain curve of the specimen, whose thermomechanical process is shown in **Fig. 3.3.1b** (series 2), deformed at a strain rate of 10^{-2} s^{-1} to various strains at 600 ℃. After the flow stress reached to the maximum value, it gradually decreased with increasing strain, and finally kept almost constant stress. As done before, ferrite fractions in each specimen at different strains were measured to compare the fraction of ferrite with the dynamic softening in flow stress. Markers on the stress-strain curve in **Fig. 3.3.4a** indicate the moment where deformation was interrupted, and the strains of square, circle, triangle, diamond and hexagon are 0.02, 0.08, 0.31, 0.5, 0.96 and 1.31, respectively. The change in the fraction of ferrite as a function of strain is shown in **Fig. 3.3.4b**. The fraction of ferrite is gradually increased with increasing strain, and it comes
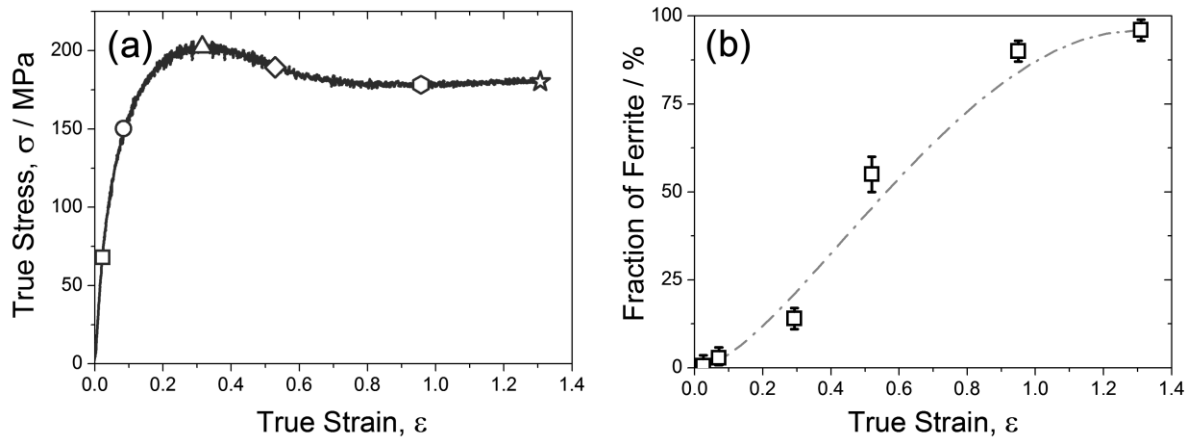
Fig. 3.3.4 (a) Stress-strain curve of the specimen deformed at a strain rate of 10^{-2} s^{-1} to different strains at 600 ℃ (series 2 in Table 3.3.1).   Square, circle, triangle, diamond, hexagon and star symbols indicate strains of 0.02, 0.08, 0.31, 0.5, 0.96 and 1.31, respectively.   (b) Change in ferrite fraction as a function of strain.

close to 95% at a large strain.

The change in the flow stress has a correlation with the increase in the fraction of ferrite as mentioned before.   By using **Eq. 3.2.2**, the flow stress in a strain range from 0.02 to 0.18 in **Fig. 3.3.4a** was fitted, and it was extrapolated to large strain region as shown in **Fig. 3.3.5a**. Fitting parameters for **Eq. 3.2.2** are shown in **Table 3.3.3**.

The solid curve in **Fig. 3.3.5a** is the stress-strain curve shown in **Fig. 3.3.4a**, and the dash-dotted curve is a result obtained from **Eq. 3.2.2**.   The dashed curve in **Fig. 3.3.5a** represents the amount of dynamic softening ($\Delta\sigma$), corresponding to the difference between the dash-dotted curve and the experimentally obtained curve.   **Figure 3.3.5b** shows the change in the amount of dynamic softening or fraction of ferrite as a function of strain.   The dynamic softening ($\Delta\sigma$) in **Fig. 3.3.5** is initiated at a strain of 0.16, and it starts to saturate at a strain of 0.8 approximately.   **Figure 3.3.5b** clearly shows that the change in the fraction of dynamically transformed ferrite shows a good agreement with the dynamic softening in flow stress.

82

Table 3.3.3 Fitting parameters of Eq. 3.2.2.

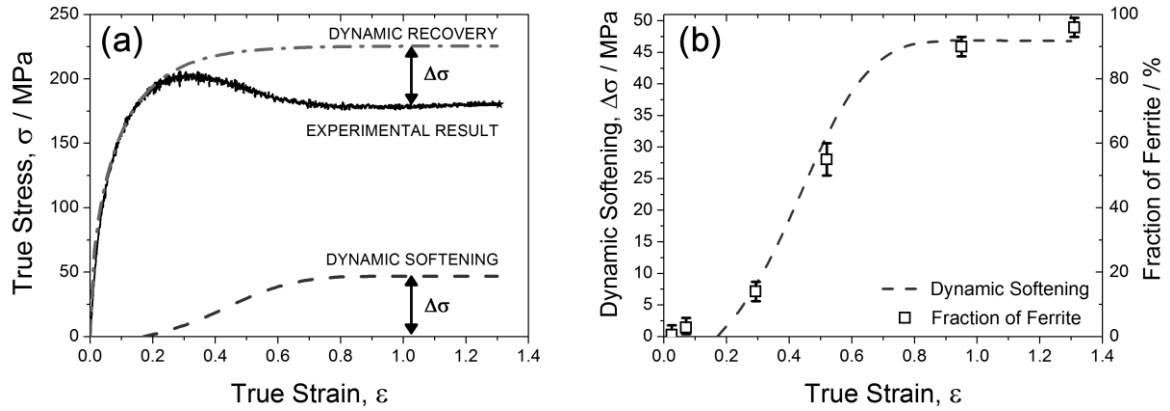| σ_0	σ_{sat}	k	d
1 MPa	225 MPa	6.7	0.5

Fig. 3.3.5 (a) Experimentally obtained stress-strain curve shown in Fig. 3.3.4a (solid line), the dynamic recovery type curve predicted by Eq. 3.2.2 (dash-dotted line) and the difference between two previous curves corresponding to the dynamic softening, $\Delta\sigma$ (dashed line).   (b) Change in dynamic softening determined in (a) (dashed line), and the fraction of dynamically transformed ferrite shown in Fig. 3.3.4b, as a function of strain.

3.3.4 Discussions

Kinetics of static transformation can be usually described by Johnson-Mehl-Avrami-Kolmogorov (JMAK) equation, expressed as following [22],

$$X = 1 - \exp\left(- p \cdot t^q\right) \qquad (3.3.1)$$

where X is the fraction of product phase, p and q are constants which reflect nucleation and growth mode during transformation, and t is time. Based on **Eq. 3.3.1**, when the values of $\log[\ln\{1/(1-X)\}]$ are plotted as a function of $\log(t)$, the slope of log-log plot is equal to the exponent, q, and the change of exponent q indicates how transformation mode varies as a function of t. In the present study, transformation happens during deformation of austenite. Thus, strain is also an important parameter for expressing the kinetics of transformation. The time in $\log[\ln\{1/(1-X)\}]$ vs. $\log(t)$ can be replaced by a parameter, strain (ε), as a form of $\log(\varepsilon - \varepsilon_c)$ where ε_c is the critical strain described before. It is assumed that dynamic transformation is initiated at a critical strain.

The change in dynamic softening of flow stress shown in **Fig. 3.3.3a** (the first series) is plotted in **Fig. 3.3.6a** and **b** as a function of time ($\log(t)$) and that of strain ($\log(\varepsilon - \varepsilon_c)$), respectively. The change in dynamic softening of flow stress shown in **Fig. 3.3.5a** (the second series) is plotted in **Fig. 3.3.6c** and **d** as a function of time ($\log(t)$) and that of strain ($\log(\varepsilon - \varepsilon_c)$), respectively, as well. In order to obtain the exponent, q values, linear fitting was done from 25% to 75% of the maximum fraction of ferrite, and those are also exhibited in each images. It should be noted that holding period before applying deformation to austenite (60 s for two series of experiments) is excluded in these calculations.

84

It is well known that in the case of isothermal static transformation, exponent, q, is usually less than 4 which is the case when the rates of nucleation and growth keep constant during transformation [23]. In **Figs. 3.3.6a** and **c**, on the other hand, the stage of transformation can be divided into three stages I, II and III. In the initial stage I, the slopes of two plots (**Figs. 3.3.6a** and **c**) are quite steeper (around 7) than those in intermediate range (stage II, 25 to 75% of the maximum fraction of ferrite). It implies that nucleation rate is extremely rapid during deformation, or growth rate might be faster than that in the static transformation under an assumption that the growth is radial [23,24]. In the intermediate range (stage II, linear fit range), q values are around 3.30 to 3.44, which implies that the nucleation rate is gradually decreased compared with that in the stage I. Such high q values in **Fig. 3.3.6** indicate that ferrite transformation is accelerated by continuous deformation.
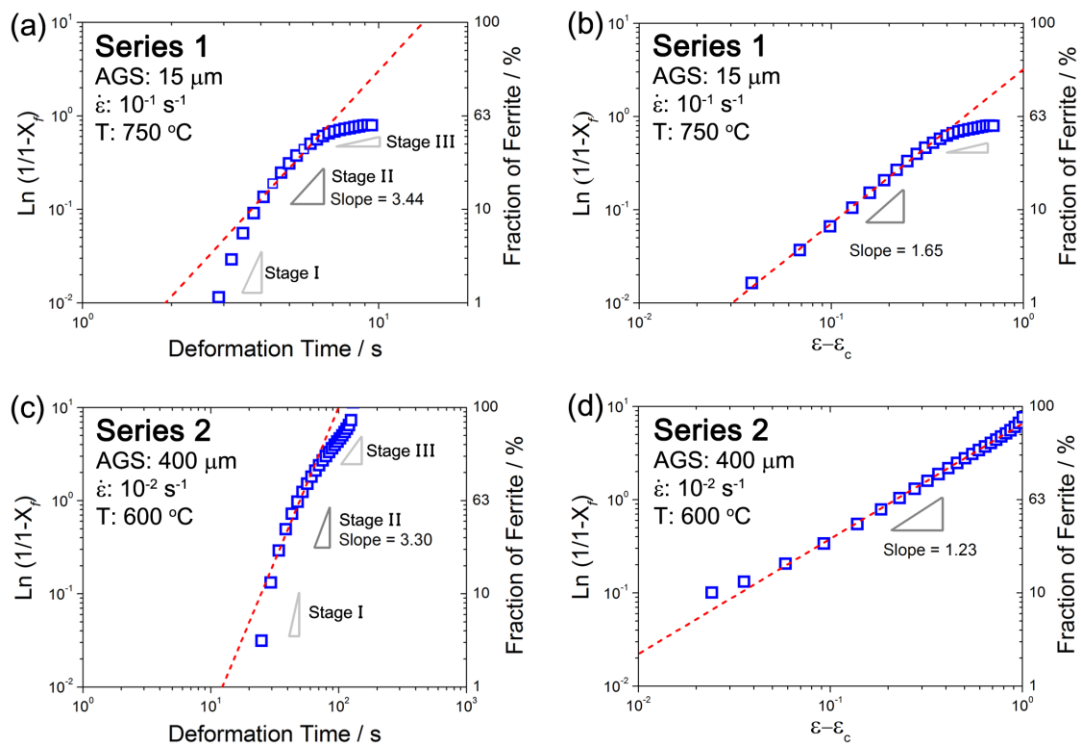

Fig. 3.3.6 Two forms of JMAK plots of the two series of experiments: (a),(b) series 1 and (c),(d) series 2. (a),(c) Plots of $\log[\ln\{1/(1-X)\}]$ vs. $\log(t)$. (b),(d) Plots of $\log[\ln\{1/(1-X)\}]$ vs. $\log(\varepsilon - \varepsilon_c)$.

In the final stage III, q values are decreased compared with those in the previous stages I and II. It reflects that the rate of dynamic transformation at final stage drops, similar to isothermal static transformation. The change in slope in three stages reveals that the modes of dynamic transformation continuously varies with the progress of transformation, and it is not constant even at the initial stage, which is a different aspect from isothermal static transformation.

In **Figs. 3.3.6b** and **d**, in contrast, the stage of transformation is not divided into few stages, but exponent, q, is almost constant in whole range. The slopes are 1.23-1.65 which would be sensitively altered by a critical strain, but insensitively varied by strain rate or austenite grain size. By comparing the exponent value in $\log[\ln\{1/(1-X)\}]$ vs. $\log(\varepsilon - \varepsilon_c)$ with those in previous plots ($\log[\ln\{1/(1-X)\}]$ vs. $\log(t)$), it could be concluded that kinetics of dynamic transformation is strongly governed by deformation, i.e., strain.

One of the distinguished features in two series of experiments is the saturation of transformation shown in only the first series. The final stage in **Figs. 3.3.6a** and **b** shows the retardation of kinetics of dynamic transformation, and it would keep constant fraction of ferrite (55%). It might be due to a saturation of *equilibrium fraction of ferrite under deformation condition* as discussed in Chapter 2.3.

3.3.5 Summary

We investigated the kinetics of dynamic ferrite transformation through two series of experiments in the 6Ni-0.1C steel.   The major results are summarized as follows:

1. The change in dynamic softening of flow stress was proportional to the increase in the fraction of dynamically transformed ferrite as a function of strain.   Therefore, stress-strain curve could be regarded to predict the kinetics of dynamic transformation corresponding to the change in flow stress during deformation.

2. Through comparing two types of Johnson-Mehl-Avrami-Kolmogorov (JMAK) equation plots, it was concluded that kinetics of dynamic transformation was significantly governed by deformation strain.   High values of exponent of JMAK equation were obtained, which indicated that the kinetics of ferrite transformation was accelerated by continuous deformation.

3.4 Conclusions

In the Chapter 3, the kinetics of dynamic transformation was studied. Following two results were derived by using the specimens having various prior austenite grain sizes. Firstly, the onset of dynamic transformation was accelerated by refinement of austenite grain size, similar to static transformation. Secondly, the decrease in flow stress was correlated with the increase in the fraction of dynamically transformed ferrite, and the fraction of ferrite proportionally increased with decreasing flow stress. Thus, the kinetics of dynamic transformation could be predicted through the change in flow stress during deformation. As a result, the modified Johnson-Mehl-Avrami-Kolmogorov plot could describe the kinetics of dynamic transformation for two series of experiments having different deformation conditions. It was concluded that kinetics of dynamic transformation was greatly controlled by deformation strain.

3.5 References

[1]   T. Sakai and J. Jonas, "Overview no. 35 Dynamic recrystallization: Mechanical and microstructural considerations," *Acta Metallurgica*, vol. 32, pp. 189–209, 1984.

[2]   C. M. Sellars, "The kinetics of softening processes during hot working of austenite," *Czechoslovak Journal of Physics*, vol. 35, pp. 239–248, 1985.

[3]   J. M. Cabrera, A. A. Omar, J. M. Prado, and J. J. Jonas, "Modeling the flow behavior of a medium carbon microalloyed steel under hot working conditions," *Metallurgical and Materials Transactions A*, vol. 28, pp. 2233–2244, 1997.

[4]   A. Hiramatsu and M. Umemoto, "Computer modelling of phase transformation from work-hardened austenite," *ISIJ International*, vol. 32, pp. 306–315, 1992.

[5]   K. C. Russell, D. M. Barnett, C. J. Altstetter, H. I. Aaronson, and J. K. Lee, "Strain energy interactions, the T0 concept and sympathetic nucleation," *Scripta Metallurgica*, vol. 11, pp. 485–490, 1977.

[6]   H. I. Aaronson, W. T. Reynolds, and G. R. Purdy, "The incomplete transformation phenomenon in steel," *Metallurgical and Materials Transactions A*, vol. 37, pp. 1731–1745, 2006.

[7]   M. R. Plichta, W. A. T. Clark, and H. I. Aaronson, "The Nucleation Kinetics, Crystallography, and Mechanism of the Massive Transformation," *Metallurgical Transactions A*, vol. 15, pp. 427–735, 1984.

[8]   J. . Rigsbee and H. . Aaronson, "A computer modeling study of partially coherent f.c.c.:b.c.c. boundaries," *Acta Metallurgica*, vol. 27, pp. 351–363, 1979.

[9]   C. Zheng, N. Xiao, L. Hao, D. Li, and Y. Li, "Numerical simulation of dynamic strain-induced austenite–ferrite transformation in a low carbon steel," *Acta Materialia*, vol. 57, pp. 2956–2968, 2009.

[10]   H. Beladi, G. Kelly, A. Shokouhi, and P. Hodgson, "Effect of thermomechanical parameters on the critical strain for ultrafine ferrite formation through hot torsion testing," *Materials Science and Engineering A*, vol. 367, pp. 152–161, 2004.

[11]   V. V Basabe and J. J. Jonas, "The ferrite transformation in hot deformed 0.036 % Nb austenite at temperatures above the Ae 3," *ISIJ international*, vol. 50, pp. 1185–1192, 2010.

[12]   J.-K. Choi, D.-H. Seo, J.-S. Lee, K.-K. Um, and W.-Y. Choo, "Formation of ultrafine ferrite by strain-induced dynamic transformation in plain low carbon steel," *ISIJ International*, vol. 43, pp. 746–754, 2003.

[13] A. Z. Hanzaki, R. Pandi, P. D. Hodgson, and S. Yue, "Continuous cooling deformation testing of steels," *Metallurgical Transactions A*, vol. 24, pp. 2657–2665, 1993.

[14] R. Wang and T. Lei, "Deformation and restoration behaviour of ferrite-austenite two-phase structures," *Materials Science and Engineering A*, vol. 165, pp. 19–27, 1993.

[15] X. Liu, J. K. Solberg, and R. Gjengedal, "Measurement of austenite-to-ferrite transformation temperature after multi-pass deformation of steels," *Materials Science and Engineering A*, vol. 194, pp. L15–L18, 1995.

[16] H. Yada, C.-M. Li, and H. Yamagata, "Dynamic $\gamma \rightarrow \alpha$ transformation during hot deformation in iron-nickel-carbon alloys," *ISIJ international*, vol. 40, pp. 200–206, 2000.

[17] E. Poliak and J. Jonas, "A one-parmenter approach to determining the critical conditions for the initiation of dynamic recrystallization," *Acta Materialia*, vol. 44, pp. 127–136, 1996.

[18] U. F. Kocks and H. Mecking, "Physics and phenomenology of strain hardening: the FCC case," *Progress in Materials Science*, vol. 48, pp. 171–273, 2003.

[19] E. Voce, "The relation between stress and strain for homogeneous deformation," *Journal of the Institute of Metals*, vol. 74, pp. 537–562, 1948.

[20] J. H. Palm, "Stress-strain relations for uniaxial loading," *Applied Scientific Research*, vol. 1, pp. 198–214, 1949.

[21] J. J. Jonas, X. Quelennec, L. Jiang, and É. Martin, "The Avrami kinetics of dynamic recrystallization," *Acta Materialia*, vol. 57, pp. 2748–2756, 2009.

[22] F. J. Humphreys and M. Hatherly, *Recrystallization and related annealing phenomena*, 2nd ed., vol. 54. Pergamon, 2004.

[23] S. E. Offerman, L. J. G. W. van Wilderen, N. H. van Dijk, J. Sietsma, M. T. Rekveldt, and S. van der Zwaag, "In-situ study of pearlite nucleation and growth during isothermal austenite decomposition in nearly eutectoid steel," *Acta Materialia*, vol. 51, pp. 3927–3938, 2003.

[24] J. Cahn and W. Hagel, *Decomposition of austenite by diffusional processes*. New York: Interscience, 1960, pp. 131–196.

CHAPTER 4

CHARACTERISTICS OF DYNAMICALLY TRANSFORMED FERRITE

4.1 Introduction

The previous chapters confirmed that dynamic transformation occurred over wide range of temperatures even above Ae_3, and the kinetics of dynamic transformation was greatly affected by deformation conditions.

Chapter 4 investigates the characteristics of dynamically transformed ferrite obtained under various deformation conditions. This chapter consists of four sections. First section studies the effect of strain on the evolution of microstructure. A nucleation and growth of ferrite grains, texture analysis of dynamically transformed ferrite, etc., are shown in this section. Additionally, crystallographic orientation features of dynamically transformed ferrite are studied as well. In the second section, the author focuses on the effect of deformation temperature on microstructure of ferrite. In the third section, the effect of strain rate on nucleation of ferrite is discussed with the deformation behavior of austenite. Lastly in the fourth section, mechanical properties of dynamically transformed ferrite are compared with those of statically transformed ferrite.

4.2 Effect of strain on microstructural evolution of dynamically transformed ferrite

4.2.1 Introduction

There are several reports about the effect of strain on microstructural evolution of dynamically transformed ferrite. However, in the most cases, relatively fine austenite grain size was used in order to obtain fine ferrite grains

. When prior austenite grain size is fine, it is hard to study mechanisms of dynamic transformation, for example, nucleation or growth of ferrite during deformation. In the present section, the effect of strain on microstructural evolution of dynamic transformation is studied using coarse prior austenite grains to reveal microstructural characteristics of dynamic transformation.

4.2.2 Experimental procedure

The material used in the present study is the same alloy (Fe-6Ni-0.1C), as that used in Chapter 2 shown in **Table 2.2.1**. As-received hot rolled plate was homogenized at 1100 ℃ for 24 hours, and then quenched in water. The detailed thermomechanical processes used in this study are shown in **Fig. 4.2.1**. After the specimens 12 mm in height and 8 mm in diameter were installed in the thermomechanical simulator, they were austenitized at 1200 ℃ for 180 s, resulting in the mean austenite grain size to be 400 μm. Then, these were cooled by N_2 gas at a cooling rate of 30 ℃ s^{-1} to 600 ℃ (below Ae_1 (613 ℃)). After 60 s holding at 600 ℃, specimens were compressed at a strain rate of 10^{-2} s^{-1} to various strains: $\varepsilon = 0.03$,
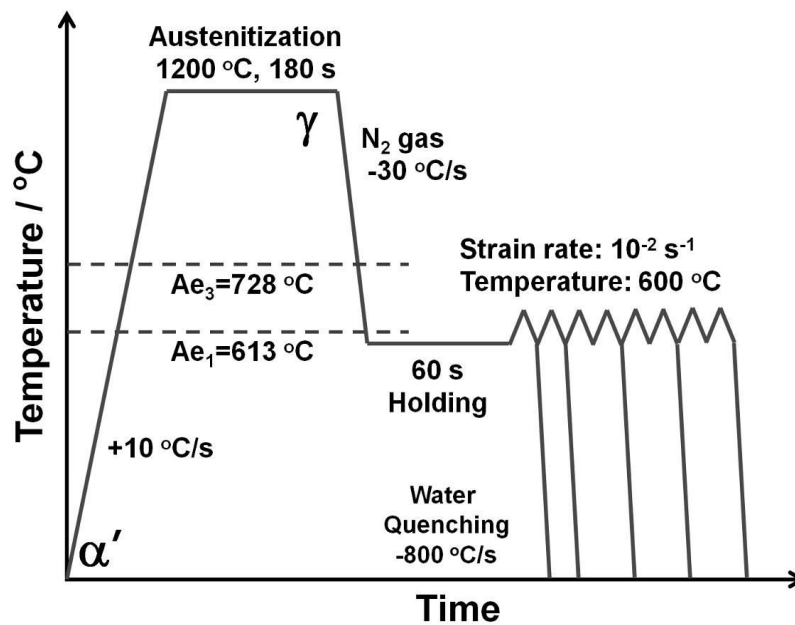
Fig. 4.2.1 Schematic illustration of the thermomechanical processes in compression deformation. Austenitized specimens were deformed at 600 ℃ at a strain rate of 10^{-2} s^{-1} to various strains: ε = 0.03, 0.07, 0.29, 0.52, 0.96 and 1.31. Ae_3 and Ae_1 calculated by Thermo-Calc were 728 ℃ and 613 ℃, respectively.

0.07, 0.29, 0.52, 0.96 and 1.31. Before compression, no static transformation occurred during holding at 600 ℃ (according to the TTT diagram shown in **Fig. 2.2.2**). When the scheduled deformation was completed, specimens were immediately quenched to room temperature by precisely controlled water-injection. The cooling rate on the surface was recorded to be 800 ℃ s^{-1}. Mica and glass powder were used in the hot-compression test as insulator and lubricant, and temperature of the specimens was precisely controlled to be kept it constant by the induction-heating system of the simulator.

Microstructural observation was carried out by an optical microscopy (OM) and an electron back-scattering diffraction (EBSD). The cross-section parallel to the compressive axis of the specimens was mechanically polished, and then electro-polished in a solution of 10% perchloric acid ($HClO_4$) and 90% acetic acid (CH_3COOH) at 25 ℃. 3% nital solution

was used to reveal microstructures of deformed specimens. For measuring texture and mean ferrite grain size, large areas (100 μm × 150 μm) of the specimens were scanned by EBSD with a step size of 0.10 or 0.12 μm to obtain statistically reliable data. The sizes of ferrite grains were determined by mean linear intercept method on the EBSD microstructures including all boundaries with misorientation above 2 °. Inverse pole figure (IPF) map, kernel average misorientation (KAM) map and texture analysis were used to analyze the EBSD microstructures of dynamically transformed ferrite. IPF map expresses the crystal orientations at each measured point parallel to a particular direction of the specimen. KAM map, which shows the average misorientation angle between an EBSD measurement point and all its neighbors, is used to evaluate the degree of misorientation in local area [1,2]. In order to quantify the texture of dynamically transformed ferrite, orientation density function (ODF) was calculated using TSL-OIM software with a harmonic series expansion under following options: a series rank 34, a Gaussian half-width equal to 5 °, and an axial symmetry.

4.2.3 Results

True stress-true strain curves of the specimens deformed to various strains at 600 ℃ at a strain rate of 10^{-2} s^{-1} are shown in **Fig. 4.2.2**.   As mentioned above, all specimens had microstructures of 100% austenite at the onset of hot-compression. The moments that deformations were interrupted are marked as square, circle, triangle, diamond, hexagon and star.   The flow stress increases with increasing strain, and it reaches to maximum value at a strain of 0.29.   The flow stress decreases with increasing strain, and finally keeps a constant value.   The stress-strain curves of the specimens agree well to each other.

OM images of the specimens deformed to various strains are displayed in **Fig. 4.2.3**. The strains applied to the specimens are shown in the upper right hand corner on each OM image.   Bright and dark areas, respectively, represent ferrite and martensite transformed from retained austenite during water-quenching after completion of the scheduled deformation.   Dashed lines in **Figs. 4.2.3a**, **e** and **f** indicate prior austenite grain boundaries.
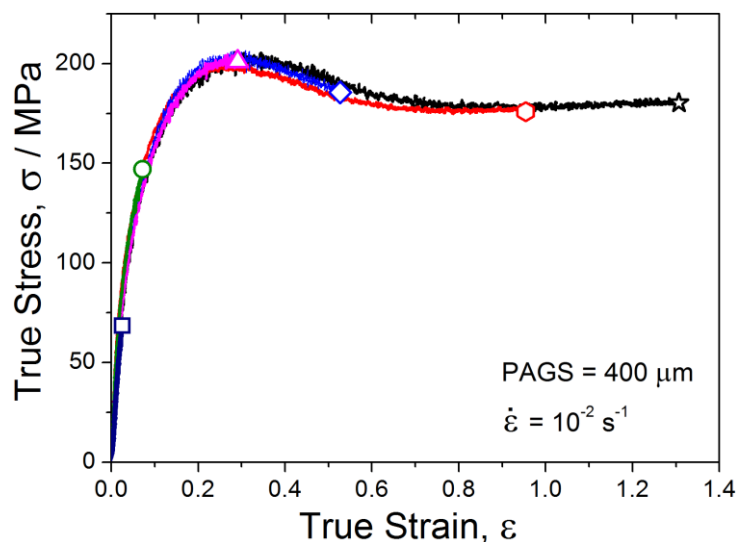

Fig. 4.2.2 True stress-true strain curves of the specimens deformed at a strain rate of 10^{-2} s^{-1} to various strains at 600 ℃.   The deformation was interrupted at various strains indicated by square ($\varepsilon = 0.03$), circle ($\varepsilon = 0.07$), triangle ($\varepsilon = 0.29$), diamond ($\varepsilon = 0.52$), hexagon ($\varepsilon = 0.96$) and star ($\varepsilon = 1.31$).

Double-headed arrows in **Figs. 4.2.3a**, **b**, **e** and **f** represent the directions along which ferrite grains seem to grow. Several needle-like ferrite grains are found in the vicinity of an austenite grain boundary in **Fig. 4.2.3a** ($\varepsilon = 0.03$). With the increase in strain, fraction of ferrite around austenite grain boundaries is increased, and ferrite grains cover most of austenite grain boundaries in **Figs. 4.2.3b** ($\varepsilon = 0.07$). When flow stress of deformation reaches to maximum (peak) value, all austenite grain boundaries and twin boundaries indicated by arrow are decorated by ferrite grains with its fraction of 14% in **Fig. 4.2.3c** ($\varepsilon = 0.29$). When the strain reaches to 0.52, the fraction of ferrite becomes approximately
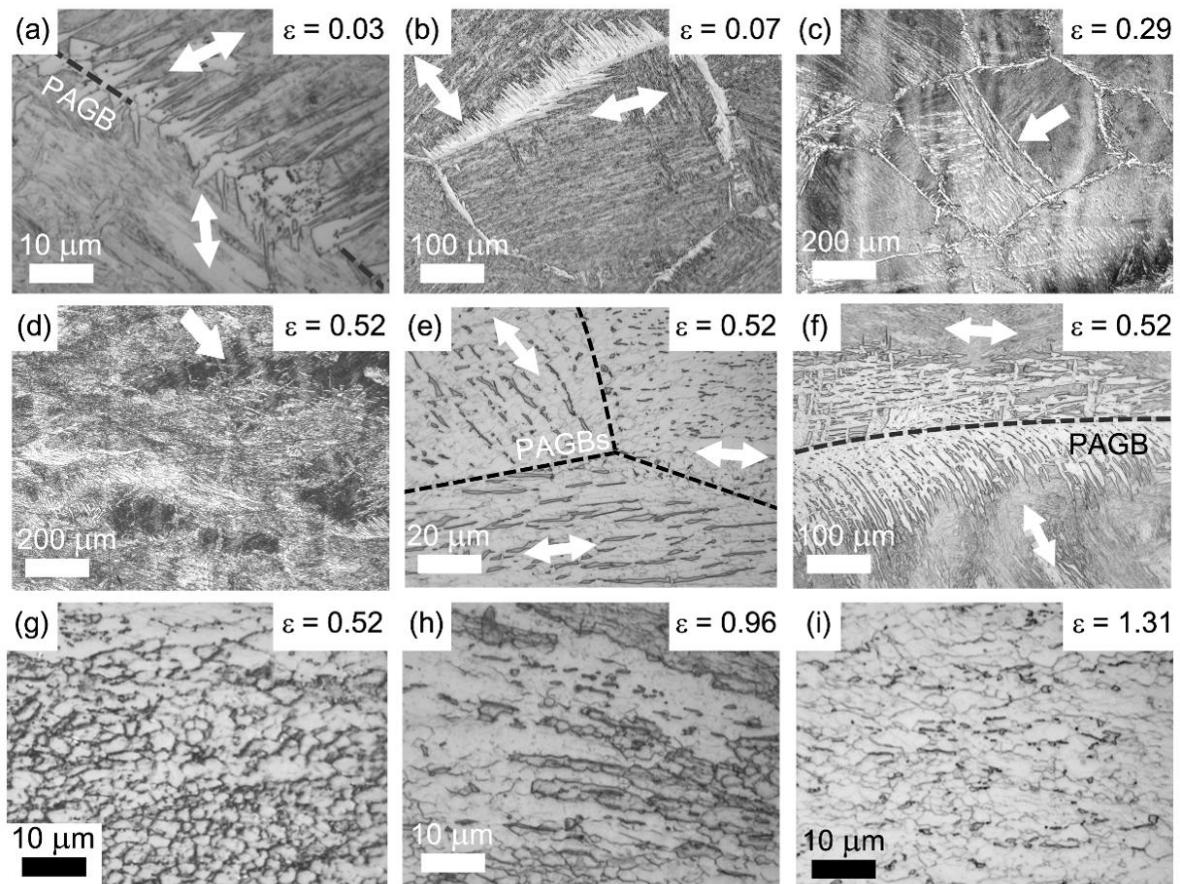

Fig. 4.2.3 Optical microscope images of specimens deformed to various strains: (a) $\varepsilon = 0.03$, (b) $\varepsilon = 0.07$, (c) $\varepsilon = 0.29$, (d-g) $\varepsilon = 0.52$, (h) $\varepsilon = 0.96$ and (i) $\varepsilon = 1.31$. Dashed lines in (a,e,f) indicate prior austenite grain boundaries. Double-headed arrows in (a,b,e,f) represent the directions along which ferrite grains seem to be elongated. Compression direction is parallel to the vertical axis of images.

96

55% in total, and some ferrite grains are formed in interior of austenite grains as pointed out by arrow in **Fig. 4.2.3d**. Microstructure in the specimen deformed to a strain of 0.52 is quite heterogeneous in local area. For example, in **Figs. 4.2.3e** and **f**, the longitudinal directions of ferrite grains are different depending on austenite grains. Ferrite grains with many martensite-austenite constituents in the upper right corner of **Fig. 4.2.3e** are elongated perpendicular to the compression direction, but ferrite grains with retained austenite grains in the upper left corner are grown to different directions, which will be described later (**Fig. 4.2.9**). Fine and equiaxed ferrite grains are also found inside the austenite grains of the identical specimen, as shown in **Fig. 4.2.3g**. When the strain reaches to 0.96, the microstructure consists of ferrite and some of martensite-austenite constituents, indicating that dynamic transformation seems to be completed, as shown in **Figs. 4.2.3h**. Fine and equiaxed ferrite grains coexist with ferrite grains elongated perpendicular to the compression direction. With further increase in strain, the morphology of ferrite grains is not changed so much as shown in **Fig. 4.2.3i** ($\varepsilon = 1.31$).
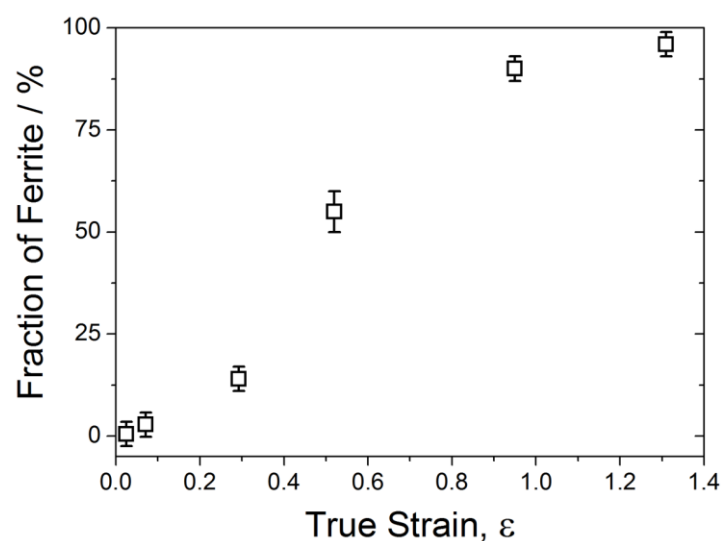

Fig. 4.2.4 The change in the fraction of dynamically transformed ferrite as a function of applied strain.

Figure 4.2.4 shows the change in the fraction of dynamically transformed ferrite as a function of strain.   The fraction of ferrite is gradually increased with increasing strain, and it comes close to 95% at a large strain.   The kinetics of dynamic transformation in this condition (prior austenite grain size: 400 μm, strain rate: 10^{-2} s^{-1} and temperature: 600 ℃) has been discussed in Chapter 3.

EBSD measurement was carried out for the specimens deformed to various strains in order to understand microstructural characteristics of dynamically transformed ferrite. **Figure 4.2.5** shows an image quality (IQ) map and corresponding IPF maps of the specimen deformed to a strain of 0.29.   Bright and dark areas in IQ map indicate ferrite and martensite, respectively.   Prior austenite grain boundary is marked as a dashed white line.   The low angle boundaries with misorientation of 2 to 15 ° and the high angle boundaries with misorientation above 15 ° are also drawn in red and green lines, respectively.   The colors in the IPF maps indicate the crystallographic orientation parallel to the compression direction at
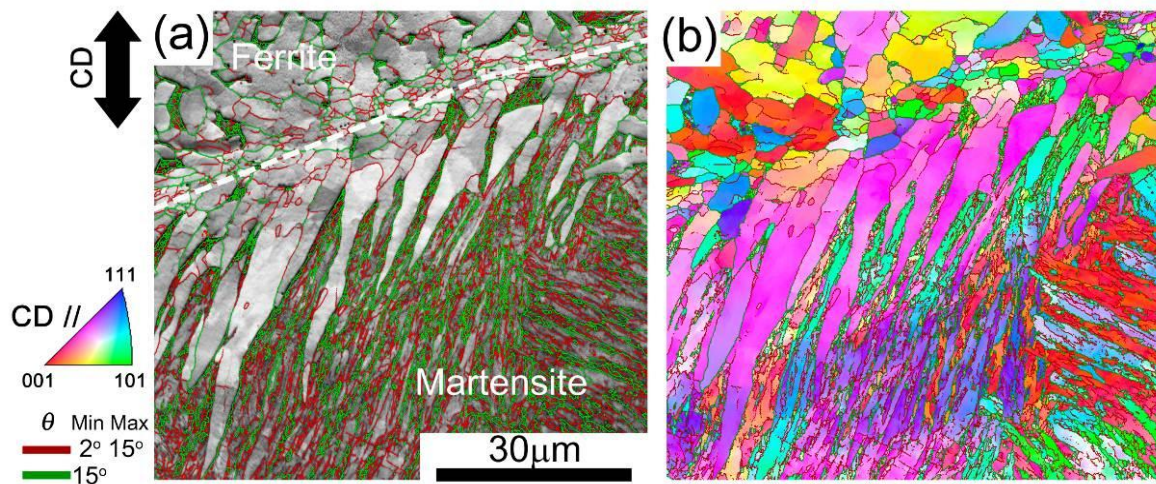

Fig. 4.2.5 (a) Image quality map and (b) corresponding inverse pole figure map of the specimen deformed to a strain of 0.29.   Bright and dark areas in (a) represent ferrite and martensite, respectively.   Dashed white line indicates prior austenite grain boundary.   Low angle boundaries with misorientation of 2 to 15 ° and high angle boundaries with misorientation above 15 ° are also drawn in red and green lines, respectively.

each measured point, according to the key stereographic triangle shown in the left hand side. Fine and equiaxed ferrite grains are formed in the vicinity of austenite grain boundaries, and the orientations of those grains are randomly distributed. Widmanstätten-like ferrite grains having elongated morphologies are found in one part of austenite grains interior, and Widmanstätten-like ferrite grains have almost the identical crystallographic orientation as shown in Fig. **4.2.5b**.

Figure 4.2.6 displays IPF maps (a-c) and corresponding KAM maps (d-f) of the specimens deformed to strains of (a,d) 0.52, (b,e) 0.96 and (c,f) 1.31 at which the fractions of ferrite are 52%, 90% and 92%, respectively, as shown in **Fig. 4.2.4**. The IPFs in **Figs. 4.2.6g-i** have the same logarithmic scale where the maximum value of the probability for finding a given orientation in a random distribution is 10. The color intensity is shown in the upper right hand corner. The specimen deformed to a strain of 0.52 (**Figs. 4.2.6a** and **d**) contains large fraction of low angle boundaries (79.2%) with irregular shape of ferrite grains surrounded by high angle boundaries. The mean GAM value of this specimen is 0.65 ° which is much higher than that of statically transformed ferrite grains (0.28 °), and the mean ferrite grain size is 7.6 μm. The IPF in **Fig. 4.2.6g** indicates that crystallographic orientation of $<111>_\alpha$ component is strong. The microstructure of the specimen deformed to a strain of 0.96 in **Figs 4.2.6b** and **e** is relatively homogeneous, compared with that of the specimen deformed to a strain of 0.52 in **Figs. 4.2.6a** and **d**. Coarse ferrite grains are elongated perpendicular to the compression direction, and fine ferrite grains surrounded by high angle boundary are also found together. The mean ferrite grain size is 3.2 μm. $<111>_\alpha$ and $<001>_\alpha$ components of ferrite in the inverse pole figure in **Fig. 4.2.6h** are stronger than those in **Fig. 4.2.6g**, and their maximum intensity values are 4.6 and 6.8, respectively. The microstructure of the specimen deformed to a strain of 1.31 in **Figs 4.2.6c** and **f** is almost
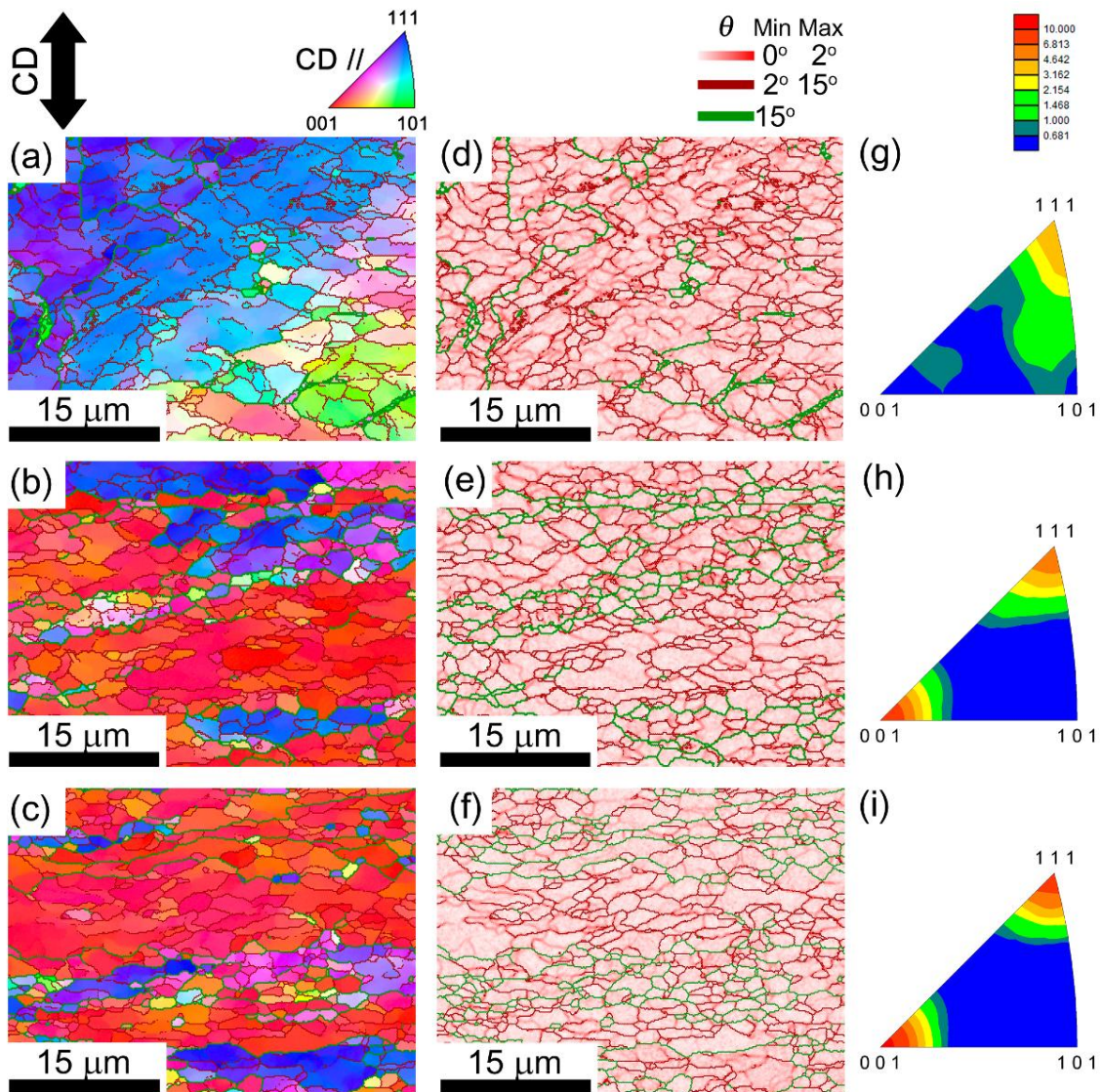
Fig. 4.2.6 (a-c) Inverse pole figure maps, (d-f) corresponding kernel average misorientation maps and (g-i) inverse pole figures of the specimens deformed to various strains: (a,d,g) ε = 0.52, (b,e,h) ε = 0.96 and (c,f,i) ε = 1.31. (a-f) The low angle boundaries with misorientation of 2 to 15 ° and the high angle boundaries with misorientation above 15 ° are also drawn in red and green lines, respectively. (d-f) The range of misorientation angle for kernel average misorientation is 0 to 2 °.

identical with that in the specimen deformed to a strain of 0.96 in **Figs 4.2.6b** and **e**. The mean GAM value of this specimen is 0.64 °, and the mean ferrite grain size is around 2.9 μm. The maximum intensities of $<111>_\alpha$ and $<001>_\alpha$ components of ferrite in **Fig. 4.2.6i** increase and reach to around 6.8 and 10.0, respectively.

The change in the fraction of high angle boundary as a function of strain is shown in **Fig. 4.2.7a**, and the representative misorientation distribution of grain boundaries of the specimen deformed to a strain of 1.31 is displayed in **Fig. 4.2.7b**. Random distribution of misorientation which is known as Mackenzie distribution [3,4] is also plotted together in **Fig. 4.2.7b**. The fraction of high angle boundary is gradually increased, and is saturated when strain is at 0.96. In other words, the fraction of low angle boundary was initially high, and it decreased as dynamic transformation progressed. This is probably due to the dynamic recovery during hot deformation. It is the reason why the mean GAM values are kept to be approximately 0.64 ° even though strain of deformation increased. Another possibility is the increase in the number of ferrite grains dynamically recrystallized during subsequent deformation. Fine ferrite grains in **Fig. 4.2.6e** and **f** surrounded by high angle boundaries contribute to the increase in the fraction of high angle boundary.

During compression, dynamically transformed ferrite and retained austenite grains are continuously deformed. It is well known that $<011>_\gamma$ component of austenite and $<001>_\alpha$
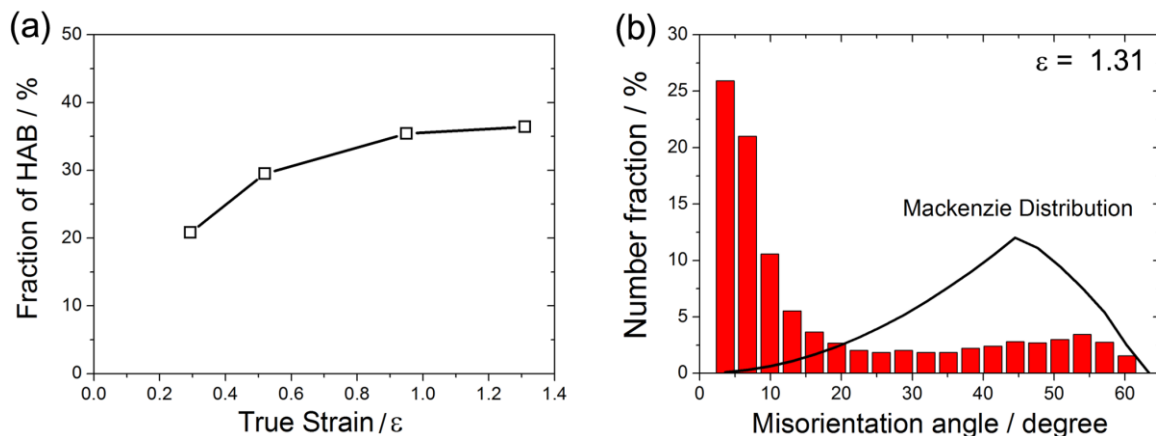

Fig. 4.2.7 (a) The change in the fraction of high angle boundaries as a function of strain. (b) The distribution of grain boundaries of the specimen deformed to a strain of 1.31 as a function of misorientation angle. Random distribution of misorientation which is known as Mackenzie distribution is plotted together [9,10].

and $<111>_\alpha$ components of ferrite, parallel to the compressive direction, are preferentially developed under compression deformation [5,6]. In **Figs. 4.2.6g-i**, components of $<111>_\alpha$ and $<001>_\alpha$ become stronger with increasing strain. The quantitative intensities of each component are displayed in **Fig. 4.2.8**. The tolerance angle of 15 ° deviated from ideal poles of each component was used. The change in the fraction of each orientation component of dynamically transformed ferrite is shown in **Fig. 4.2.8a**. The change of $<001>_\alpha$ component drastically increases with increasing strain. The fraction of $<111>_\alpha$ component is high at small strains of deformation, and it gradually increases as strain increases. On the other hand, the fraction of $<011>_\alpha$ component gradually decreases as the strain increases. The sum of $<001>_\alpha$ and $<111>_\alpha$ components is shown in **Fig. 4.2.8b**. As shown in Fig. **4.2.8a**, the sum of $<001>_\alpha$ and $<111>_\alpha$ components is increased with increasing strain, and reaches to almost 88% at a strain of 1.31.
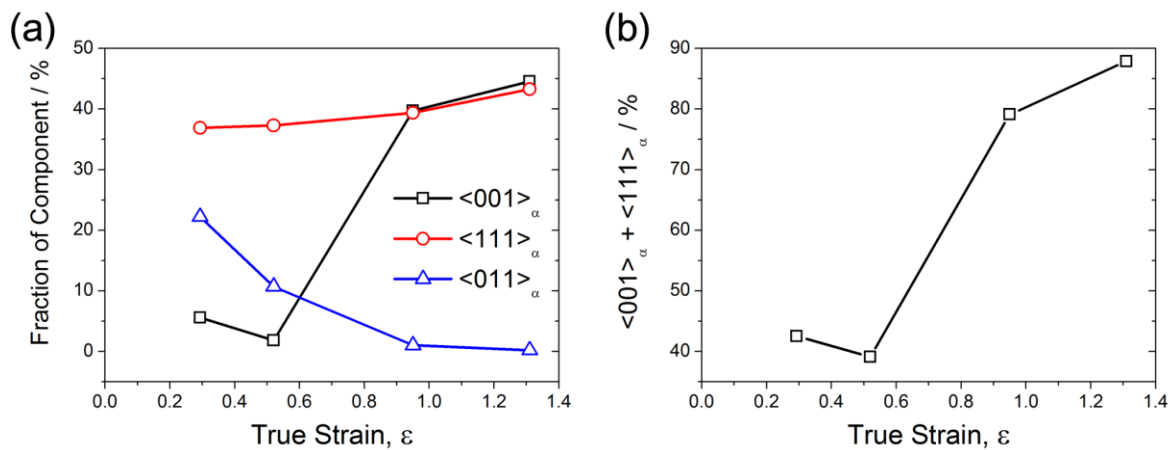

Fig. 4.2.8 The change in the fraction of texture components of ferrite as a function of strain. (a) Each component of ferrite. Square: $<001>_\alpha$, circle: $<111>_\alpha$ and triangle: $<011>_\alpha$. (b) Sum of $<001>_\alpha$ and $<111>_\alpha$.

4.2.4 Discussion

4.2.4.1 Formation of Widmanstätten-like ferrite grains

Figure 4.2.3 shows microstructures of dynamically transformed ferrite at different strains. Ferrite grains were preferentially nucleated at austenite grain boundaries, and they grew into interior of austenite grains. With increasing strain the fraction of ferrite increased, and it was almost 95% at strains larger than 0.96. One of interesting characteristics of the microstructures of dynamically transformed ferrite grains is the morphology of ferrite. As shown in **Figs. 4.2.3a-f** and **4.2.5**, Widmanstätten-like ferrite grains are aligned to some specific directions.

Many previous reports about transformation behaviors of Widmanstätten ferrite in steels have been published [7–17], but few studies are reported about the effects of elastic or plastic deformation of austenite on morphologies of Widmanstätten ferrite grains [12,14]. Yang et al. [12] reported that extremely large and straight Widmanstätten ferrite grains were formed with a strong selection of crystallographic variant of ferrite under the elastic deformation with a constant external stress of 50 MPa. Larn et al. [14] reported the effect of ausforming on the formation of Widmanstätten ferrite during isothermal holding. Although the onset of the formation of Widmanstätten ferrite was accelerated by plastic deformation of austenite, the fraction of Widmanstätten ferrite was decreased since orientation of austenite was locally rotated due to plastic deformation of austenite so that growth of Widmanstätten ferrite was interrupted.

The difference in the present experiment from those in the previous reports is the level of flow stress which exceeds the yield stress of austenite. As a result, Widmanstätten-like ferrite with different morphology formed during plastic deformation. Plate type ferrite

grains similar to the typical Widmanstätten ferrite grains were found, but simultaneously, curved ferrite grains were also observed in **Fig. 4.2.3**. In order to understand the reason why different morphologies of ferrite grains were formed, EBSD measurement was conducted as shown in **Fig. 4.2.9**.

Figure 4.2.9 represents IQ map, IPF map and phase map of the specimen deformed to a strain of 0.52. Bright and black areas in IQ map (**Fig. 4.2.9a**) indicate ferrite (F) and martensite (M), respectively. Dashed white line represents the prior austenite grain
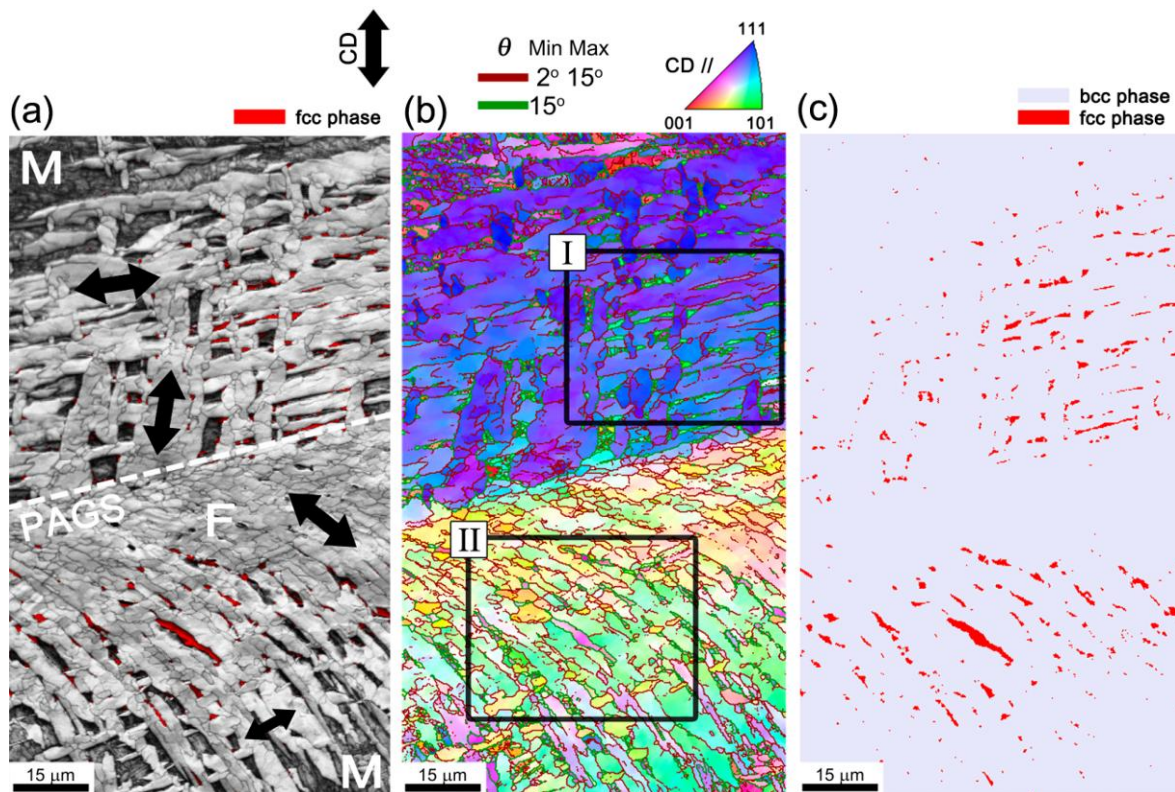

Fig. 4.2.9 (a) Image quality map, (b) inverse pole figure map and (c) phase map of the specimen deformed at a strain of 0.52. Bright and dark areas in (a) represent ferrite (F) and martensite (M), respectively. Dashed line indicates prior austenite grain boundary. Double-headed arrows in (a) show the directions to which ferrite grains were grown. Red and light purple in (c) indicate fcc phase (austenite) and bcc phase (ferrite and martensite), respectively. (b) The low angle boundaries with misorientation of 2 to 15 ° and the high angle boundaries with misorientation above 15 ° are also drawn in red and green lines, respectively. Regions I and II will be shown in Fig. 4.2.10.

boundary, and double-headed arrows indicate the directions to which Widmanstätten-like ferrite grains were grown. Light purple and red areas in the phase map (**Fig. 4.2.9c**) show bcc phase (ferrite and martensite) and fcc phase (retained austenite), respectively. It should be noted that a number of retained austenite grains are found between Widmanstätten-like ferrite grains, and the detailed discussion concerning the retained austenite is done in Chapter 4.2.4.3. The scanned area contains two prior austenite grains, and the representative areas of each prior austenite grains are highlighted as regions I and II in **Fig. 4.2.9b**. In the region I, the orientations of the retained austenite and ferrite are close to $<101>_\gamma$ and $<111>_\alpha$ parallel to compression direction (//C.D.), which are the preferred orientations of austenite and ferrite under uniaxial compression, respectively. Thus, both austenite and ferrite are not significantly influenced by plastic deformation so that the morphology of plate type ferrite grains might be kept during subsequent plastic deformation. In region II, on the other hand, the orientations of the retained austenite and ferrite are far from their preferred orientations, and, in this area, curved and large ferrite grains were observed. The formation of such Widmanstätten-like ferrite grains could be attributed to the rotation of orientations of both austenite and ferrite to the preferred ones during subsequent deformation. The detailed crystallographic analysis of Widmanstätten-like ferrite will be discussed in the following section.

4.2.4.2 Crystallographic characteristics of Widmanstätten-like ferrite

It is well known in steels that the product b.c.c. phases transformed from austenite satisfy the Kurdjumov-Sachs (K-S) orientation relationship (OR) or the Nishiyama-Wassermann (N-W) OR with austenite [18–20]. The detailed information of those relationships are displayed in **Table 4.2.1** [21]. It has been reported that (statically

Table 4.2.1 Possible γ-α orientation relationships [21].

Relationship	Parallel planes	Directions	Misorientation angle	Axis
K-S	$\{111\}_\gamma \parallel \{011\}_\alpha$	$<110>_\gamma \parallel <111>_\alpha$	42.85°	<17.8 17.8 96.8>
N-W	$\{111\}_\gamma \parallel \{011\}_\alpha$	$<112>_\gamma \parallel <011>_\alpha$	45.99°	<8.3 20.1 97.6>

transformed) Widmanstätten ferrite grains grew into an austenite grain, satisfying K-S OR with the austenite grain [22,23]. **Figure 4.2.10a** and **b** show the phase maps, which are the enlarged parts in **Fig. 4.2.9** as marked regions I and II, respectively. Areas colored by light purple and red in **Fig. 4.2.10** represent bcc and fcc phases, respectively. Blue and black lines indicate the boundaries with K-S and N-W ORs, respectively, and the tolerance angle of 1.57 ° from the ideal misorientation of K-S or N-W OR shown in **Table 4.2.1** is used. Dynamically transformed ferrite and austenite grains partially satisfy K-S or N-W OR, and the fraction of N-W OR in both regions I and II is larger than that of K-S OR. The ratios of total boundary length of N-W/K-S ORs in **Figs. 4.2.10a** and **b** are 4.3 and 7.6, respectively.
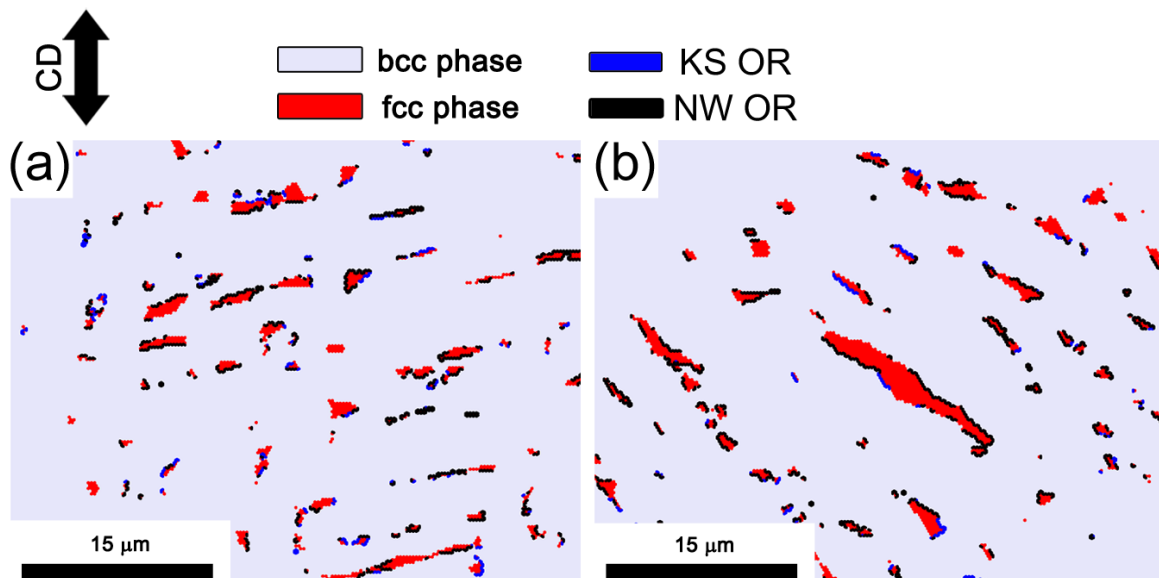

Fig. 4.2.10 Phase maps of the specimen deformed to a strain of 0.52. (a-b) Enlarged parts of regions I and II in Fig. 4.2.9b. Light purple and red areas indicate bcc (ferrite and martensite) and fcc phases (austenite), respectively. Blue and black lines represent the parts where K-S and N-W OR are satisfied. Tolerance angle from the ideal misorientation is set to be 1.57 °.
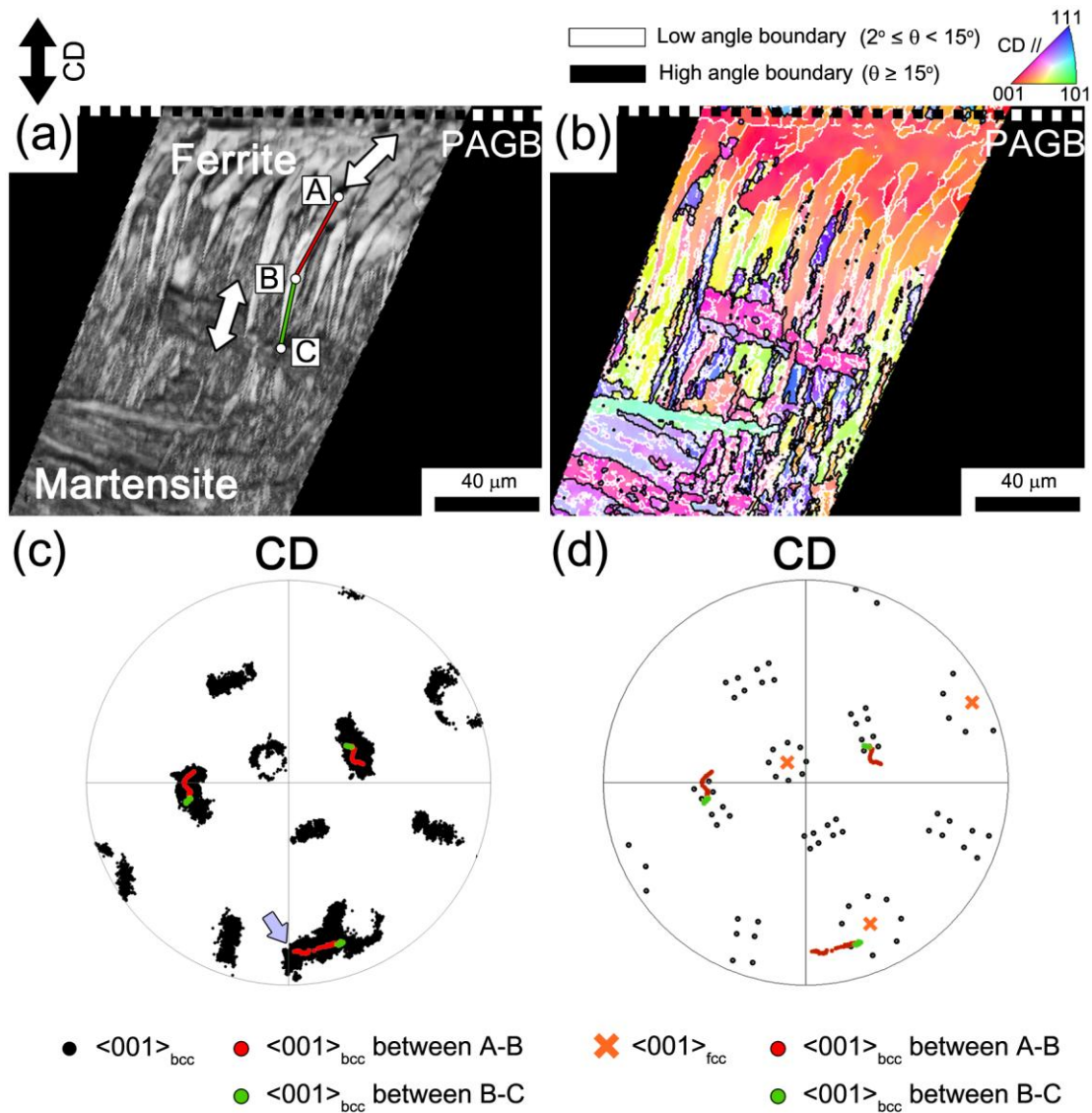
Fig. 4.2.11 (a) Image quality map and (b) corresponding inverse pole figure map of the specimen deformed at a strain of 0.52. Bright and dark areas in (a) represent ferrite and martensite, respectively. Dashed line indicates prior austenite grain boundary. Double-headed arrows in (a) show the directions ferrite grains were grown. (b) The low angle boundaries with misorientation of 2 to 15 ° and the high angle boundaries with misorientation above 15 ° are also drawn in red and green lines, respectively. (c) The $<001>_\alpha$ pole figure of bcc phase of the lower prior austenite grain in (a). (d) The ideal positions of 24 variants of martensite (black circles) with $<001>_\gamma$ (multiplication marks). Two straight lines, as marked as red (A to B) and green (B to C), are drawn in (a), and the changes in orientation of two lines are shown in (c) and (d). Arrow in (c) indicates the orientation of position A.

The change in the orientation of Widmanstätten-like ferrite in the vicinity of prior austenite grain boundary during continuous deformation is shown in **Fig. 4.2.11** that represents IQ map and corresponding IPF map of the specimen deformed to a strain of 0.52.   Bright and dark areas in IQ map indicate ferrite and martensite, respectively.   Prior austenite grain boundary is marked as a dashed line.   The low and high angle boundaries are also drawn in white and black lines, respectively.   Double-headed arrows indicate the directions to which ferrite grains seem to be elongated or grown within austenite grains.   **Figure 4.2.11c** is a pole figure of bcc phase in **Fig. 4.2.11a**.   Because it is well known that martensite in low carbon steels satisfies K-S OR with respect to austenite, 24 variants can be formed from a single grain of austenite. [24,25].   Based on the positions of various variants of martensite, it is possible to speculate the orientation of prior austenite grain.   In **Fig. 4.2.11d**, the multiplication marks is the $<001>_\gamma$//C.D., and black circles represent the ideal 24 variants of $<001>_\alpha$//C.D.   which correspond with those of martensite in **Fig. 4.2.11c**.   The change in orientation of dynamically transformed ferrite along two straight lines, as marked as red (A to B) and green (B to C), in **Fig. 4.2.11a** is tracked.   The position, C, is the place where ferrite formed at last, and the position, A, indicated by arrow in **Fig. 4.2.11c** is the part in which ferrite was formed prior to the formation of ferrite at the place of C.   The changes in orientation along two lines are shown in **Figs. 4.2.11c** and **d**.   The orientations from B to C (green) are close to one of the ideal positions of 24 K-S variants of bcc phase.   However, from A to B (red), the orientation of ferrite drafts apart from the ideal position of bcc phase as shown in **Fig. 4.4.11d**, but is close to $<001>_\alpha$//C.D. in **Fig. 4.4.11b**, which is one of the preferred orientations of ferrite under uniaxial compression, as mentioned above.   This indicates that Widmanstätten-like ferrite initially kept K-S OR with neighboring austenite, but the orientation of ferrite was rotated to its preferred orientations during continuous plastic deformation.

Another interesting feature is that only few numbers (less than four) of the selected variants of Widmanstätten-like ferrite were observed in each prior austenite grain, as seen in the IPF maps of **Figs. 4.2.9b** and **4.2.11b**. Such variant selections of martensite, bainite as well as Widmanstätten ferrite formed through various thermomechanical processes have been reported [6,26–31]. However, in the present study, the number of observations is not enough to discuss the issue statistically.

4.2.4.3 Diffusion of carbon in dynamic transformation

One of the controversial topics about dynamic transformation is whether transformation mechanism of dynamic ferrite transformation accompanies diffusion of carbon or not. Yada, who is one of the pioneers of dynamic transformation studies, and his colleague proposed a massive transformation of ferrite occurred during deformation [32,33]. Massive transformation is the transformation in which the product phase has a different crystal structure but the same chemical composition with the matrix phase. [34–41]. Some reports have been published that massive transformation of ferrite occurred during deformation of austenite [42,43]. In contrast, some other groups reported that C diffused during dynamic transformation [44,45]. Recently, a Monte Carlo simulation worked by Tong et al. [46,47] showed that diffusion of C during dynamic transformation was strongly dependent on strain rate of deformation. When strain rate is high enough, C cannot diffuse into austenite, and a concentration of C in ferrite exceeds its solubility at a given temperature. When strain rate is low, on the other hand, it diffuses into austenite, resulting in different C concentrations between ferrite and austenite.

Figure 4.2.9c clearly showed the existence of retained austenite grains. In order to obtain retained austenite grains in water-quenched specimens of the present alloy at room temperature, the concentrations of C and/or Ni must be enriched in local area [48]. It is possible for Ni to be segregated in the homogenized plate. The concentration of Ni in the as-quenched specimen after homogenization treatment at 1100 ℃ for 24 h is shown in **Fig. 4.2.12**. The concentration of Ni was measured by an energy-dispersive X-ray spectroscopy (EDS) equipped in a scanning electron microscope (SEM) operated at 15 kV of accelerating voltage. Step size of scanning was 0.6 μm, and every point was exposed for enough duration time (22 s / point). The maximum fluctuation of Ni concentration in a wide range of distance is ± 0.75%. It could be mentioned that there is no serious segregation of Ni in the homogenized specimen because the deviation level (± 0.75%) is within the error range of EDS measurement for Ni. Because diffusion of substitutional atoms, for example, Ni, is very slow at such a low temperature (600 ℃), large amount of C atoms should diffuse into
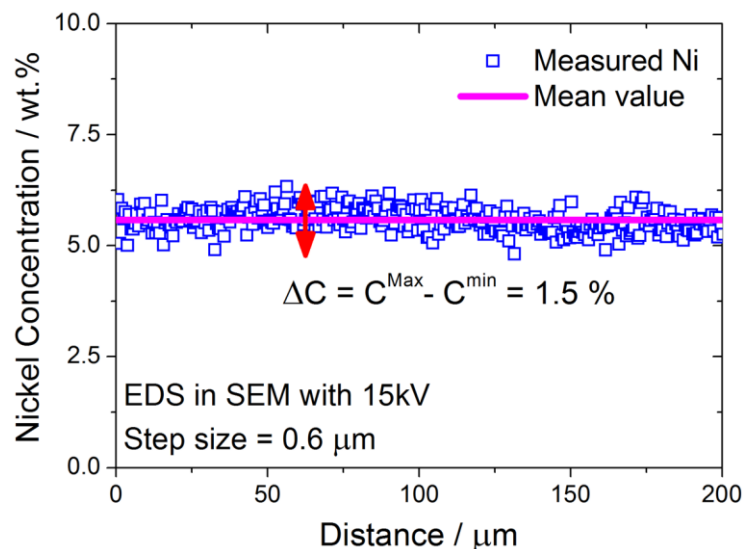

Fig. 4.2.12 Ni concentration in the homogenized specimen used in the present study (Fe-6Ni-0.1C), measured by energy-dispersive X-ray spectroscopy (EDS). Scan step size between each datum point was 0.6 μm, and every point was exposed for enough duration time (22 s / point). Solid line represents the mean value of all data displayed by squares.

austenite during dynamic transformation for retaining the austenite grains at room temperature. Therefore, the existence of the retained austenite grains at room temperature indicates that dynamic ferrite transformation accompanies diffusion of carbon.

4.2.4.4 Evolution of microstructure during dynamically transformed ferrite

Schematic illustrations shown in **Fig. 4.2.13** summarize the microstructure evolution in dynamic ferrite transformation from austenite with increasing deformation strain. Red and black lines represent low and high angle boundaries. (a)-(b) Initial austenite grain is plastically deformed in compression, and deformation structures, such as microbands with large numbers of dislocations, are introduced. (c) With increasing strain, the austenite grain is elongated perpendicular to the compressive direction, and ferrite grains are formed preferentially in the vicinity of austenite grain boundaries and partially at deformation structures within the austenite grain. (d) Further deformation results in the growth of ferrite or the formation of ferrite grains having the identical crystallographic orientation with that of existing neighbor ferrite grains, resulting in the formation of Widmanstätten-like ferrite plates (**Fig. 4.2.5**). Most of austenite grain boundaries are decorated by ferrite grains. (e) Continuous deformation results in the change of crystallographic orientations of austenite and ferrite simultaneously. This introduces low angle boundaries within the ferrite grains. (f) Although some ferrite grains are heavily deformed, the mean GAM values are kept nearly constant owing to dynamic recovery of ferrite with development of low angle boundaries. The fraction of ferrite and the number of fine ferrite grains are increased with increasing strain. (g) Dynamic transformation is completed at large strain of deformation. However, some austenite grains surrounded by ferrite grains remain due to high concentration of C that diffuses from ferrite during dynamic transformation. Ferrite grains seem to be elongated

perpendicular to the compressive direction with containing large numbers of dislocations. Fine and equiaxed ferrite grains are also formed by either final stage of dynamic transformation or dynamic recrystallization of previously transformed ferrite. The mean grain size of ferrite is decreased with increasing strain. The mean ferrite grain size of 3 μm was obtained in the present study.
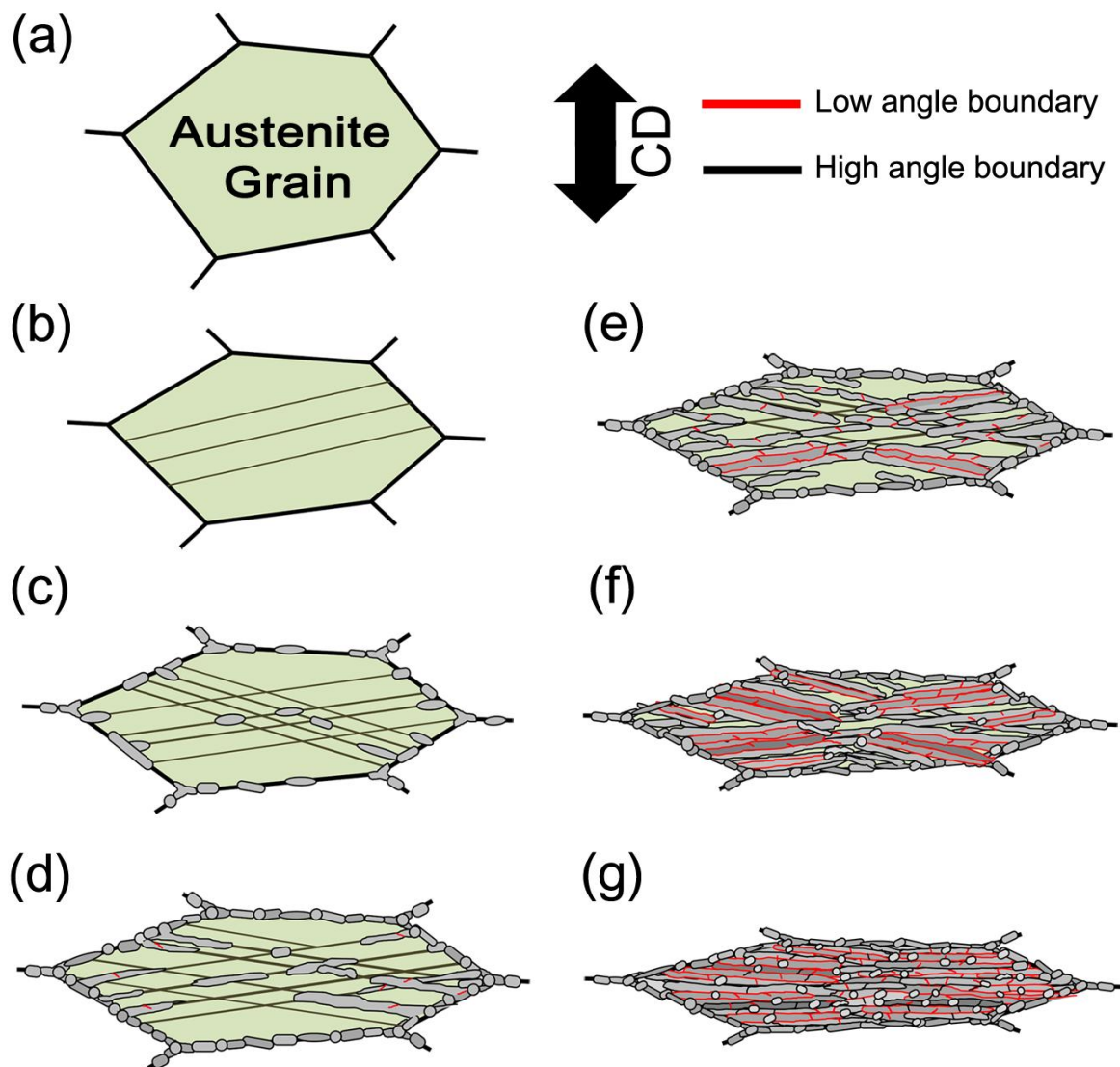

Fig. 4.2.13 Schematic illustrations showing the evolution of microstructures during dynamic ferrite transformation from austenite with increasing plastic strain. Solid red and black lines represent low and high angle boundaries.

4.2.5 Summary

We investigated the microstructural evolution in dynamic ferrite transformation as a function of applied strain at a temperature below Ae_1.   The major results are summarized as follows:

1. Widmanstätten-like ferrite grains initially formed in the vicinity of austenite grain boundaries during plastic deformation of austenite.   With increasing strain, the growth of the Widmanstätten-like ferrite grains was dominant, and the mean grain size of ferrite was decreased to be 3 μm with increasing strain.

2. Widmanstätten-like ferrite satisfied crystallographic orientation relationship (OR) with prior austenite.   It grew into austenite grain inside with keeping K-S or N-W ORs during deformation.

3. The crystallographic orientation of ferrite showed extremely strong texture components of $<001>_\alpha$ and $<111>_\alpha$ parallel to the compressive direction.

4. Carbon atoms diffused during dynamic transformation, and C-enriched austenite found at room temperature.

4.3 Effect of deformation temperature on microstructure of dynamically transformed ferrite

4.3.1 Introduction

Last 40 years, one of the hot issues in metallurgical engineering fields was dynamic recrystallization or recovery. Especially in steel science, dynamic recrystallization of austenite or ferrite was highlighted to achieve finer grain size [49–55]. However, only a few reports have been published about microstructures in the specimens deformed at intercritical temperatures ranging from Ae_3 to Ae_1 where ferrite coexists with austenite [56,57]. The occurrence of dynamic ferrite transformation over wide temperature range has been discussed through both stress-strain curves analyses and microstructural observations in Chapter 2 and Chapter 3. Based on the results and discussion in the present study, the effect of deformation temperature on microstructure of dynamically transformed ferrite is systematically studied over wide temperature range, including temperature above Ae_3 in the present section.

4.3.2 Experimental procedure

The material used in the present study is the Fe-6Ni-0.1C alloy, same as that in the previous section. The detailed chemical composition is shown in **Table 2.2.1**. As-received hot rolled plate of the Fe-6Ni-0.1C steel was homogenized at 1100 ℃ for 24 hours, and then quenched in water. The detailed thermomechanical processes used in this study are shown

in **Fig. 4.3.1**. After austenitization at 800 ℃ for 180 s, cylindrical specimens 12 mm in height and 8 mm in diameter were cooled to various deformation temperatures ranging from 600 to 780 ℃, and then held isothermally for 10 s (600 ℃) or 60 s (at temperatures ranging from 650 to 780 ℃) before compression to make temperature in the specimens homogenous. The holding time for 60 s at temperatures ranging from 650 to 780 ℃ is short enough to avoid isothermal (static) transformation to ferrite before applying deformation. In contrast, the holding time was 10 s in the case of 600 ℃ deformation because isothermal transformation is initiated around 10 s at this temperature. The fraction of isothermally transformed ferrite during holding for 10 s at 600 ℃ measured by optical microscopy (OM) was 5%. Uniaxial compression was applied to the specimens at a constant strain rate of 10^{-1} s^{-1} to a strain of 0.96, and then all deformed specimens were immediately cooled by water-injection, at a cooling rate of approximately 800 ℃ s^{-1}. Mica and glass powder were used in the hot-compression test as insulator and lubricant, respectively.

Microstructural observation was carried out by OM, EBSD and TEM. 3% nital solution was used to reveal microstructure of the specimens. For the EBSD observation, specimens were electro-polished using a solution of 10% perchloric acid ($HClO_4$) and 90%
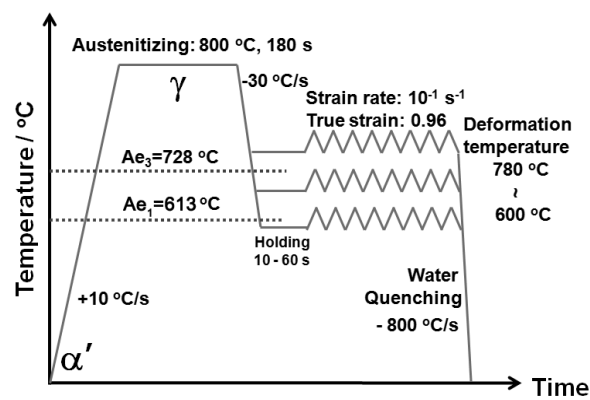

Fig. 4.3.1 Schematic illustration of the thermomechanical processes in compression for dynamic transformation.

acetic acid (CH_3COOH) at 25 ℃. The sizes of ferrite grains were determined by mean linear intercept method on the EBSD microstructures including all boundaries with misorientation above 2 °. The grain average misorientation (GAM) obtained by EBSD, which is the average misorientation angle among all pairs of adjacent points in a grain, is used to evaluate the degree of misorientation inside the grains [1]. For measuring texture and mean ferrite grain size, large area of 100 μm × 150 μm was scanned with a step size of 0.08 or 0.12 μm to obtain statistically reliable data.   Orientation density function (ODF) was calculated using TSL-OIM software with a harmonic series expansion under following options: a series rank 34, a Gaussian half-width equal to 5 °, and an axial symmetry.   For the TEM observation, thin-foil specimens were prepared by twin-jet electro-polishing using the same solution as that used for the EBSD observation.

4.3.3 Results and discussion

OM images of the specimens deformed at (a) 770 ℃, (b) 750 ℃, (c) 700 ℃ and
(d) 600 ℃ are shown in **Fig. 4.3.2**. Compression direction is parallel to the vertical axis of
the images.   Arrows indicate ferrite grains in **Figs. 4.3.2a** and **b**, and black particles in **Figs.
4.3.2c** and **d** are cementites or martensite-austenite (MA) constituents.   When the
deformation temperature is 770 ℃ (**Fig. 4.3.2a**), ferrite grains are observed in the vicinity of
prior austenite grain boundaries.   The mean grain size of austenite was around 15 μm.
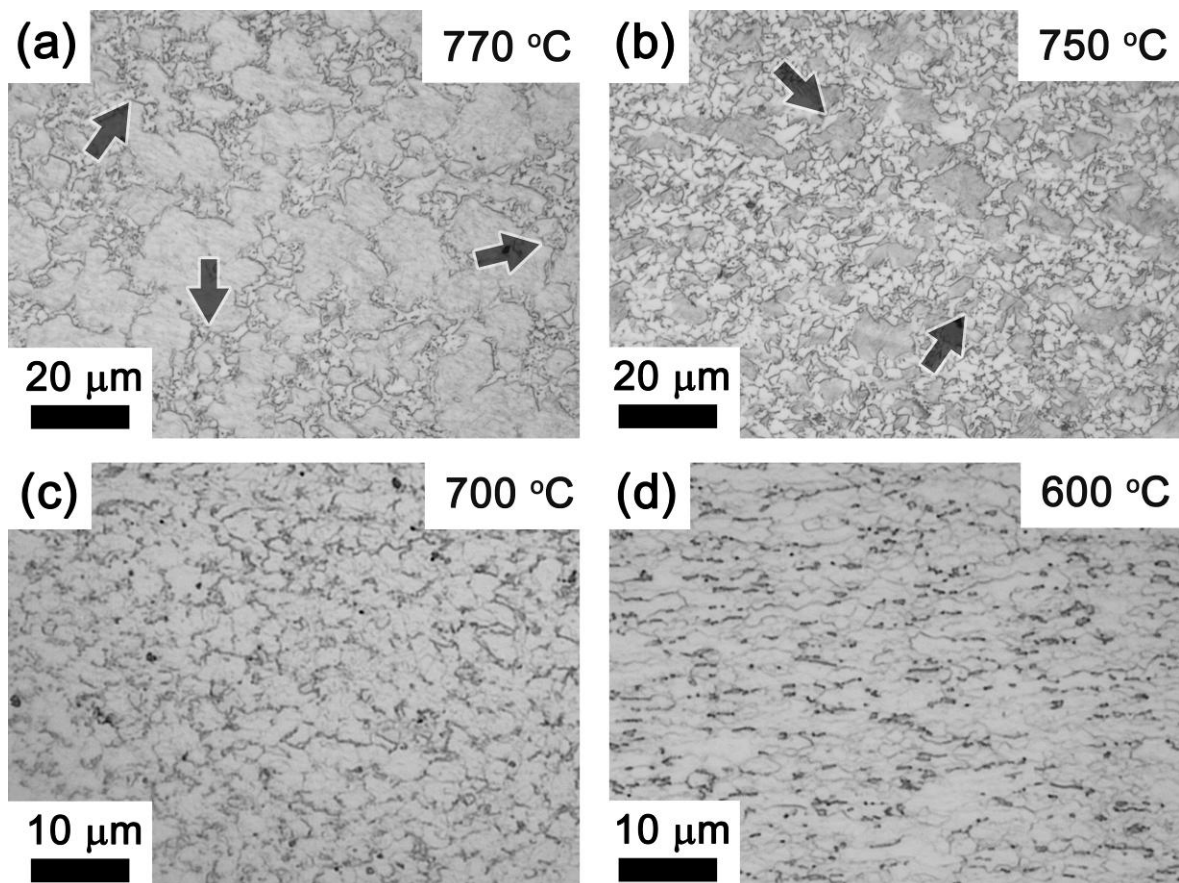With decreasing the deformation temperature to 750 ℃ (**Fig. 4.3.2b**) or 700 ℃ (**Fig. 4.3.2c**),

Fig. 4.3.2 Optical microscope images of the specimens deformed at a strain rate of 10^{-1} s^{-1} to
a strain of 0.96 at various temperatures: (a) 770 ℃, (b) 750 ℃, (c) 700 ℃ and (d) 600 ℃.
Arrows indicate ferrite grains.   Compression direction is parallel to the vertical axis of the images.

the morphology of dynamically transformed ferrite becomes more equiaxed. In contrast, dynamically transformed ferrite grains at 600 °C (**Fig. 4.3.2d**) are elongated perpendicular to the compression direction, and cementites or MA constituents are located between elongated ferrite grains. The change in the fraction of dynamically transformed ferrite has been shown as a function of deformation temperature in **Fig 2.3.5a**, where the fraction of ferrite increases with lowering deformation temperature. As discussed in Chapter 2, addition of extra energy in austenite phase raises Ae_3 as well as Ae_1 (refer to **Fig. 2.3.7**). Ae_3 and Ae_1 rise from 728 °C to 806 °C and 613 °C to 645 °C, respectively, after the addition of extra energy of 180 $J\ mol^{-1}$ to austenite phase. Consequently, it is natural that the maximum fraction of ferrite under deformation condition at a given temperature is larger than that of ferrite without any deformation of austenite. For example, the fraction of ferrite dynamically transformed at 650 °C in **Fig. 2.3.5a** was around 100%, but that of ferrite statically transformed at the same temperature shown in **Fig. 2.2.8b** was approximately 70%.

Figure 4.3.3 shows EBSD results of the specimens deformed at various temperatures: (a-b) 750 °C, (c-d) 730 °C, (e-f) 700 °C and (g-h) 600 °C. Figures on the left- and right-hand sides represent (a,c,e,g) image quality (IQ) maps and (b,d,f,h) corresponding inverse pole figure (IPF) maps, respectively. Compression direction is parallel to the vertical axis of the images. The colors in the IPF maps indicate the crystallographic orientation parallel to the compression direction at each measured point, according to the key stereographic triangle shown in the figure. The low angle boundaries with misorientation of 2 to 15 ° and the high angle boundaries with misorientation above 15 ° are drawn in white and black lines, respectively. 'F' and 'M' in **Figs. 4.3.3a-d** indicate ferrite and martensite, respectively. In **Figs. 4.3.3a-f**, polygonal ferrite grains are observed, but ferrite grains in **Figs. 4.3.3g-h** are elongated perpendicular to the compression direction. The change of colors within identical
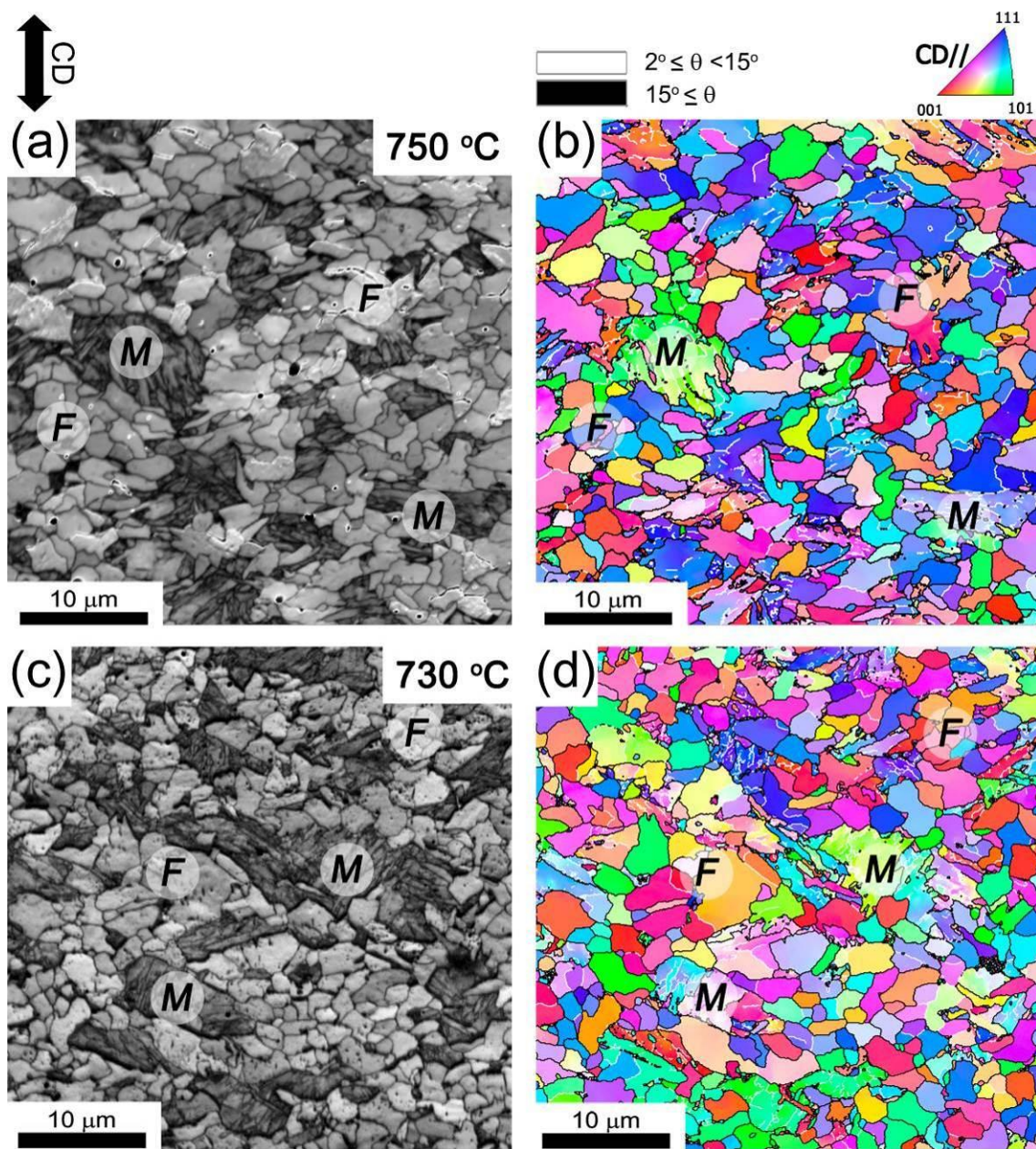
Fig. 4.3.3 Image quality maps (a,c,e,g) and corresponding inverse pole figure maps (b,d,f,h) of the specimens deformed at a strain rate of 10^{-1} s^{-1} to a strain of 0.96 at various temperatures: (a-b) 750 ℃, (c-d) 730 ℃, (e-f) 700 ℃ and (g-h) 600 ℃.　Compression direction is parallel to the vertical axis in the images.　The low angle boundaries with misorientation of 2 to 15 ° and the high angle boundaries with misorientation above 15 ° are also drawn in white and black lines, respectively.　'F' and 'M' in (a-d) indicate ferrite and martensite, respectively.
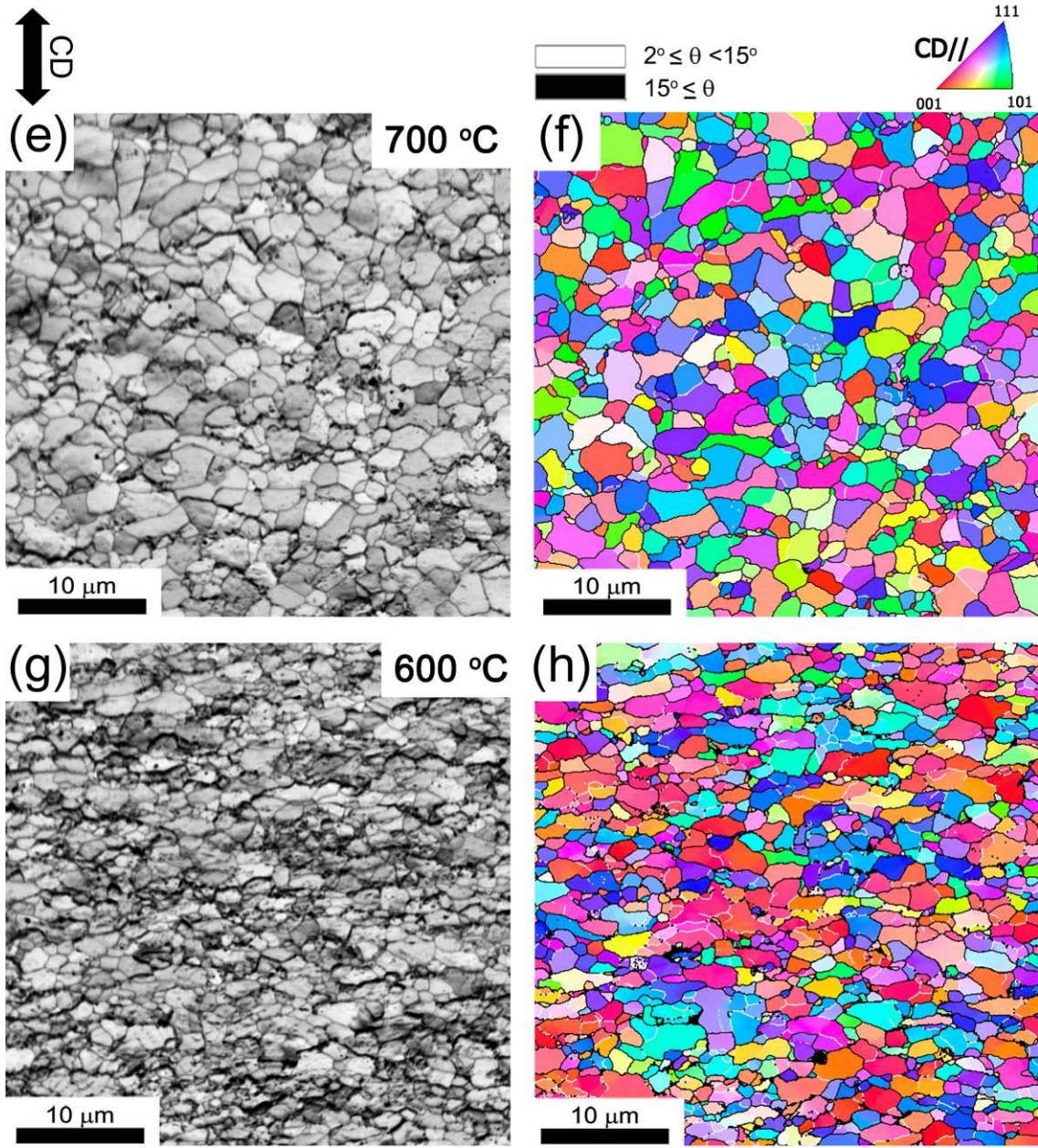
119

Fig. 4.3.3 (continued)

120

ferrite grains in the IPF maps indicates that ferrite grains were subsequently deformed after nucleation, as discussed in Chapter 2.   As a result, the number of ferrite grains containing low angle boundaries is increased with decreasing deformation temperature.

Figure 4.3.4 illustrates the inverse pole figures of the specimens deformed at various temperatures: (a) 750 ℃, (b) 730 ℃, (c) 700 ℃, (d) 650 ℃ and (e) 600 ℃.   The identical logarithmic scale with maximum 1.5 multiples of a random distribution (MRD) is set to compare texture intensities quantitatively, and its color intensity is shown in the upper right hand corner.   As mentioned above, components $<001>_\alpha$ and $<111>_\alpha$ parallel to the compression direction are preferentially developed in the ferrite grains.   However, ferrite grains in the specimens deformed at high temperatures above 700 ℃ (**Figs. 4.3.4a-c**) do not have any specific texture component, but show nearly random distribution of crystallographic
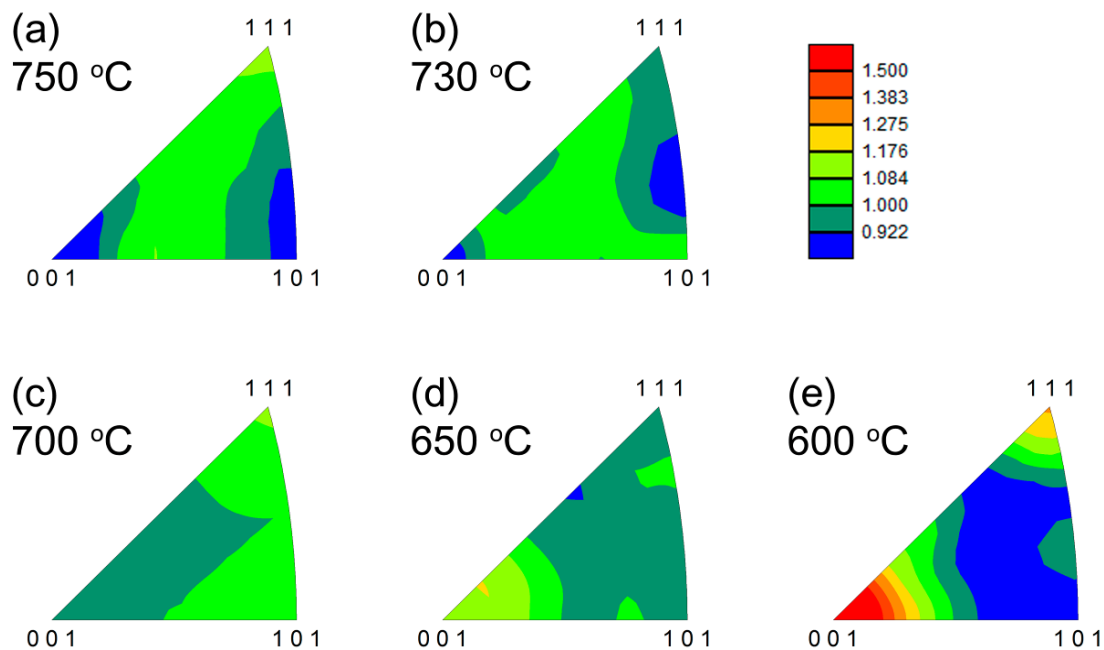

Fig. 4.3.4 Inverse pole figures of the specimens deformed at a strain rate of 10^{-1} s^{-1} to a strain of 0.96 at various temperatures: (a) 750 ℃, (b) 730 ℃, (c) 700 ℃, (d) 650 ℃ and (e) 600 ℃. The identical logarithmic scale with 1.5 multiples of a random distribution (MRD) maximum is set to compare texture components quantitatively, and its color intensity is shown in the upper right hand corner.

orientations.   Meanwhile, ferrite grains in the specimens deformed at low temperatures, i.e.
650 and 600 ℃ (**Figs. 4.3.4d-e**), have preferred orientation of $<001>_\alpha$ and $<111>_\alpha$ although
intensities of texture components are much weaker than those shown in **Fig. 4.2.6**.

   Figure 4.3.5 shows the distributions of grain average misorientation (GAM) obtained
from EBSD measurement of ferrite grains in the specimens deformed at various
temperatures: (a) 730 ℃, (b) 700 ℃, (c) 650 ℃ and (d) 600 ℃.   The mean GAM values are
also displayed in each figure.   The change in the mean GAM values as a function of
deformation temperature is illustrated in **Fig. 4.3.5e**.   As shown in Chapter 2.2, the mean
GAM value of statically transformed ferrite grains was 0.28 °.   As deformation temperature
decreases, the width of distribution increases, and the mean GAM values simultaneously
increases as shown in **Fig. 4.3.5e**.

   Figure 4.3.6 shows the distributions of misorientation angle between neighboring grains
in the specimens deformed at various temperatures: (a) 730 ℃, (b) 700 ℃, (c) 650 ℃ and (d)
600 ℃.   Solid lines in each figure indicate random distribution of misorientation which is
known as Mackenzie distribution [3,4].   Because it is difficult to extract boundaries between
ferrite and martensite, some portion of misorientation angles might be overestimated in **Figs.
4.3.6a** and **b** where the microstructure of the specimens consists of martensite and ferrite
together.   Fractions of low angle boundaries in the specimens deformed at low temperatures
are much larger than those deformed at high temperatures.

   Figures 4.3.2 to **4.3.6** revealed that the dynamically transformed ferrite consists of
deformation microstructures when the deformation temperature decreases.   One interesting
feature is that the morphology of ferrite grains at high temperatures was equiaxed without any
strong texture although the specimens were plastically deformed and containing high mean
GAM values.   In general, plastically deformed metallic materials have preferred
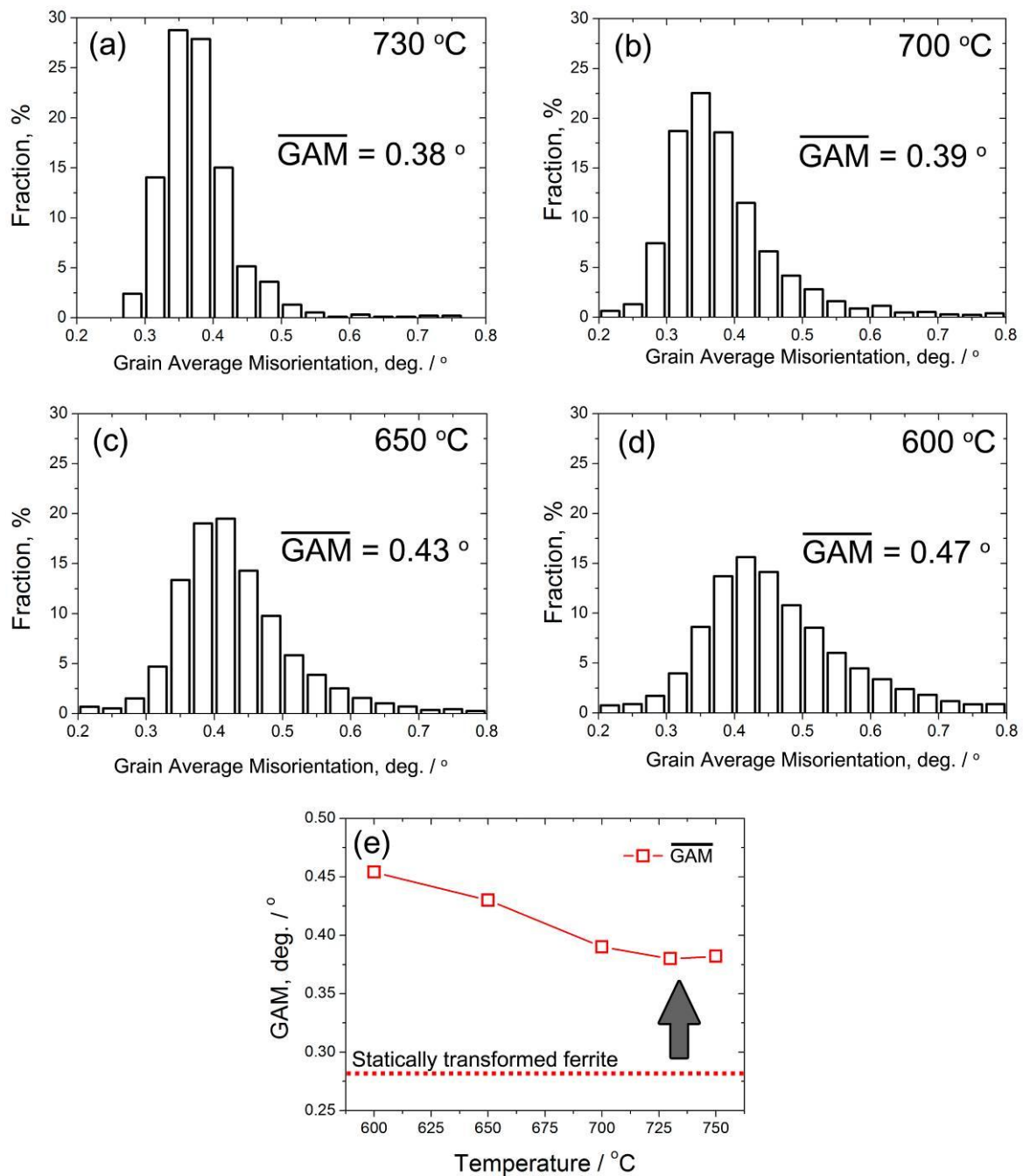
Fig. 4.3.5 Distributions of grain average misorientation (GAM) obtained from EBSD measurements in the specimens deformed at a strain rate of 10^{-1} s^{-1} to a strain of 0.96 at various temperatures: (a) 730 ℃, (b) 700 ℃, (c) 650 ℃ and (d) 600 ℃. (e) The change in the mean GAM values as a function of deformation temperature. The mean GAM value of statically transformed ferrite grains (0.28 °) is marked as a dashed line in (e).
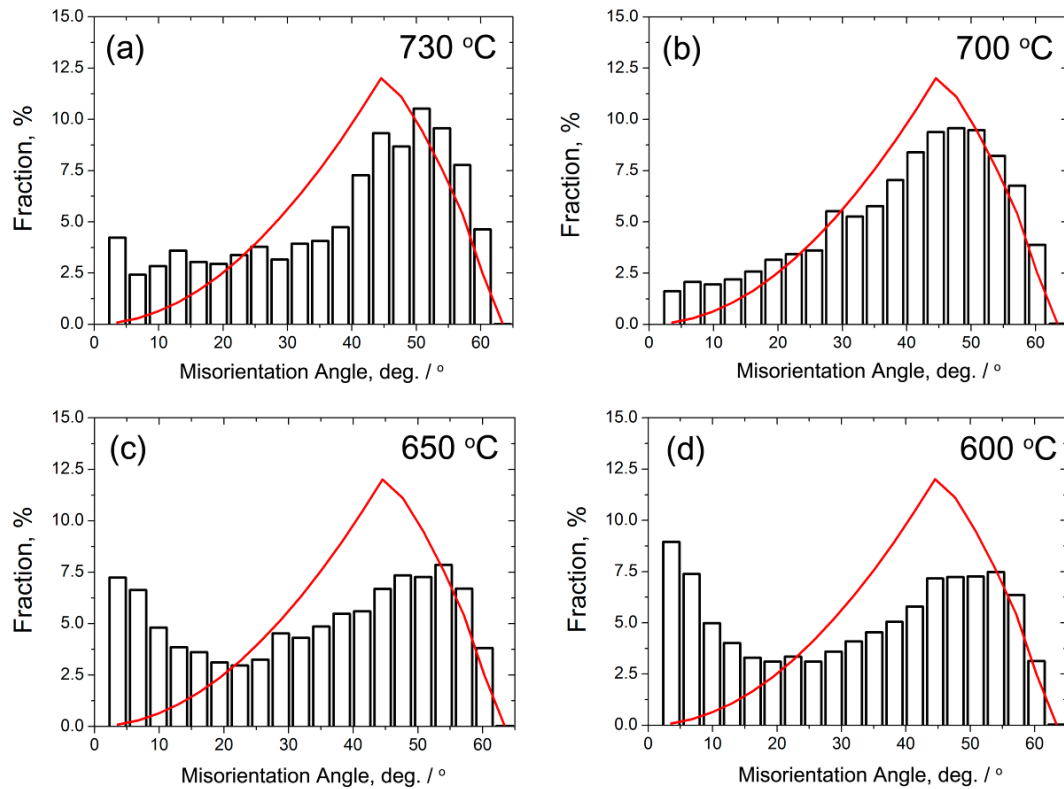
crystallographic

Fig. 4.3.6 Distributions of misorientation angle between neighboring grains in the specimens deformed at a strain rate of 10^{-1} s^{-1} to a strain of 0.96 at various temperatures: (a) 730 ℃, (b) 700 ℃, (c) 650 ℃ and (d) 600 ℃ obtained from EBSD measurements.   Solid lines in each figure indicate random distribution of misorientation.

crystallographic orientations, i.e., deformation texture, depending on deformation mode, and grains deformed by compression are usually elongated perpendicular to the compression direction.   Additionally, it is well known that ferrite grains could be easily recovered during deformation, i.e., dynamic recovery.   When dynamically transformed ferrite grains coexisting with austenite are recovered during subsequently deformation, the ferrite grains are essentially elongated perpendicular to the compression direction, and subgrains are developed inside due to dynamic recovery of ferrite.   However, morphology of ferrite grains in the specimens deformed at higher temperatures ranging from 700 to 750 ℃ in **Fig. 4.3.3** is not elongated, but equiaxed although the mean GAM values of ferrite grains in the specimens are higher than that of statically transformed ferrite grains.

There is another possibility that ferrite grains transformed at higher temperatures are subsequently deformed, so that the free energy of ferrite itself rises due to the increase in stored energy in ferrite as shown in **Fig. 2.3.8**.   These ferrite grains containing high free energy, compared to the free energy of undeformed austenite at a given temperature, could not be stable any longer, resulting in reverse transformation to austenite.   It was discussed in Chapter 3 that fraction of ferrite at 750 ℃ was kept constant during deformation, and it meant that dynamic ferrite transformation and reverse transformation to austenite was a reversible phenomenon.   Such a reversible transformation between ferrite and austenite during deformation might give us hints to explain why round and non-textured polygonal ferrite grains are formed.   The mechanism of reverse transformation from deformed ferrite to undeformed austenite at a give high temperature, for example, interphase boundary migration or nucleation of austenite, is not clarified yet in the present study.

Another possibility to explain the observed morphology is the rotation of ferrite grains during further deformation.   Wang et al. [57] reported (so-called) continuous dynamic recrystallization of ferrite (by continuous rotation of ferrite subgrains during rolling) in 0.17C-0.34Si-0.46Mn (wt.%) steel at intercritical temperatures regime, and it was described as follows.   At high strains, ferrite subgrain boundaries are pinned by the interphase boundary, and dynamic recovery in ferrite cannot be continued.   These constrained sub-boundaries absorb dislocations continuously on further straining.   As a result, the misorientation between subgrains is gradually increased with increasing strain, and continuous dynamic recrystallization takes place.   More intensive study is required in order to clarify the reasons why the morphology of ferrite grains at high temperatures was equiaxed without any strong texture although the specimens were plastically deformed.

125

Figures **4.3.7a** and **b** show TEM images of the specimens deformed at lower temperatures (650 ℃ and 600 ℃, respectively). Double-headed arrows indicate the compression direction. Ferrite grains in both images are equiaxed, but slightly elongated perpendicular to the compression direction. Because dynamically transformed ferrite grains at these temperatures were subsequently deformed, those ferrite grains include many dislocations. The mean grain size of ferrite in **Figs. 4.3.7a** and **b** are about 1.2 μm and 0.8 μm, respectively. Concerning refinement of dynamically transformed ferrite, Hodgson et al. [58] mentioned the possibility of the occurrence of dynamic recrystallization of ferrite after dynamic ferrite transformation in a 0.06C-0.59Mn (wt.%) steel, but they also insisted that dynamic recrystallization of ferrite appears only in interstitial free steels with large amount of strains. Ok et al. [42] concluded, on the other hand, that ferrite was formed during deformation of austenite by massive transformation in a 0.15C-0.25Si-1.1Mn (wt.%) steel, and the grain refinement of dynamically transformed ferrite was achieved by dynamic recrystallization of massive ferrite. In the near future, it is necessary to investigate the roles of deformation both on austenite to occur dynamic transformation as well as on dynamically transformed ferrite.
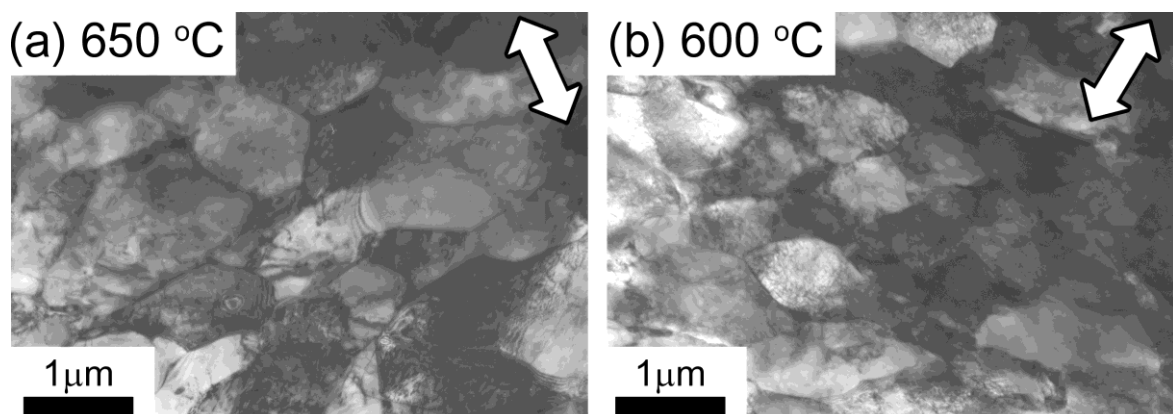

Fig. 4.3.7 TEM images of the specimens deformed at a strain rate of 10^{-1} s^{-1} to a strain of 0.96 at (a) 650 ℃ and (b) 600 ℃. Double-headed arrows indicate the compression direction.

The mean grain size of statically transformed ferrite at 650 °C from austenite having prior grain size of austenite of 15 μm in **Fig. 2.2.8** was around 6 μm, but that of dynamically transformed ferrite at the identical temperature in **Fig. 4.3.7a** was 1.2 μm, indicating that dynamic transformation with subsequent plastic deformation can achieve grain refinement of ferrite. The average grain size of dynamically transformed ferrite with subsequent deformation to a strain of 0.96 is decreased with decreasing the deformation temperature as seen in **Fig. 4.3.3**, and **Fig. 4.3.8a** shows the change in the average ferrite grain size as a function of deformation temperature. It is well-known that the size of dynamically recrystallized grains decreases with increasing Zener-Hollomon parameter. The average ferrite grain size shown in **Fig. 4.3.8a** is plotted again in **Fig. 4.3.8b** as a function of Zener-Hollomon parameter using an apparent activation energy of $Q = 254$ kJ mol^{-1} [55]. **Figure 4.3.8b** also includes the data in previous reports [55,59,60]. Tsuji et al. [55] reported the sizes of dynamically recrystallized ferrite grains and subgrains in the deformed specimens of a Ti-added interstitial free steel. Ohmori et al. [59] reported the change in ferrite grain sizes
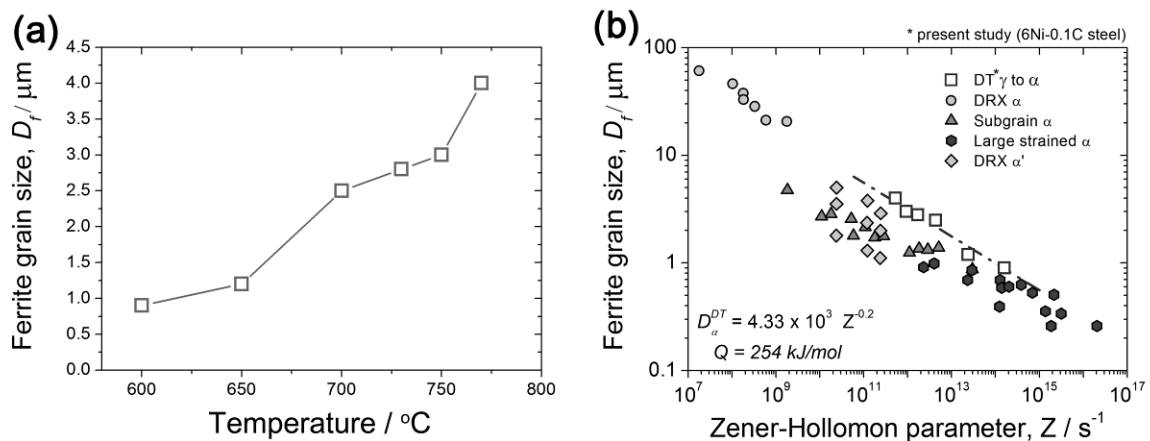

Fig. 4.3.8 Change in the average ferrite grain size as functions of (a) deformation temperature and (b) Zener-Hollomon parameter with an apparent activation energy of 254 kJ mol^{-1}. Open squares in (b) are the data obtained in the present study. Data from Refs. [55,59,60] are included in (b): circles and triangles from Ref. [55], hexagons from Ref. [59] and diamonds from Ref. [60].

in the specimens deformed to large strain using a 0.16C-1.43Mn-0.41Si steel (wt.%). Grain sizes of ferrite formed through deformation of tempered martensite were also reported using a (0.1-0.8)C-2Mn steels (wt.%) [60]. All those reports including the present study reveal that the change in the ferrite grain size, regardless of a chemical composition or a deformation mode, is governed by Zener-Hollomon parameter of deformation. One interesting point in the present study is that the ferrite grain size at higher temperature is obeyed by Zener-Hollomon parameter although microstructure at these temperatures in specimens consists of ferrite and austenite together.

4.3.4 Summary

We investigated the effect of deformation temperature on microstructures of dynamically transformed ferrite at wide temperature ranges.   When deformation temperature was high, equiaxed ferrite grains having random crystallographic orientation were formed. On the other hand, when deformation temperature was low, ferrite grains were elongated perpendicular to the compression axis, and contained many low angle boundaries with a number of dislocations.   Crystallographic textures, $<001>_\alpha$ and $<111>_\alpha$ parallel to uniaxial compressive direction, were developed in the ferrite grains formed at low temperature.   The mean GAM values of ferrite in all specimens fabricated in the present study were much higher than that of statically transformed ferrite.   The mean grain size of ferrite was governed by Zener-Hollomon parameter.   It decreased with decreasing deformation temperature under a constant strain rate, and reached down to 0.8 μm at 600 ℃ deformation.

4.4 Effect of strain rate on microstructure of dynamically transformed ferrite

4.4.1 Introduction

In section 4.2, the effects of strain and deformation temperature on microstructural evolution in dynamic transformation was revealed. With increasing plastic strain, Widmanstätten-like ferrite grains formed initially in the vicinity of austenite grain boundaries and they grew into interior of austenite grains. Finally dynamic transformation was completed, and plastic deformation of ferrite only took place, resulting in the ferrite grains elongated perpendicular to the compression direction with strong compression texture of ferrite.

It is well known that the evolution of deformed microstructure and the amount of lattice defects are significantly influenced by the deformation condition, such as temperature and strain rate [61–75]. The defects in deformed austenite would play important roles as nucleation sites or growth paths for dynamically transformed ferrite [66,67]. In this section, it is discussed how nucleation sites or growth paths for dynamic transformation are affected by strain rate in austenite deformation, by comparing microstructures of dynamically transformed ferrite in the Fe-6Ni-0.1C alloy with that of deformed austenite in a Fe-31Ni alloy.

4.4.2 Experimental procedure

The material used in the present study is the Fe-6Ni-0.1C alloy used in the previous section, as shown in **Table 2.2.1**. As-received hot rolled plate of the 6Ni-0.1C steel was homogenized at 1100 ℃ for 24 hours, and then quenched in water. The detailed thermomechanical processes used in this study are shown in **Fig. 4.4.1**. After austenitization at 1200 ℃ for 180 s, cylindrical specimens 12 mm in height and 8 mm in diameter were cooled to the deformation temperature (650 ℃), and held for 60 s. To simulate the effect of strain rate on dynamic transformation, the specimens were deformed at strain rates of 10^{-1} or 10^{-2} s^{-1} at 650 ℃ to a strain of 0.96 (60% reduction in height) as shown in **Fig. 4.4.1a**. The Fe-31Ni alloy, of which microstructure was 100% austenite at room temperature, was used to study microstructure of deformed austenite. The detailed chemical composition of the Fe-31Ni is shown in **Table 4.4.1**. Cylindrical specimens 9 mm in height and 6 mm in diameter of the Fe-31Ni were compressed at 750 ℃ at strain rates of 10^{-1} and 10^{-2} s^{-1} after annealing at 1200 ℃ for 180 s as shown in **Fig. 4.4.1b**. After compression, all specimens were immediately cooled by water-injection, at a cooling rate of approximately
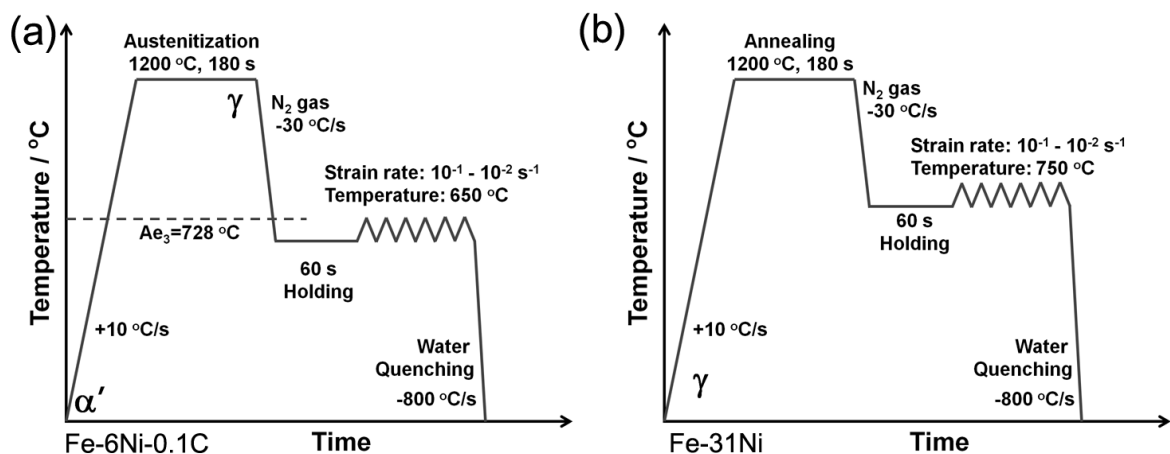

Fig. 4.4.1 Schematic illustrations of the thermomechanical processes in compression for (a) dynamic transformation and (b) deformation of the Fe-31Ni austenite steel.

800 °C s^{-1}.   Mica and glass powder were used in the hot-compression test as insulator and lubricant.   Microstructural observation was carried out by EBSD and transmission electron microscopy.

Table 4.4.1 Chemical composition of the Fe-31Ni alloy (wt.%).

C	Si	Mn	P	S	Ni	Fe
0.005	0.005	0.01	0.002	0.008	30.8	Bal.

4.4.3 Results

Figure 4.4.2 shows (a) the image quality (IQ) map and (b) corresponding inverse pole figure (IPF) map of the Fe-6Ni-0.1C specimen deformed at a strain rate of 10^{-1} s^{-1} to a strain of 0.96 at 650 ℃. Bright and dark areas in the IQ map (**Fig. 4.4.2a**) indicate dynamically transformed ferrite grains and martensite, respectively. Dashed white lines represent prior austenite grain boundaries, and double-headed arrows indicate the directions along which
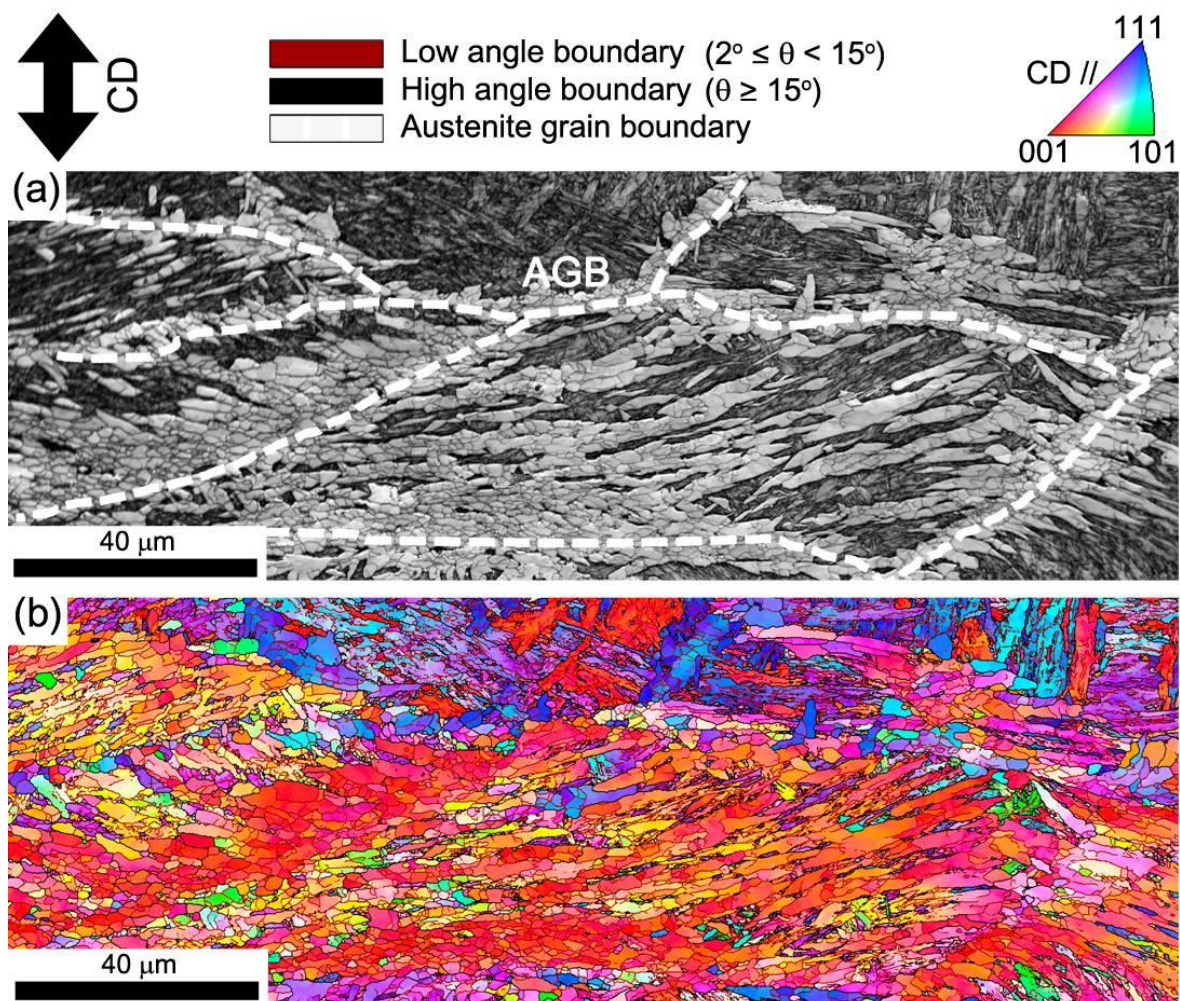

Fig. 4.4.2 (a) Image quality (IQ) map and (b) corresponding inverse pole figure (IPF) map of the specimen deformed at a strain rate of 10^{-1} s^{-1} to a strain of 0.96 at 650 ℃. Bright and dark areas in (a) indicate ferrite and martensite, respectively. Dashed white lines indicate prior austenite grain boundaries. The low angle boundaries with misorientation of 2-15° and the high angle boundaries with misorientation above 15° are also drawn in red and black lines, respectively.

ferrite grains grew. The colors in the IPF maps in **Fig. 4.4.2b** indicate the crystallographic orientation parallel to the compression direction at each measured point, according to the key stereographic triangle shown in the figure. The low angle boundaries with misorientation of 2 to 15 ° and the high angle boundaries with misorientation above 15 ° are also drawn in red and black lines, respectively. The fraction of ferrite grains is different depending on the austenite grains. Most of the austenite grain boundaries are covered by fine ferrite grains, and large numbers of ferrite grains are found within austenite grains. Widmanstätten-like ferrite plates grew along identical directions in each austenite grain, and these directions are different depending on the austenite grains. The ferrite grains in each austenite grain have similar orientation as shown in **Fig. 4.4.2b**.

Figure 4.4.3 shows the (a) IQ map and (b) corresponding IPF map of the Fe-6Ni-0.1C specimen deformed at a strain rate of 10^{-2} s^{-1} to a strain of 0.96 at 650 ℃. As shown in **Figs. 4.4.3a** and **b**, austenite grain boundaries indicated by dashed white lines are decorated by equiaxed ferrite grains. Some grains are surrounded by high angle boundaries. In addition, many Widmanstätten-like ferrite plates grew into austenite grains, and the growth direction of the ferrite grains is almost identical in each austenite grain. In the Widmanstätten-like ferrite grains, deformation microstructures with large numbers of low angle boundaries are developed. Containing many low angle boundaries and the changes in orientation within the ferrite grains indicate that dynamically transformed ferrite was subsequently deformed after nucleation, as discussed in Chapter 4.

Microstructural differences of dynamically transformed ferrite grains between **Fig. 4.4.2** and **Fig. 4.4.3** are possibly due to the difference in strain rate in deformation. In order to understand microstructural development of ferrite at different strain rates, it is necessary to study the microstructure of deformed austenite before dynamic transformation, because
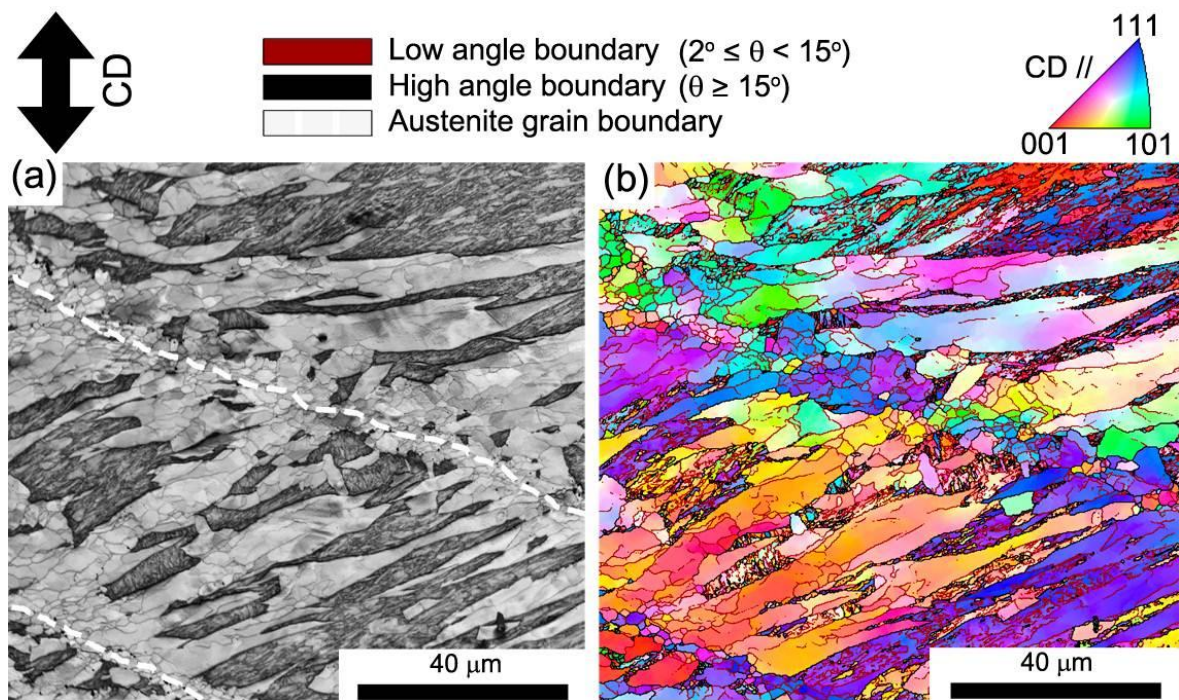
Fig. 4.4.3 (a) Image quality (IQ) map and (b) corresponding inverse pole figure (IPF) map of the specimen deformed at a strain rate of 10^{-2} s^{-1} to a strain of 0.96 at 650 ℃. Bright and dark areas in (a) indicate ferrite and martensite, respectively. Dashed white lines show prior austenite grain boundaries. The low angle boundaries with misorientation of 2-15 ° and the high angle boundaries with misorientation above 15 ° are also drawn in red and black lines, respectively.

lattice defects in deformed austenite play important roles for nucleation and growth of ferrite grains during transformation [65–67,75]. The deformation microstructures of austenite in the Fe-31Ni, which is deformed at a strain rate of 10^{-1} s^{-1} to a strain of 0.96 at 750 ℃, are shown in **Fig. 4.4.4**. IQ map and corresponding IPF map show that coarse austenite grain in the middle is surrounded by many fine recrystallized austenite grains. The deformed coarse grain contains large numbers of low angle boundaries, and the crystallographic orientation of this grain shows a typical deformation texture, $<101>_\gamma$, of austenite under uniaxial compression in **Fig. 4.4.4b**. A local area marked by a dashed square is chosen in **Fig. 4.4.4b**, and its KAM map and $\{111\}_\gamma$ pole figure are displayed in **Figs. 4.4.4c** and **d**, respectively. The traces of low angle boundaries are overlapped with those of KAM contrast in **Figs. 4.4.4c**.
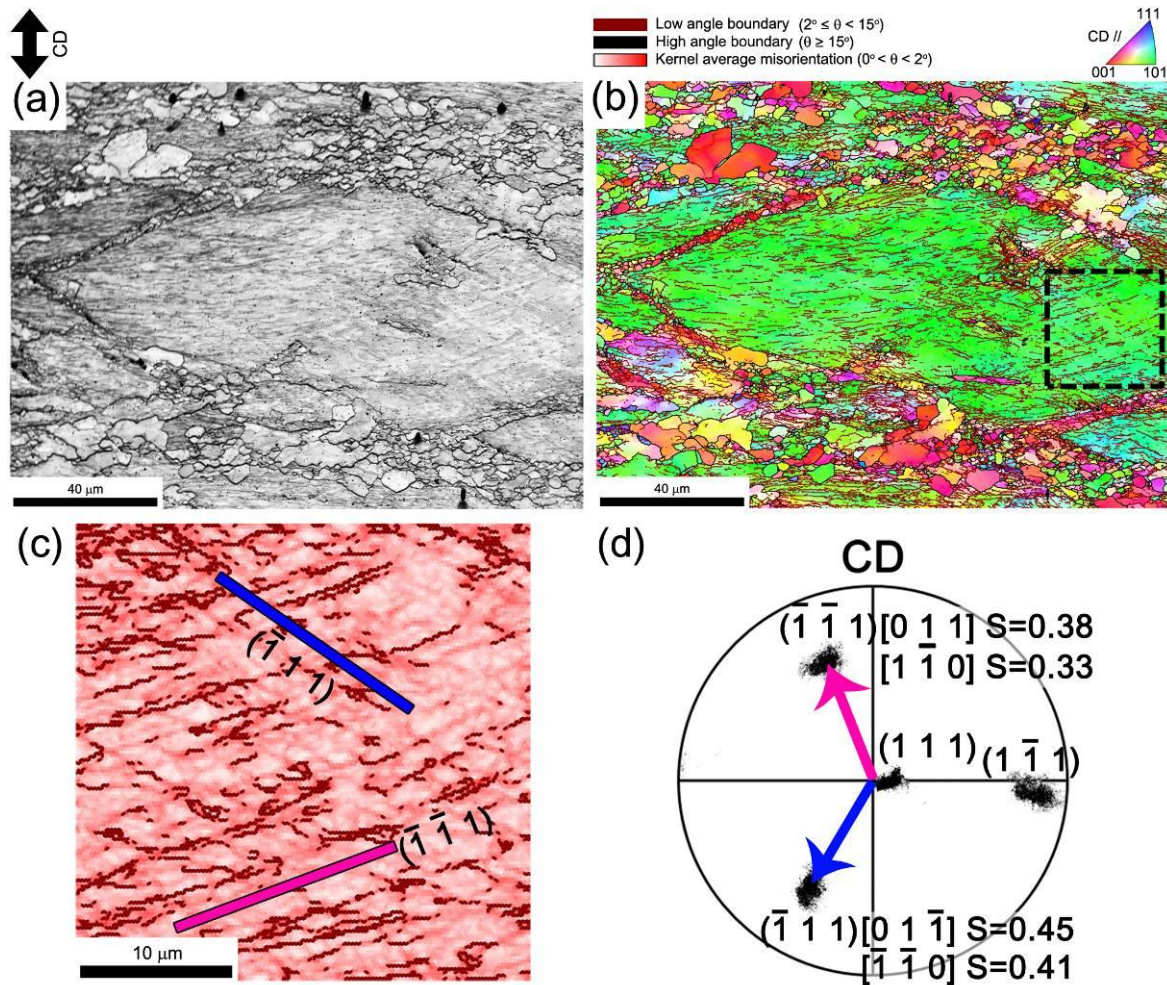
135

Fig. 4.4.4 (a) Image quality (IQ) map and (b) corresponding inverse pole figure (IPF) map obtained from EBSD measurement of a Fe-31Ni alloy deformed at a strain rate of 10^{-1} s^{-1} to a strain of 0.96 at 750 ℃. (c) Kernel average misorientation maps of the region marked in (b). (d) $\{111\}_\gamma$ pole figure showing crystallographic orientation of austenite along compression direction. The low angle boundaries with misorientation of 2-15° and the high angle boundaries with misorientation above 15° are also drawn in red and black lines, respectively. Slip system which shows high Schmid factor is displayed in (d) with its Schmid factor, S.

Those traces are parallel to the traces of $\{111\}_\gamma$ planes of austenite in **Figs. 4.4.4c**. The $\{111\}_\gamma$ planes whose traces are parallel to the traces of low angle boundaries are slip planes having high values of Schmid factors in **Fig. 4.4.4d**.

136

Figures **4.4.5a** and **b** are TEM images showing the microstructures of the Fe-31Ni alloy specimens deformed to a strain of 0.96 at 750 ℃ at strain rates of 10^{-1} and 10^{-2} s^{-1}, respectively.　　Arrows in **Figs. 4.4.5a** and **b** indicate microbands in austenite.　　In **Fig. 4.4.5a**, two series of microbands elongated to different directions are obviously observed with a large number of dislocations.　　In **Fig. 4.4.5b**, on the other hand, microbands are not well developed compared with those in **Fig. 4.4.5a**, but there are numerous dislocations.
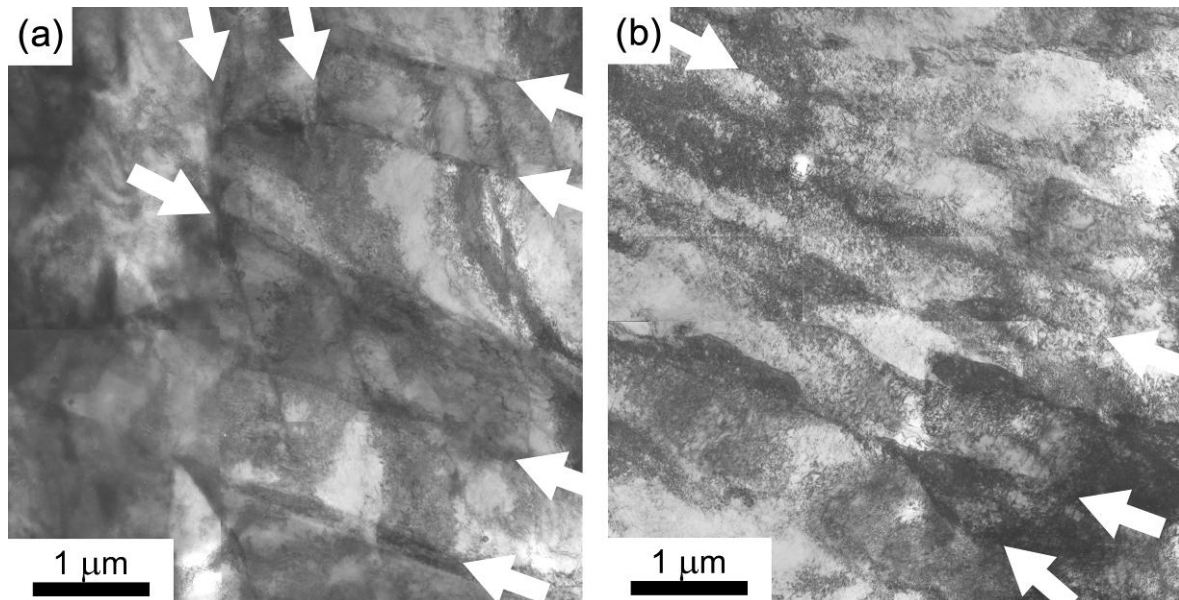

Fig. 4.4.5 TEM images of the Fe-31Ni alloy deformed at 750 ℃ to a strain of 0.96 at different strain rates: (a) $\dot{\varepsilon} = 10^{-1}$ s^{-1}, (b) $\dot{\varepsilon} = 10^{-2}$ s^{-1}.　　Microbands are indicated by arrows.

4.4.4 Discussion

The number density and the size of ferrite grains are apparently different depending on strain rate as shown in **Fig. 4.4.2** and **Fig. 4.4.3**, and such differences possibly are generated by different strain rates in deformation. Planar deformation structures (such as microbands) along $\{111\}_\gamma$ were found in the deformed austenite (**Fig. 4.4.4**), and different deformation microstructure owing to different strain rates of austenite deformation are seen in **Fig. 4.4.5**. Hurley et al. [66] have suggested that intragranular ferrite grains may nucleate along the microband interface. When a high strain rate is applied to austenite, large amount of microbands are formed, and it may be enough to lower the activation energy for nucleation of ferrite in austenite grain interior. As a result, high number density and fine size of intragranular ferrite grains could form, i.e., nucleation dominant process happens. When austenite is deformed at a relatively low strain rate, on the other hand, the density of defects in austenite grains interior might not be enough to form intragranular ferrite grains, but sufficient to assist the growth of ferrite grains, i.e., growth-dominant process occurs.

Based on these results together with the materials discussed in Chapter 4.2 (the effect of strain on microstructural evolution in dynamic transformation), the effect of strain rate on the mechanism of dynamic transformation could be classified into two processes, i.e., nucleation- or growth-dominant ones, and these are schematically illustrated in **Fig. 4.4.6**. Specimens having coarse austenite grains are compressed at different strain rates, i.e., high and low strain rates. (a) Austenite is plastically deformed at a high strain rate, and microbands are well developed within austenite grains. (b) With increasing strain, the austenite grain is elongated perpendicular to the compressive direction, and ferrite grains are dynamically formed at austenite grain boundaries. In addition, many intragranular ferrite grains form on microbands inside the austenite grain, for example, intersections of different microbands as
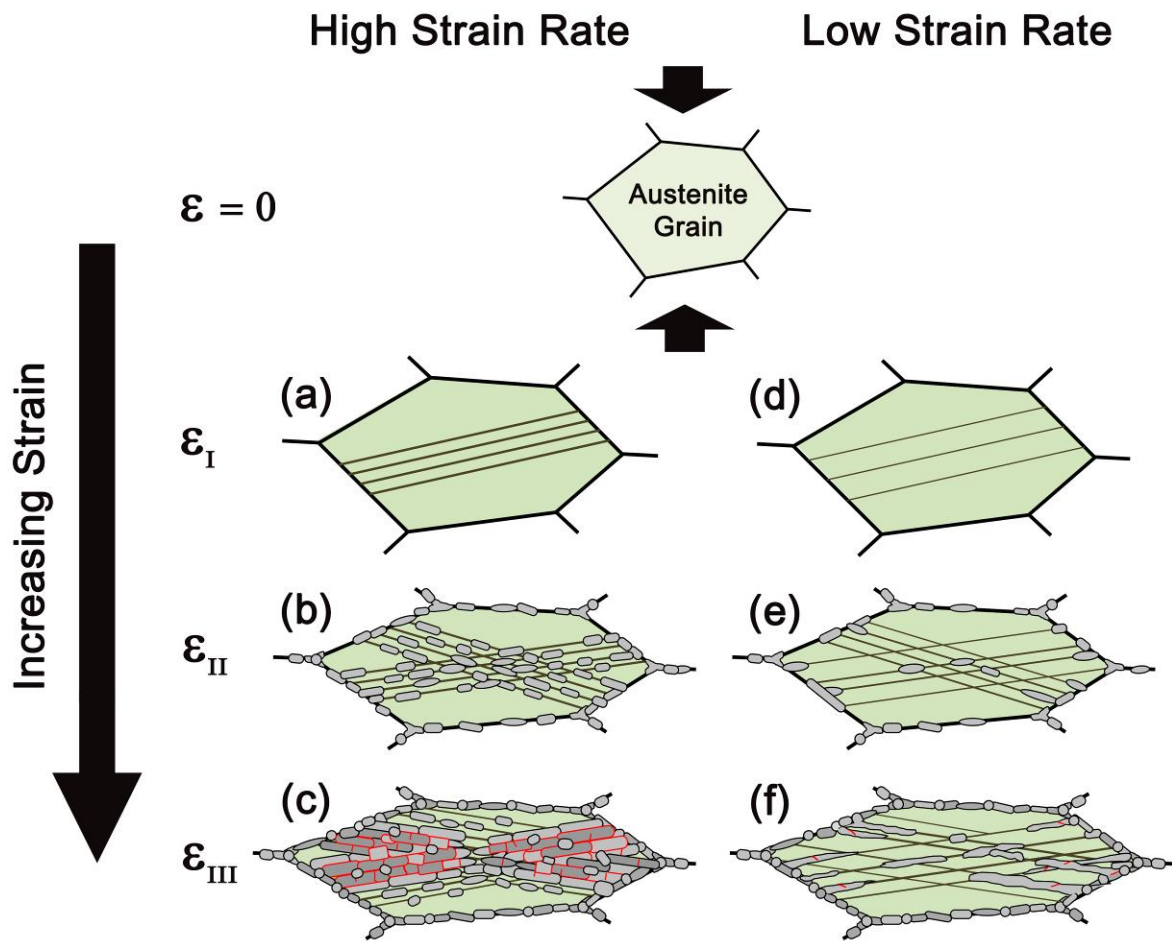
High Strain Rate   **Low Strain Rate**

$\varepsilon = 0$

Austenite Grain

Increasing Strain

(a) ε_{I} (d)

(b) $\varepsilon_{\mathrm{II}}$ (e)

(c) $\varepsilon_{\mathrm{III}}$ (f)

Fig. 4.4.6 Schematic illustration showing the evolution of microstructures in austenite and ferrite under deformation at different strain rates.   The low and high angle boundaries are drawn in red and black lines, respectively.

t***spacers**** re

shown in **Fig. 4.4.5a**.   (c) With increasing deformation strain of austenite, some ferrite grains grow along the microbands.   Coalescence of these ferrite grains forms plate-shaped ferrite involving low angle boundaries, because those ferrite grains have similar orientation. Equiaxed ferrite grains are also formed within the austenite grain.   (d) When the strain rate is low, in contrast, large numbers of dislocations are generated and are aligned on specific slip planes as shown in **Fig. 4.4.5b**.   (e) Ferrite grains are preferentially formed on austenite grain boundaries, and few numbers of ferrite grains are formed in austenite grains.   (f) With

increasing strain, the existing ferrite grains grow along microbands or dislocation boundaries so that the fraction of plate-shaped (Widmanstätten-like) ferrite increases. Some of the grown Widmanstätten-like ferrite grains are subsequently deformed or new Widmanstätten-like ferrite grains are formed near the tip of their former plates, resulting in development of low angle boundaries inside or between the grains. Equiaxed ferrite grains form in the vicinity of austenite grain boundaries as well. Therefore, it could be summarized that, depending on strain rate, the microstructural development through dynamic transformation is different; when the strain rate is high, nucleation of ferrite occurs dominantly in austenite grain interior, while growth dominant process of dynamically transformed ferrite grains would occur when the strain rate is low.

4.4.5 Summary

We investigated the effect of strain rate on microstructure of dynamic ferrite transformation.   The major results are summarized as follows:

1. When the strain rate was high, a lot of intragranular ferrite grains were found.   Those grains had similar crystallographic orientations.   In contrast, when the strain rate was low, plate-shaped ferrite grains grew from austenite grain boundaries into austenite grain interior. In both cases, fine ferrite grains primarily formed in the vicinity of austenite grain boundaries, and deformation microstructures were seen within the ferrite grains.

2. In order to understand the effect of strain rate on microstructural evolution in dynamic ferrite transformation, microstructures of the Fe-31Ni alloy deformed at different strain rates were observed.   When strain rate of austenite deformation was high, microbands were frequently formed, which might enable intragranular ferrite formation in dynamic transformation.   When the strain rate was low, dislocation cell structures were generated, which would assist a growth of ferrite grains in dynamic transformation.

3. Consequently, the microstructural evolution in dynamic transformation is classified into two types.   When the strain rate is high, nucleation of ferrite in austenite grains is dominant. When the strain rate is low, in contrast, ferrite grains can easily grow into austenite grains from austenite grain boundaries.

4.5 Mechanical properties of dynamically transformed ferrite

4.5.1 Introduction

Ferrite grain refinement, which is one of the strengthening mechanisms in steels, has been a hot issue in metallurgical engineering field to improve mechanical properties without losing ductility and toughness. There are many reports studying grain refinement of ferrite in low-carbon steels through thermomechanical controlled processing. Dynamic transformation to ferrite studied in the present study is also one way to achieve finer ferrite grain size. Even though many research groups studied about dynamic transformation, there are few reports about the mechanical properties of dynamically transformed ferrite [58,76,77]. This section studies mechanical properties of dynamically transformed ferrite.

4.5.2 Experimental procedure

4.5.2.1 Thermomechanical processes

The material used in the present study is the same alloy (Fe-6Ni-0.1C), as shown in **Table 2.2.1**. As-received hot rolled plate was homogenized at 1100 ℃ for 24 hours, and then quenched in water. Three different heat treatments shown in **Fig. 4.5.1**were conducted. In order to obtain the specimens with statically transformed ferrite (**Fig. 4.5.1a**), a thin plate whose dimension was 20 mm × 5 mm × 2 mm was austenitized at 800 ℃ for 180 s in a salt bath. The austenitized plate was cooled slowly at an average cooling rate of 1.5 ℃ min^{-1} from 800 ℃ to 100 ℃. The second and third specimens were fabricated using the thermomechanical simulator. After the specimens 12 mm in height and 8 mm were installed
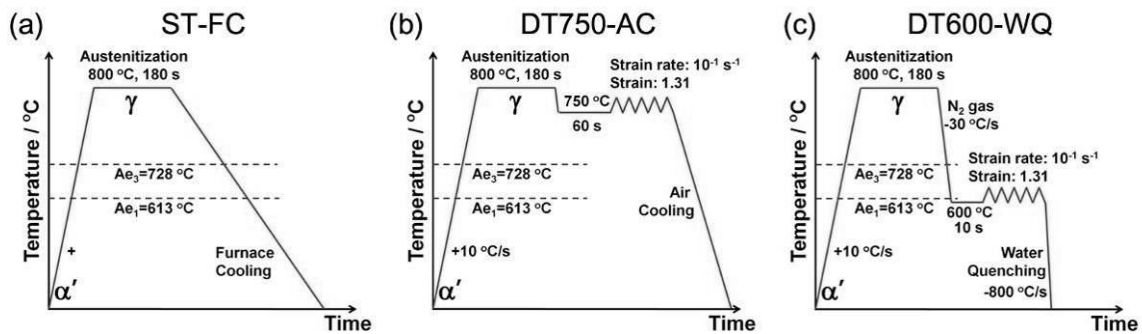
Fig. 4.5.1 Schematic illustrations of the thermomechanical processes in compression deformation. Ae_3 and Ae_1 calculated by Thermo-Calc were marked at 728 °C and 613 °C, respectively.

in the machine, they were austenitized at 800 °C for 180 s. Austenitized specimens were cooled by N_2 gas at a cooling rate of 30 °C s^{-1} to different temperatures. As shown in **Fig. 4.5.1b**, the austenitized specimen was cooled to 750 °C in the second procedure. After keeping at 750 °C for 60 s, the specimen was compressed at a strain rate of 10^{-1} s^{-1} to a strain of 1.31 in order to obtain a microstructure with dynamically transformed ferrite (fraction of 55%), as shown in section 2.3. And then, the compressed specimen was cooled by N_2 gas at a cooling rate of 5 °C s^{-1} after releasing compression loading. In the third procedure, the specimen was cooled to 600 °C after austenitization at 800 °C, as shown in **Fig. 4.5.1c**. After keeping at 600 °C for 10 s, the specimen was deformed at a strain rate of 10^{-1} s^{-1} to a strain of 1.31, and then it was quenched to room temperature by precisely controlled water-injection. Mica and glass powder were used in the hot-compression test as insulator and lubricant. Hereafter, those three specimens are named as ST-FC, DT750-AC and DT600-WQ. First term, ST or DT indicates an occurrence of static or dynamic transformation, and 750 or 600 means the deformation temperature. The last term, FC, AC or WQ, represents a cooling method (furnace cooling, air cooling or water quenching).

4.5.2.2 Miniature tensile test

Sheet type miniature tensile test specimens were obtained from the compressed samples, as shown in **Fig. 4.5.2**.   The tensile direction was perpendicular to the compression direction as marked on the right hand side.   The center position of the deformed specimens was chosen to be the gauge part of the tensile test specimen, and the top and bottom surfaces of the compressed sample were mechanically polished.   The dimension of the gauge in the tensile test specimen is 2.0 mm (length) $\times$ 1.0 mm (width) $\times$ 0.5 mm (thickness).   In order to measure precise elongation during tensile test by using a CCD camera, indentation markers were carved by Vickers hardness tester with 4.40 N load (0.5Hv) for 10 s.   Tensile test was conducted at an initial strain rate of 8.3×10^{-4} s^{-1} at room temperature.   During setting a specimen on the tensile test machine, pre-strain was applied on a specimen, but it did not exceed 40 MPa (0.020 kN) which was lower than the yield strength of ferrite at room temperature.   10 images per second were captured by the CCD camera to measure a precise displacement of a tensile specimen.   Captured images were analyzed by image correlation software to measure the position of two markers on a tensile test specimen.
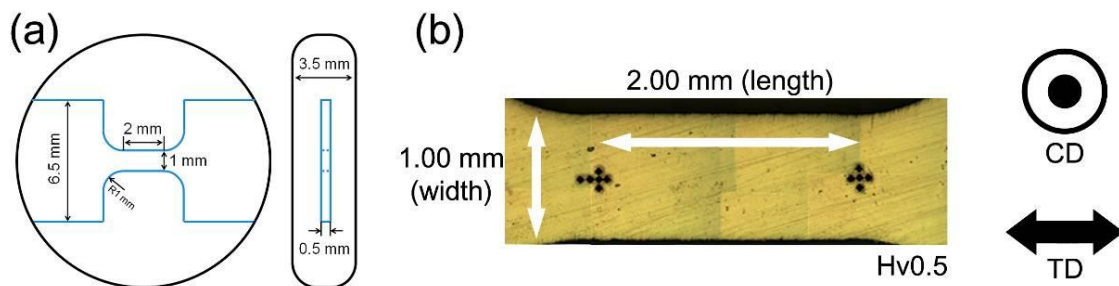

Fig. 4.5.2 (a) Illustrations of top and side views of a specimen deformed in compression to a strain of 1.31 to fabricate tensile test sample.   The dimension of a tensile test sample is 2.00 mm (length) $\times$ 1.0 mm (width) $\times$ 0.5 mm (thickness).   (b) Optical microscope image of the gauge part in a tensile specimen.   Directions of the compression in thermomechanical test and the tensile test are marked on the right hand side.

4.5.2.3 Microstructure observation

Microstructural observation was carried out by optical microscopy (OM) and electron back-scattering diffraction (EBSD) installed in SEM before the tensile test. The cross-section parallel to the compressive axis of the specimens was mechanically polished, followed by electro-polishing in a solution of 10% of perchloric acid ($HClO_4$) and 90% of acetic acid (CH_3COOH) at 25 ℃. 3% nital solution was used to reveal microstructures of the specimens. For the TEM observation, thin-foil specimens were prepared by twin-jet electro-polishing using the same solution as that used for the EBSD observation.

OM observation revealed that microstructures of both specimens, ST-FC and DT750-AC, consisted of ferrite and small amount of pearlite, but that of the specimen, DT600C-WQ, was composed of ferrite and martensite-austenite (MA) constituent. After tensile test, the fractured surfaces were observed by SEM.

4.5.3 Results and discussion

Figure 4.5.3 shows inverse pole figure (IPF) maps of the specimens (a) ST-FC, (b) DT750-AC and (c) DT600-WQ. The low angle boundaries with misorientation of 2 to 15 ° and the high angle boundaries with misorientation above 15 ° are drawn in red and black lines, respectively. Fraction of high angle boundary in **Fig. 4.5.3a** (ST-FC) is 93%, and the mean ferrite grain size is 8.0 μm when the grain size is measured using only high angle boundaries. On the other hand, when both low and high angle boundaries are used together to measure mean ferrite grain size, it is 7.5 μm. The value of mean grain average misorientation (GAM) in EBSD measurement is around 0.23 °. Detailed information of three specimens is summarized in **Table 4.5.1** as well. In the case of DT750-AC, fraction of dynamically transformed ferrite at 750 ℃ was around 55% as discussed in Chapter 3, and retained austenite is thought to transform to ferrite or pearlite during air cooling. In the IPF
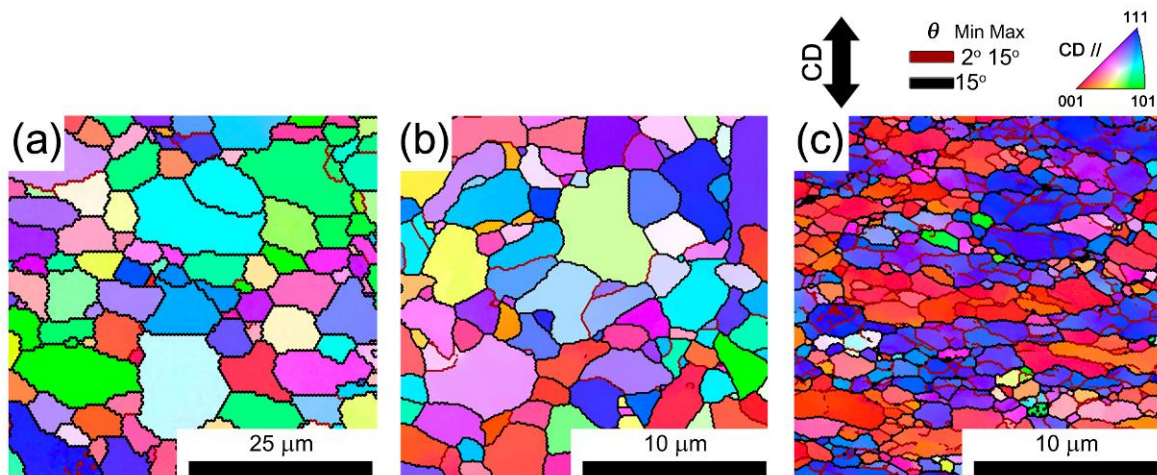

Fig. 4.5.3 Inverse pole figure maps of the specimens (a) ST-FC, (b) DT750-AC and (c) DT600-WQ. The low angle boundaries with misorientation of 2 to 15 ° and the high angle boundaries with misorientation above 15 ° are also drawn in red and black lines, respectively. Compression direction is parallel to the vertical axis of figures.

146

Table 4.5.1 Detailed information about microstructure observation results for three specimens.

		ST-FC	DT750-AC	DT600-WQ
Ferrite grain size	High angle boundary	8.0 μm	3.8 μm	3.5 μm
	All boundaries	7.5 μm	2.9 μm	1.2 μm
f_{HAB}		93%	89%	55%
Mean GAM		0.23 °	0.26 °	0.47 °

map of **Fig. 4.5.3b**, polygonal ferrite grains are observed with large fraction of high angle boundary (89%), and the mean ferrite grain size is much finer than that of the ST-FC specimen. The mean GAM value is 0.26 °, which indicates that the ferrite does not contain deformation microstructure so much. However, in the case of the DT600-WQ specimen (**Fig. 4.5.3c**), elongated ferrite grains containing large fraction of low angle boundaries are observed. Few numbers of equiaxed ferrite grains surrounded by high angle boundary are found. The mean GAM value of the ferrite structure is 0.47 °, which suggests that ferrite grains involve significant amount of deformation substructures and dislocations. TEM image of the specimen DT600-WQ is shown in **Fig. 4.3.7b**. Those ferrite grains contain large numbers of dislocations, which coincides with high GAM value in EBSD measurement.

Figure 4.5.4 shows stress-strain curves of three specimens, ST-FC, DT750-AC and DT600-WQ obtained by tensile test. All specimens show discontinuous yielding with Lüders deformation at the initial stage of deformation. Lower yield strength and tensile strength are increased with grain refinement, and total elongation is decreased with decreasing ferrite grain size. The detailed mechanical properties of the specimens are summarized in **Table 4.5.2**.
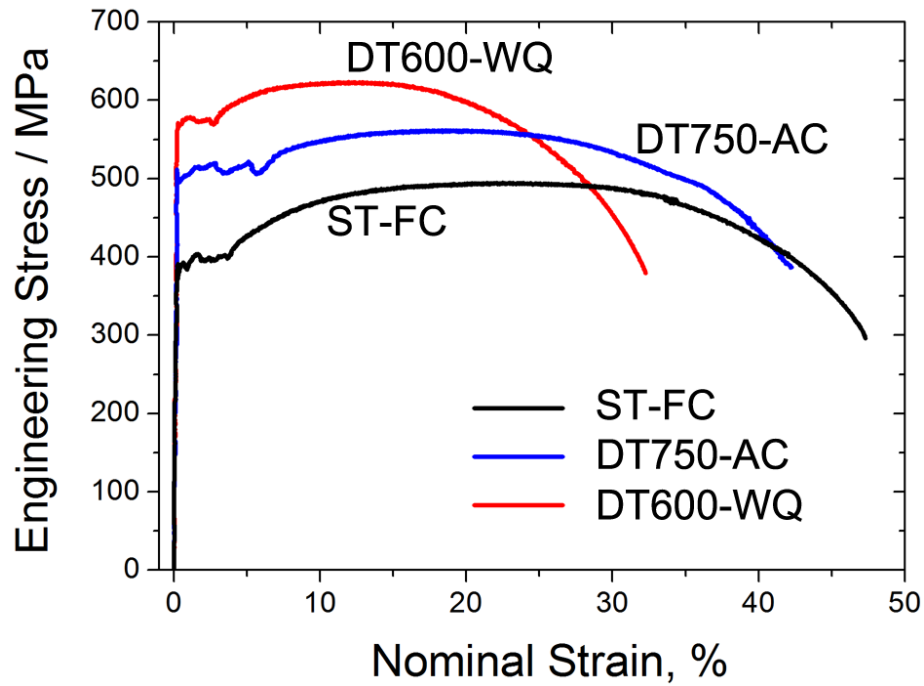
Fig. 4.5.4 Tensile stress-strain curves of three specimens, ST-FC, DT750-AC and DT600-WQ

Table 4.5.2 Detailed information about tensile test results for three specimens.

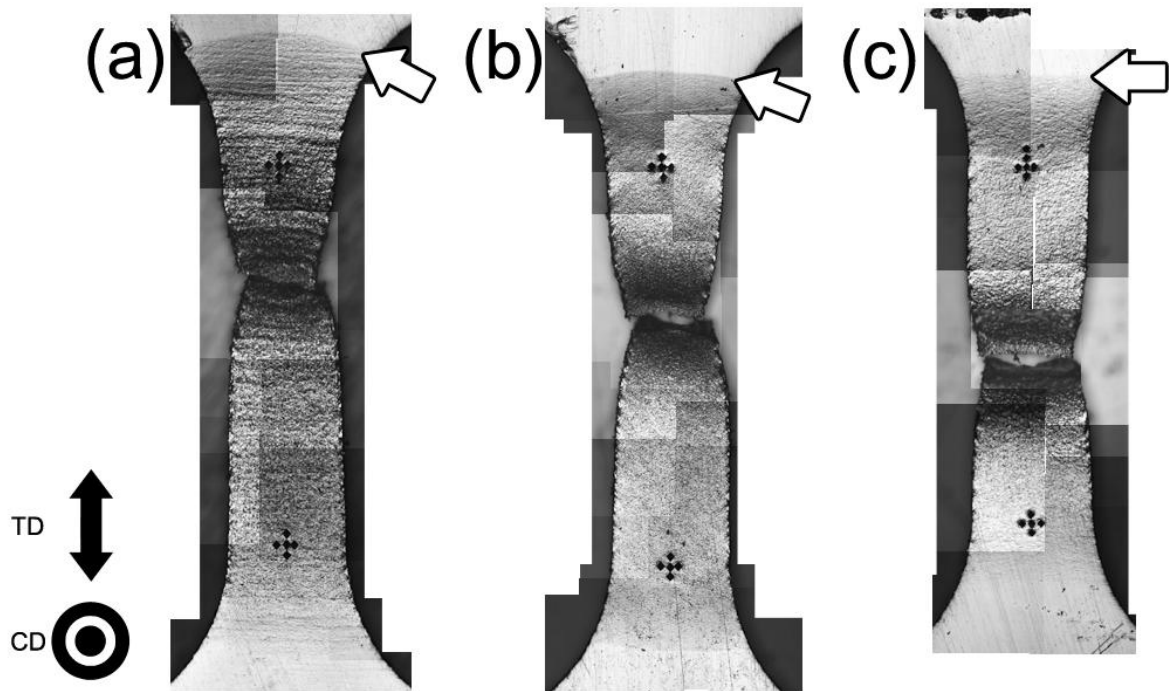|	ST-FC	DT750-AC	DT600-WQ
Lower yield strength	396 MPa	490 MPa	570 MPa
Tensile strength	495 MPa	560 MPa	623 MPa
Uniform elongation	23%	20%	12%
Total elongation	47%	42%	32%
Toughness	213 MPa	222 MPa	185 MPa
Reduction of area	75%	73%	69%

Fig. 4.5.5 Optical microscope images of fractured specimens. (a) ST-FC, (b) DT750-AC, (c) DT600-WQ. Arrows indicate the end of Lüders bands. Directions of both the compression in thermomechanical test and the tensile test are marked on the left hand corner.
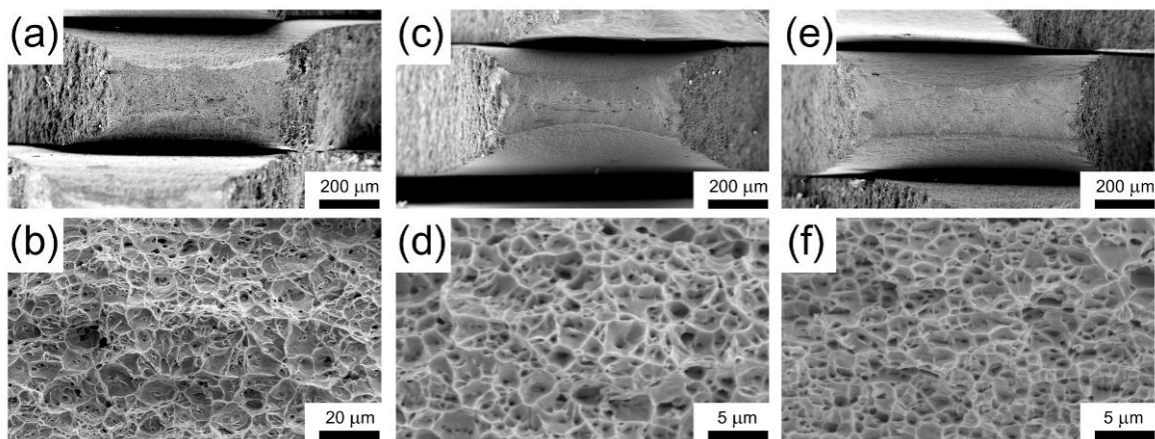

Fig. 4.5.6 SEM images of fractured surfaces in the specimens (a,b) ST-FC, (c,d) DT750-AC and (e,f) DT600-WQ.

Figure 4.5.5 shows the appearance of the specimens, (a) ST-FC, (b) DT750-AC and (c) DT600-WQ, after tensile test. All specimens are fractured within the gauge part, and it is clearly seen that Lüders band was expanded beyond gauge part as pointed by arrows. The widths near fractured parts in the ST-FC and DT750-AC are much narrower than that in the DT600-WQ.

Figure 4.5.6 shows SEM images of the fractured surfaces in the three specimens: (a,b) ST-FC, (c,d) DT750-AC and (e,f) DT600-WQ. Reductions in area (RA) obtained from **Figs. 4.5.6a,c** and **e** are 75, 73 and 69%, respectively. The change in RA also corresponds to the total elongation shown in **Fig. 4.5.5**. SEM images in **Figs. 4.5.6b,d** and **f** show that fracture surfaces consist of spherical dimples which is a typical characteristic of ductile fracture.

It is well known in polycrystalline metallic materials that yield strength is proportional to the inverse square root of grain size, which is so called Hall-Petch relationship [78–82]. **Figure 4.5.7** shows lower yield strengths of the specimens as a function of inverse square root of the grain size. Square, circle and triangle indicate the data of the specimens ST-FC, DT750-AC and DT600-WQ, respectively. Dashed line represents a conventional Hall-Petch relationship of low carbon steels ($\sigma_y [MPa] = 100 + 600 \times d^{-1/2} [\mu m]$) [82]. Dash-dotted line has the same gradient ($600 MPa \cdot \mu m^{1/2}$) of the dashed line, and passes through points of the present specimens, ST-FC and DT750-AC. The mean ferrite grain size was measured by two different definition in the present study as mentioned above (**Table 4.5.1**), and only that obtained from high angle boundaries were regarded as ferrite grain size in **Fig. 4.5.7**. The difference between dashed line and dash-dotted line is around 84 MPa, and this could be considered as a sum of the solid solution hardening due to 6 wt.% Ni in ferrite and the hardening due to small amount of pearlite. In the case of the specimen DT600-WQ, on the other hand, there is an extra hardening of around 67 MPa from the dash-dotted line. A
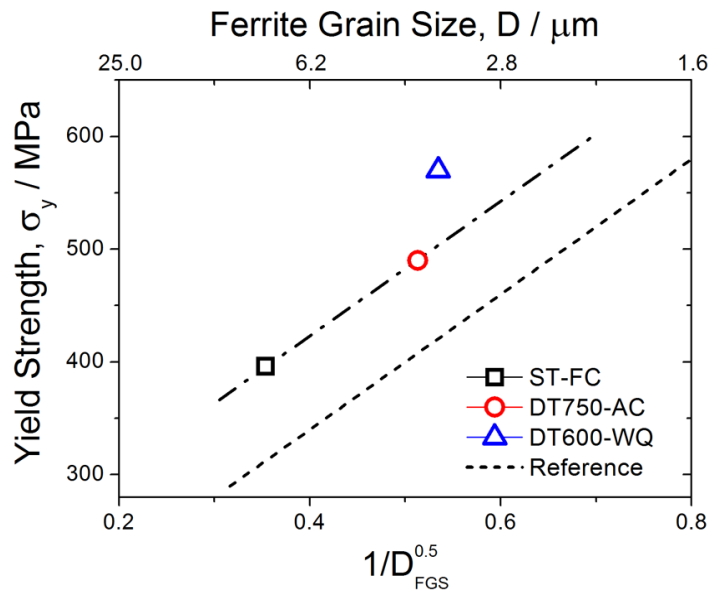
Fig. 4.5.7 Lower yield strengths of the specimens (square: ST-FC, circle: DT750-AC, triangle: DT600-WQ) in the present study as a function of the inverse square root of the ferrite grain size. Dashed line represents the conventional Hall-Petch relationship of low carbon steels [82]. Dash-dotted line is a parallel shift of the dashed line passing through ST-FC datum.

dislocation hardening or an existence of MA constituents could be attributed to the increase in the yield strength of the DT600-WQ specimen. As seen in **Fig. 4.5.4** and high mean GAM in **Table 4.5.1**, ferrite is strain hardened and contains a numbers of dislocations. 5% of MA constituents might improve strength of the material, too.

One interesting finding in the present study is the change in Lüders strain in **Fig. 4.5.5**. It has been reported that Lüders strain increases with decreasing ferrite grain size [83,84], or with decreasing carbon concentration [84]. However, the Lüders strain of the specimen DT600-WQ in **Fig. 4.5.5**. is shortened even though ferrite grain size is decreased. If carbon concentration in dynamically transformed ferrite is higher than its solubility at a given temperature as reported by Tong et al. [46,47], a shortening of Lüders band would happen even though the grain size of dynamically transformed ferrite is decreased. A precise chemical analysis is required to understand this mechanism in detail.

4.5.4 Summary

The mechanical properties of dynamically transformed ferrite were compared with those of statically transformed ferrite in the 6Ni-0.1C steel through tensile test using miniaturized specimens.   The major results are summarized as follows:

1. Dynamically transformed ferrite had higher yield and tensile strengths compared to statically transformed ferrite.   It could be attributed to dislocation hardening or existence of MA constituents in the DT materials.   However, total elongation of dynamically transformed ferrite was slightly smaller than that of the statically transformed ferrite.

2. The decrease in Lüders elongation was observed when the mean ferrite grain size decreased.   Further systematic studies are required to unveil the hardening mechanisms of dynamically transformed ferrite in future.

4.6 Conclusions

In this chapter, the characteristics of dynamically transformed ferrite were investigated. First of all, the effect of strain on microstructure evolution of ferrite was discussed. Widmanstätten-like ferrite grains were formed, and its crystallographic orientation had Kurdjumov-Sachs and Nishiyama-Wassermann relationships with austenite depending on the portions. Dynamically transformed ferrite with subsequent deformation showed typical deformation textures of ferrite under uniaxial compression ($<001>_\alpha$ and $<111>_\alpha$).

Secondly, the effect of deformation temperature on dynamic transformation was investigated. Polygonal ferrite grains were obtained at high temperatures, but elongated ferrite grains containing many low angle boundaries were formed at low temperatures. Grain size of dynamically transformed ferrite was decreased with decreasing deformation temperature.

Next, nucleation behavior of ferrite was studied at different strain rates. When the strain rate was high, large numbers of intragranular ferrite grains were observed. On the other hand, when the strain rate was low, grain growth of ferrite was dominant. It was concluded that nucleation density of ferrite within austenite could be modulated by changing the strain rate.

Finally, miniature tensile test was carried out to study the mechanical properties of dynamically transformed ferrite. Both yield and ultimate tensile strengths of dynamically transformed ferrite increased compared with those of statically transformed ferrite, which was attributed to strain hardening or existence of martensite-austenite constituents. Lüders strain of dynamically transformed ferrite was shortened even though the grain size of ferrite decreased.

4.7 References

[1] R. Yoda, T. Yokomaku, and N. Tsuji, "Plastic deformation and creep damage evaluations of type 316 austenitic stainless steels by EBSD," *Materials Characterization*, vol. 61, pp. 913–922, 2010.

[2] M. Calcagnotto, Y. Adachi, D. Ponge, and D. Raabe, "Deformation and fracture mechanisms in fine- and ultrafine-grained ferrite/martensite dual-phase steels and the effect of aging," *Acta Materialia*, vol. 59, pp. 658–670, 2011.

[3] J. Mackenzie and M. J. Thomson, "Some statistics associated with the random disorientation of cubes," *Biometrika*, vol. 44, pp. 205–210, 1957.

[4] J. K. Mason and C. a. Schuh, "The generalized Mackenzie distribution: Disorientation angle distributions for arbitrary textures," *Acta Materialia*, vol. 57, pp. 4186–4197, 2009.

[5] F. J. Humphreys and M. Hatherly, *Recrystallization and related annealing phenomena*, 2nd ed., vol. 54. Pergamon, 2004.

[6] G. Miyamoto, N. Iwata, N. Takayama, and T. Furuhara, "Quantitative analysis of variant selection in ausformed lath martensite," *Acta Materialia*, vol. 60, pp. 1139–1148, 2012.

[7] M. Hillert, "On the Formation of Widmanstätten Austenite," *Metallurgical Transactions A*, vol. 17, p. 741, 1986.

[8] A. Ali and H. K. D. H. Bhadeshia, "Nucleation of Widmanstätten ferrite," *Materials Science and Technology*, vol. 6, pp. 781–784, 1990.

[9] M. Enomoto, "Thermodynamics and kinetics of the formation of Widmanstätten ferrite plates in ferrous alloys," *Metallurgical and Materials Transactions A*, vol. 25, pp. 1947–1955, 1994.

[10] Y. Ohmori, H. Ohtsubo, Y. C. Jung, S. Okaguchi, and H. Ohtani, "Morphology of bainite and Widmanstätten ferrite," *Metallurgical and Materials Transactions A*, vol. 25, pp. 1981–1989, 1994.

[11] G. Spanos and M. G. Hall, "The formation mechanism(s), morphology, and crystallography of ferrite sideplates," *Metallurgical and Materials Transactions A*, vol. 27, pp. 1519–1534, 1996.

[12] J. Yang and L. Chang, "The effect of stress on the Widmanstätten ferrite transformation," *Materials Science and Engineering A*, vol. 223, pp. 158–167, 1997.

[13] S. Jones and H. K. D. H. Bhadeshia, "Kinetics of the Widmanstätten ferrite transformation in steel," *International Conference on Displacive Phase Transformations and Their Applications in Materials Engineering*, pp. 419–426, 1998.

[14] R. . Larn and J. . Yang, "The effect of compressive deformation of austenite on the Widmanstätten ferrite transformation in Fe–Mn–Si–C steel," *Materials Science and Engineering A*, vol. 264, pp. 139–150, 1999.

[15] C. H. Shek, C. Dong, J. K. L. Lai, and K. W. Wong, "Early-stage Widmanstätten growth of the gamma phase in a duplex steel," *Metallurgical and Materials Transactions A*, vol. 31, pp. 15–19, 2000.

[16] D. Phelan and R. Dippenaar, "Widmanstätten ferrite plate formation in low-carbon steels," *Metallurgical and Materials Transactions A*, vol. 35, pp. 3701–3706, 2004.

[17] M. V. Kral and G. Spanos, "Three-dimensional analysis and classification of grain-boundary-nucleated proeutectoid ferrite precipitates," *Metallurgical and Materials Transactions A*, vol. 36, pp. 1199–1207, 2005.

[18] K. G and S. G., "Kurdjumov-Sachs orientation relationship," *Zeitschrift für Physik*, vol. 64, p. 325, 1930.

[19] Z. Nishiyama, *Sci. Rep. Tohoku Univ.*, vol. 23, p. 637, 1934.

[20] G. Wassermann, *Arch. Eisenhüttenwes*, vol. 6, pp. 347–351, 1933.

[21] S. Zaefferer, J. Ohlert, and W. Bleck, "A study of microstructure, transformation mechanisms and correlation between microstructure and mechanical properties of a low alloyed TRIP steel," *Acta Materialia*, vol. 52, pp. 2765–2778, 2004.

[22] J. D. Watson and P. G. McDougall, "The crystallography of widmanstätten ferrite," *Acta Metallurgica*, vol. 21, pp. 961–973, 1973.

[23] A. D. King and T. Bell, "Morphology and crystallography of Widmanstätten proeutectoid ferrite," *Metal Science*, vol. 8, pp. 253–260, 1974.

[24] S. Morito, H. Tanaka, R. Konishi, T. Furuhara, and T. Maki, "The morphology and crystallography of lath martensite in Fe-C alloys," *Acta Materialia*, vol. 51, pp. 1789–1799, 2003.

[25] H. Kitahara, R. Ueji, N. Tsuji, and Y. Minamino, "Crystallographic features of lath martensite in low-carbon steel," *Acta Materialia*, vol. 54, pp. 1279–1288, 2006.

[26] J. R. Patel and M. Cohen, "Criterion for the action of applied stress in the martensitic transformation," *Acta Metallurgica*, vol. 1, pp. 531–538, 1953.

[27] S. Kundu, K. Hase, and H. K. D. H. Bhadeshia, "Crystallographic texture of stress-affected bainite," *Proceedings of the Royal Society A: Mathematical, Physical and Engineering Sciences*, vol. 463, pp. 2309–2328, 2007.

[28] M. P. Butrón-Guillén, C. S. Costa Viana, and J. J. Jonas, "A variant selection model for predicting the transformation texture of deformed austenite," *Metallurgical and Materials Transactions A*, vol. 28, pp. 1755–1768, 1997.

[29] J. J. Jonas, Y. He, and S. Godet, "The possible role of partial dislocations in facilitating transformations of the Nishiyama–Wassermann type," *Scripta Materialia*, vol. 52, pp. 175–179, 2005.

[30] N. J. Wittridge and J. J. Jonas, "The austenite-to-martensite transformation in Fe–30%Ni after deformation by simple shear," *Acta Materialia*, vol. 48, pp. 2737–2749, 2000.

[31] W. Gong, Y. Tomota, M. S. Koo, and Y. Adachi, "Effect of ausforming on nanobainite steel," *Scripta Materialia*, vol. 63, pp. 819–822, 2010.

[32] H. Yada, T. Matsumura, and T. Senuma, "No Title," *Proc. Int. Conf. Physical Metallurgy of Themomechanical Processing of Steels and Other Metals, ISIJ*, vol. Thermec 88, pp. 200–207, 1988.

[33] Y. Matsumura and H. Yada, "Evolution deformation of ultrafine-grained ferrite in hot successive deformation," *Transactions ISIJ*, vol. 27, pp. 492–498, 1987.

[34] T. B. Massalski, S. K. Bhattacharyya, and J. H. Perepezko, "Enhancement of plastic flow during massive transformations," *Materials Transactions A*, vol. 9, pp. 53–56, 1978.

[35] T. Massalski, "Distinguishing features of massive transformations," *Metallurgical and Materials Transactions A*, vol. 15, pp. 421–425, 1984.

[36] M. R. Plichta, W. A. T. Clark, and H. I. Aaronson, "The nucleation kinetics, crystallography, and mechanism of the massive transformation," *Metallurgical Transactions A*, vol. 15, pp. 427–735, 1984.

[37] M. Hillert, "Thermodynamics of the massive transformation," *Metallurgical Transactions A*, vol. 15, pp. 411–419, 1984.

[38] T. B. Massalski, "Massive transformations revisited," *Metallurgical and Materials Transactions A*, vol. 33, pp. 2277–2283, 2002.

[39] H. I. Aaronson, S. Mahajan, G. R. Purdy, and M. G. Hall, "Origins of internal structure in massive transformation products," *Metallurgical and Materials*, vol. 33, pp. 2347–2351, 2002.

[40] M. Hillert, "Communications: Nature of massive transformation," *Metallurgical and Materials Transactions A*, vol. 35, pp. 351–352, 2004.

[41] H. I. Aaronson, "Mechanisms of the massive transformation," *Metallurgical and Materials Transactions A*, vol. 33, pp. 2285–2297, 2002.

[42] S. Y. Ok and J. K. Park, "Dynamic austenite-to-ferrite transformation behavior of plain low carbon steel within (α+γ) 2-phase field at low strain rate," *Scripta Materialia*, vol. 52, pp. 1111–1116, 2005.

[43] J. K. Park, K. H. Kim, J. H. Chung, and S. Y. Ok, "Deformation-induced austenite-to-ferrite massive transformation in medium carbon steel," *Metallurgical and Materials Transactions A*, vol. 39, pp. 235–242, 2008.

[44] C. Zheng, N. Xiao, L. Hao, D. Li, and Y. Li, "Numerical simulation of dynamic strain-induced austenite–ferrite transformation in a low carbon steel," *Acta Materialia*, vol. 57, pp. 2956–2968, 2009.

[45] C. Zheng, D. Li, S. Lu, and Y. Li, "On the ferrite refinement during the dynamic strain-induced transformation: A cellular automaton modeling," *Scripta Materialia*, vol. 58, pp. 838–841, 2008.

[46] M. Tong, D. Li, Y. Li, J. Ni, and Y. Zhang, "Monte carlo-method simulation of the deformation-induced ferrite transformation in the Fe-C system," *Metallurgical and Materials Transactions A*, vol. 35, pp. 1565–1577, 2004.

[47] M. Tong, J. Ni, Y. Zhang, D. Li, and Y. Li, "Temporal oscillatory behavior in deformation induced ferrite transformation in an Fe–C binary system," *Scripta Materialia*, vol. 50, pp. 909–913, 2004.

[48] A. Shibata, "Substructure and crystallographic features of ferrous lenticular martensite," Kyoto University, 2007.

[49] T. Sakai and J. Jonas, "Overview no. 35 Dynamic recrystallization: Mechanical and microstructural considerations," *Acta Metallurgica*, vol. 32, pp. 189–209, 1984.

[50] J. Savoie, R. Ray, M. Butronguillen, and J. Jonas, "Comparison between simulated and experimental transformation textures in a Nb microalloyed steel," *Acta Metallurgica et Materialia*, vol. 42, pp. 2511–2523, 1994.

[51] L. Briottet, J. J. Jonas, and F. Montheillet, "A mechanical interpretation of the activation energy of high temperature deformation in two phase materials," *Acta Materialia*, vol. 44, pp. 1665–1672, 1996.

[52] J. J. Jonas, X. Quelennec, L. Jiang, and É. Martin, "The Avrami kinetics of dynamic recrystallization," *Acta Materialia*, vol. 57, pp. 2748–2756, 2009.

[53] N. Tsuji, Y. Matsubara, and Y. Saito, "Dynamic recrystallization of ferrite in interstitial free steel," *Scripta Materialia*, vol. 37, pp. 477–484, 1997.

[54] L. Longfei, Y. Wangyue, and S. Zuqing, "Dynamic recrystallization of ferrite in a low-carbon steel," *Metallurgical and Materials Transactions A*, vol. 37, pp. 609–619, 2006.

[55] N. Tsuji, Y. Matsubara, Y. Saito, and T. Maki, "Occurrence of dynamic recrystallization in ferritic iron," *Journal of Japan Institute of Metals*, vol. 62, pp. 967–976, 1998.

[56] R. Wang and T. Lei, "Deformation and restoration behaviour of ferrite-austenite two-phase structures," *Materials Science and Engineering A*, vol. 165, pp. 19–27, 1993.

[57] R. Z. Wang and T. C. Lei, "Dynamic recrystallization of ferrite in a low carbon steel during hot rolling in the (F+A) two-phase range," *Scripta Metallurgica et Materialia*, vol. 31, pp. 1193–1196, 1994.

[58] P. Hodgson, M. R. Hickson, and R. K. Gibbs, "Ultrafine ferrite in low carbon steel," *Scripta Materialia*, vol. 40, pp. 1179–1184, 1999.

[59] A. Ohmori, S. Torizuka, K. Nagai, N. Koseki, and Y. Kogo, "Effect of deformation temperature and strain rate on evolution of ultrafine grained structure through single-pass large-strain warm deformation in a low carbon," *Materials transactions*, vol. 45, pp. 2224–2231, 2004.

[60] B. Poorganji, G. Miyamoto, T. Maki, and T. Furuhara, "Formation of ultrafine grained ferrite by warm deformation of lath martensite in low-alloy steels with different carbon content," *Scripta Materialia*, vol. 59, pp. 279–281, 2008.

[61] A. Belyakov, Y. Kimura, and K. Tsuzaki, "Microstructure evolution in dual-phase stainless stee during severe deformation," *Acta Materialia*, vol. 54, pp. 2521–2532, 2006.

[62] Y. T. Zhu, X. Z. Liao, and X. L. Wu, "Deformation twinning in nanocrystalline materials," *Progress in Materials Science*, vol. 57, pp. 1–62, 2012.

[63] X. Liu, J. K. Solberg, and R. Gjengedal, "Measurement of austenite-to-ferrite transformation temperature after multi-pass deformation of steels," *Materials Science and Engineering A*, vol. 194, pp. L15–L18, 1995.

[64] B. Eghbali, "Study on the ferrite grain refinement during intercritical deformation of a microalloyed steel," *Materials Science and Engineering A*, vol. 527, pp. 3407–3410, 2010.

[65] H. Ohtsuka, M. Umemoto, and I. Tamura, "Deformation structures in a work-hardened austenite," *Trans. Iron Steel Inst. Jpn.*, vol. 27, pp. 408–414, 1987.

[66] P. J. Hurley, B. C. Muddle, P. Hodgson, C. H. J. Davies, B. P. Wynne, P. Cizek, and M. R. Hickson, "Comparison of the Deformation Characteristics of a Ni-30wt% Fe Alloy and Plain Carbon Steel," *Materials Science Forum*, vol. 284–286, pp. 159–166, 1998.

[67] P. J. Hurley, B. C. Muddle, and P. D. Hodgson, "The production of ultrafine ferrite during hot torsion testing of a 0.11 wt pct C steel," *Metallurgical and Materials Transactions A*, vol. 33, pp. 2985–2993, 2002.

[68] G. Miyamoto, N. Iwata, N. Takayama, and T. Furuhara, "Variant selection of lath martensite and bainite transformation in low carbon steel by ausforming," *Journal of Alloys and Compounds*, 2012.

[69] T. Benjamin Britton and A. J. Wilkinson, "Stress fields and geometrically necessary dislocation density distributions near the head of a blocked slip band," *Acta Materialia*, vol. 60, pp. 5773–5782, 2012.

[70] B. Bay, N. Hansen, D. A. Hughes, and D. Kuhlmann-Wilsdorf, "Overview no. 96 evolution of f.c.c. deformation structures in polyslip," *Acta Metallurgica et Materialia*, vol. 40, pp. 205–219, 1992.

[71] D. Kuhlmann-Wilsdorf and N. Hansen, "Geometrically necessary, incidental and subgrain boundaries," *Scripta Metallurgica et Materialia*, vol. 25, pp. 1557–1562, 1991.

[72] N. Hansen, "Deformation microstructures," *Scripta Metallurgica et Materialia*, vol. 27, pp. 1447–1452, 1992.

[73] N. Hansen and D. J. Jensen, "Development of microstructure in FCC metals during cold work," *Philosophical Transactions of the Royal Society A: Mathematical, Physical and Engineering Sciences*, vol. 357, pp. 1447–1469, 1999.

[74] N. Hansen, R. F. Mehl, and A. Medalist, "New discoveries in deformed metals," *Metallurgical and Materials Transactions A*, vol. 32, pp. 2917–2935, 2001.

[75] A. Hiramatsu and M. Umemoto, "Computer modelling of phase transformation from work-hardened austenite," *ISIJ International*, vol. 32, pp. 306–315, 1992.

[76] R. Priestner and A. K. Ibraheem, "Processing of steel for ultrafine ferrite grain structures," *Materials Science and Technology*, vol. 16, pp. 1267–1272, 2000.

[77] Y. Choi, W. Y. Choo, and D. Kwon, "Analysis of mechanical property distribution in multiphase ultra-fine-grained steels by nanoindentation," *Scripta Materialia*, vol. 45, pp. 1401–1406, 2001.

[78] E. O. Hall, "The deformation and ageing of mild steel: III Discussion of results," *Proceedings of the Physical Society. Section B*, vol. 64, pp. 747–753, 1951.

[79] N. J. Petch, *Journal of the Iron and Steel Institute*, vol. 174, p. 25, 1953.

[80] X. Liu, M. Nagumo, and M. Umemoto, "The Hall-Petch relationship in nanocrystalline materials," *Materials transactions*, vol. 38, pp. 1033–1039, 1997.

[81] N. Hansen, "Hall-Petch relation and boundary strengthening," *Scripta Materialia*, vol. 51, pp. 801–806, 2004.

[82] K. Takeda, N. Nakada, T. Tsuchiyama, and S. Takaki, "Effect of interstitial elements on Hall–Petch coefficient of ferritic iron," *ISIJ International*, vol. 48, pp. 1122–1125, 2008.

[83] N. Tsuchida, Y. Tomota, K. Nagai, and K. Fukaura, "A simple relationship between Lüders elongation and work-hardening rate at lower yield stress," *Scripta Materialia*, vol. 54, pp. 57–60, 2006.

[84] R. Song, *Microstructure and mechanical properties of ultrafine grained C-Mn steels*. Shaker Verlag, 2004.

CHAPTER 5

SUMMARY AND CONCLUSIONS

In the present dissertation, the dynamic ferrite transformation has been studied in a Fe-6Ni-0.1C (wt.%) alloy. Ferrite was dynamically formed under certain deformation conditions, and the characteristics of dynamically transformed ferrite were investigated. The key results achieved in each chapter are summarized as follows.

In **Chapter 1**, the background and purpose of the present study were indicated.

In **Chapter 2**, the occurrence of dynamic transformation was confirmed and systematically investigated at various strain rates and temperatures by analyzing the stress-strain curves and observing the microstructures. The softening of the maximum flow stresses resulting from the occurrence of dynamic transformation was observed under certain deformation conditions determined by a critical Zener-Hollomon parameter (Z_C). When deformation condition, which was a combination of strain rate and deformation temperature, satisfied this criterion of the occurrence of dynamic transformation, the softening of the maximum stress happened. It was found that the stress-strain analysis could be a good measure for dynamic transformation. Dynamic transformation above equilibrium transformation temperature, Ae_3, was also confirmed. A thermodynamics approach enabled to interpret the formation of ferrite at temperatures above Ae_3. Microstructural observations revealed that dynamically transformed ferrite contained characteristics of deformation microstructures, such as a number of dislocations, sub-boundaries and so on, resulting in relatively large misorientation within each ferrite grain.

In **Chapter 3**, the kinetics of dynamic transformation was investigated under different deformation conditions by analyzing the stress-strain curves with microstructural observations.   In order to understand the relation between the change (softening) in flow stress and the kinetics of dynamic transformation, following two aspects were preferentially investigated.   Firstly, it was found that the onset of dynamic transformation was accelerated by refinement of austenite grain, similar to static transformation, because prior austenite grain boundaries acted as primary nucleation sites for ferrite.   Secondly, it was clarified that the decrease in flow stress was proportional to the increase in the fraction of dynamically transformed ferrite.   Consequently, the kinetics of dynamic transformation could be predicted through the change in flow stress.   The kinetics of dynamic transformation for two series of experiments with different deformation conditions were interpreted by the conventional and modified Johnson-Mehl-Avrami-Kolmogorov plots.   It was concluded in Chapter 3 that kinetics of dynamic transformation firmly depended on the amount of strain under given deformation conditions, and it was well fitted with the modified Johnson-Mehl-Avrami-Kolmogorov plot.

In **Chapter 4**, the effects of deformation conditions, such as strain, deformation temperature and strain rate, on microstructures of dynamically transformed ferrite were studied, and the miniature tensile test was carried out to investigate mechanical properties of dynamically transformed ferrite.   Retained austenite grains were found at room temperature when the austenitized specimen was deformed at a strain rate of 10^{-1} s^{-1} at 600 °C.   The retained austenite was considered to contain high concentration of carbon, which implied that dynamic ferrite transformation accompanied the partition (diffusion) of carbon from dynamically transformed ferrite into austenite.   Coarse Widmanstätten-like ferrite grains and fine equiaxed ferrite grains were formed together when the prior austenite grain size was

coarse (approximately 400 μm). The crystallographic orientations of Widmanstätten-like ferrite grains were almost identical within each prior austenite grain, but they involved certain misorientations within each plate. Kurdjumov-Sachs and Nishiyama-Wassermann orientation relationships between the retained austenite and the dynamically transformed ferrite were both observed.

The microstructure of dynamically transformed ferrite was also influenced by deformation temperature. With lowering deformation temperature, the grain size of dynamically transformed ferrite was decreased, and the change of ferrite grain size was organized a function of Z parameter. The degree of plastic deformation of ferrite was increased with decreasing deformation temperature.

The process of dynamic ferrite transformation was different depending on strain rate. When the strain rate was high, a number of intragranular ferrite grains were observed, indicating nucleation dominant process in dynamic transformation. When the strain rate was low, on the other hand, limited numbers of ferrite grains penetrated from prior austenite grain boundaries into inside of austenite, implying growth dominant process in dynamic transformation.

Mechanical properties of dynamically transformed ferrite were compared with those of statically transformed ferrite through miniature tensile test. Lower yield strength and tensile strength of dynamically transformed ferrite were higher than those of statically transformed ferrite, because dynamically transformed ferrite grains were strain-hardened during continuous deformation after the nucleation. Total elongation of dynamically transformed ferrite was shorter than that of statically transformed ferrite. The shortening of Lüders elongation was found in dynamically transformed ferrite even though the grain size of dynamically transformed ferrite was finer than that of statically transformed ferrite.

In this dissertation, the occurrence of dynamic ferrite transformation in a Fe-6Ni-0.1C alloy was systematically investigated and discussed from viewpoints of both thermodynamics and kinetics of ferrite transformation. Additionally, many interesting characteristics of dynamically transformed ferrite were found through microstructural observations and tensile test. Further investigations are required to unveil natures of dynamic transformation.

ACKNOWLEDGEMENTS

"Our Father in heaven, hallowed be your name, your kingdom come,

your will be done, on earth as it is in heaven."   Matthew 6:9-10

LIST OF PUBLICATIONS

International Journal Papers

N. Park, S. Khamsuk, A. Shibata, and N. Tsuji, "Effect of austenite grain size on kinetics of dynamic ferrite transformation in low carbon steel," *Scripta Materialia*, vol. 68, pp. 611–614, 2013.

N. Park, S. Khamsuk, A. Shibata, and N. Tsuji, "Occurrence of dynamic ferrite transformation in low-carbon steel above Ae_3," *Scripta Materialia*, vol. 68, pp. 538–541, 2013.

N. Park, A. Shibata, D. Terada, and N. Tsuji, "Flow stress analysis for determining the critical condition of dynamic ferrite transformation in 6Ni–0.1C steel," *Acta Materialia*, vol. 61, pp. 163–173, 2013.

S. Khamsuk, N. Park, H. Adachi, D. Terada, and N. Tsuji, "Evolution of ultrafine microstructures in commercial purity aluminum heavily deformed by torsion," *Journal of Materials Science*, vol. 47, pp. 7841–7847, 2012.

International Proceeding Papers

N. Park, S. Khamsuk, A. Shibata, and N. Tsuji, "Dynamic softening of flow stress during dynamic ferrite transformation," *Materials Science Forum* in press, 2013.

N. Park, S. Khamsuk, A. Shibata, and N. Tsuji, "Relationship between ferrite grain size and deformation conditions for dynamic transformation," *International Workshop on Bulk Nanostructured Metals*, pp. 57–60, 2012.

N. Park, A. Shibata, and N. Tsuji, "Systematic approach to clarify the mechanism of dynamic transformation in Fe-6Ni-0.1C alloy," *Advanced Materials Research*, vol. 409, pp. 707–712, 2012.

Presentations in International Conferences

N. Park, S. Khamsuk, A. Shibata, and N. Tsuji, "Dynamic ferrite transformation above equilibrium transformation temperature in 6Ni-0.1C steel," in *16th International Conference on Strength of Materials*, 19-24 Aug., 2012.

N. Park, S. Khamsuk, A. Shibata, and N. Tsuji, "Relationship between ferrite grain size and deformation conditions for dynamic transformation," in *International Workshop on Bulk Nanostructured Metals*, 26-29, June, 2012.

N. Park, A. Shibata, and N. Tsuji, "Systematic approach to clarify the mechanism of dynamic transformation in Fe-6Ni-0.1C alloy," in *International Conference on Processing & Manufacturing of Advanced Materials, THERMEC*, 1-5 Aug., 2011.

N. Park, A. Shibata, and N. Tsuji, "Dynamic transformation from austenite to ferrite in 6Ni-0.1C steel," in *Joint Symposium on Materials Science and Engineering for the 21 Century*, 19-23 June, 2011.

N. Park, A. Shibata, and N. Tsuji, "Fundamental study on dynamic transformation in steels," in *Joint Symposium on Materials Science and Engineering for the 21 Century*, 27-29 June, 2010.

Presentations in Domestic Conferences (Japan)

N. Park, S. Khamsuk, A. Shibata, and N. Tsuji, "Relationship between deformation condition and grain size of dynamically transformed ferrite in 6Ni-0.1C steel," in *Proceedings of ISIJ Annual Meeting, CAMP-ISIJ*, 17-19 Sept., 2012.

N. Park, A. Shibata, and N. Tsuji, "Critical Zener-Hollomon parameter for the occurrence of dynamic transformation of ferrite in 6Ni-0.1C steel," in *Proceedings of ISIJ Annual Meeting, CAMP-ISIJ*, 28-30 Mar., 2012.

N. Park, A. Shibata, and N. Tsuji, "Critical deformation condition for dynamic ferrite transformation in 6Ni-0.1C steel," in *Proceedings of ISIJ Annual Meeting, CAMP-ISIJ*, 20-22 Sept., 2011.

N. Park, A. Shibata, and N. Tsuji, "Dynamic ferrite transformation behavior at various deformation temperatures," in *Proceedings of ISIJ Annual Meeting, CAMP-ISIJ*, 25-27 Mar., 2011.

Presentations in Domestic Conferences (Korea)

N. Park, S. Khamsuk, A. Shibata, and N. Tsuji, "Dynamic ferrite transformation in austenite single-phase regime," in *Fall Conference of the Korean Institute of Metals and Materials*, 25-26, Oct., 2012.

N. Park, S. Khamsuk, A. Shibata, and N. Tsuji, "Dynamic ferrite transformation above equilibrium transformation temperature in 6Ni-0.1C steel," in *Spring Conference of the Korean Institute of Metals and Materials*, 26-27, Apr., 2012.

Award

"Student Award" from *International Conference on Processing & Manufacturing of Advanced Materials, THERME' 2011*, Quebec, Canada.